

Design and synthesis of luminescent poly(arylene vinylene)s and poly(arylene ethynylene)s



Dissertation

Zur Erlangung des akademischen Grades

Doktor der Naturwissenschaften

(Dr. rer. Nat.)

Eingereicht in der Fakultät für Mathematik und Naturwissenschaften
der Bergischen Universität Wuppertal

von

Isabell Sophia Geisler

geb. am 27.08.1992 in Leverkusen, Deutschland

Wuppertal, 10.12.2020

The PhD thesis can be quoted as follows:

urn:nbn:de:hbz:468-20210211-113009-5

[<http://nbn-resolving.de/urn/resolver.pl?urn=urn%3Anbn%3Ade%3A468-20210211-113009-5>]

DOI: 10.25926/9t2n-ay93

[<https://doi.org/10.25926/9t2n-ay93>]

Die vorliegende Arbeit wurde in der Zeit von August 2017 bis Dezember 2020 am Lehrstuhl für Makromolekulare Chemie der Fakultät für Mathematik und Naturwissenschaften an der Bergischen Universität Wuppertal unter Anleitung von *Prof. Dr. Ullrich Scherf* angefertigt.

1. Gutachter: *Prof. Dr. Ullrich Scherf (Bergische Universität Wuppertal)*

2. Gutachter: *Prof. Dr. Michael W. Tausch (Bergische Universität Wuppertal)*

Dissertation eingereicht am 10.12.2020

Abstract

Luminescent conjugated polymers like poly(arylene vinylene)s (PAV) and poly(arylene ethynylene)s (PAE) have been widely studied due to their versatile applicability, for example as chemosensors or as active component of light emitting diodes. Therefore, a synthetic challenge is to design and develop optimised polymers of increased efficiency.

In the first part of this work side and main chains of poly(arylene vinylene)s were varied systematically to obtain soluble conjugated polymers of intrinsic microporosity (C-PIM) and aggregation-induced emission (AIE) activity. The obtained polymers were compared for understanding the structural requirements for the desired combination of properties. To get a deeper insight, model compounds were synthesized and used for comparison. The resulting poly(arylene vinylene)s showed S_{BET} surface areas of up to $417 \text{ m}^2\text{g}^{-1}$ and AIE effects leading to high fluorescence efficiency. One polymer was applied in explosive sensing experiments where it proved its high sensitivity towards picric acid with a very low detection limit of 1.5 ppm. Furthermore, a N-carbazolyl-substituted poly(arylene vinylene) was electrooxidatively cross-linked and the influence of the cross-linking on optical properties and S_{BET} surface areas was investigated.

In the second part of this work a soluble poly(anthrylene ethynylene) was synthesized by a novel procedure. The polymer was characterized and compared to a monomeric model compound. Fluorescence anisotropy measurements revealed that the defined transition dipole moment of anthracene is blurred by the incorporation of the anthryl units into the polymer chain.

Zusammenfassung

Lumineszente, konjugierte Polymere wie zum Beispiel Poly(arylenvinyl)en (PAV) und Poly(arylenethinyl)en (PAE) wurden dank ihrer vielfältigen Einsatzmöglichkeiten, wie zum Beispiel als Chemosensoren oder als aktive Komponente in Leuchtdioden, eingehend studiert. Aufgrund dessen ist die Herausforderung nun optimierte Polymere zu entwickeln die die vorhandenen Materialien in ihrer Effizienz noch übertreffen.

Im ersten Teil dieser Arbeit wurden die Haupt- und Seitenketten von Poly(arylenvinyl)en systematisch variiert mit dem Ziel ein lösliches, konjugiertes Polymer mit intrinsischer Mikroporosität und einem aggregationsinduziertem Emissionseffekt zu erhalten. Die so erhaltenen Polymere wurden charakterisiert, um Rückschlüsse auf die Struktur-Eigenschaftsbeziehungen ziehen zu können. An geeigneter Stelle wurden Modellverbindungen synthetisiert und zum Vergleich eingesetzt, um beobachtetes Verhalten tiefergehend zu analysieren. Die so erhaltenen Poly(arylenvinyl)en zeigten spezifische BET-Oberflächen bis zu $417 \text{ m}^2\text{g}^{-1}$ und aggregationsinduzierte Emissionseffekte mit hohen Fluoreszenzquantenausbeuten. Anhand von Sprengstoffdetektionsexperimenten mit Pikrinsäure konnte für eines der Polymere eine sehr hohe Nachweisgenauigkeit mit einer unteren Grenze von 1.5 ppm gezeigt werden. Zusätzlich wurde ein N-carbazolyl-substituiertes Poly(arylenvinyl)en elektrooxidativ vernetzt und der Einfluss der Vernetzung auf die optischen Eigenschaften und die spezifischen BET-Oberflächen des resultierenden Netzwerkes untersucht.

Im zweiten Teil dieser Arbeit wurde ein lösliches Poly(anthracenethinyl)en mittels einer neu entwickelten Methode synthetisiert. Das Polymer wurde charakterisiert und mit einer monomeren Modellverbindung verglichen. Durch Messung der Fluoreszenzanisotropie konnte gezeigt werden, dass das definierte Übergangsdipolmoment des Anthracens durch Integration der Struktur in die Polymerkette verwischt.

Table of contents

1	General introduction.....	1
1.1	Aggregation-caused quenching.....	1
2	Poly(arylene vinylene)s with AIE characteristics and enhanced surface for explosive detection.....	3
2.1	Introduction.....	3
2.1.1	Aggregation-induced emission (AIE).....	3
2.1.2	Application of AIE molecules in explosive detection.....	6
2.1.3	AIE-active, microporous polymers.....	8
2.2	Objective and strategy.....	10
2.3	Results and discussion.....	11
2.3.1	Synthesis of the diketo monomers.....	13
2.3.2	Synthesis of the poly(arylene vinylene)s.....	17
2.3.3	Variation of the main chain structure.....	21
2.3.4	Variation of the side chain structure.....	28
2.3.5	Combinations of different side and main chains.....	32
2.3.6	Synthesis and characterization of tetraphenylethylene model compounds.....	36
2.3.7	Explosives detection with PPV-DP _t Bu.....	48
2.3.8	Electrochemical cross-linking of PPV-DPC as linear precursor.....	49
2.4	Conclusions and Outlook.....	56
3	Synthesis and Characterization of a Poly(anthrylene ethynylene).....	59
3.1	Introduction.....	59
3.1.1	Anthracene as chromophoric building block.....	60
3.1.2	Fluorescence anisotropy.....	60
3.2	Objective and strategy.....	61
3.3	Results and discussion.....	62
3.3.1	Synthesis of the bis-geminal tetrabromide monomer.....	63

3.3.2	Synthesis and Characterization of PAAE	65
3.3.3	Fluorescence anisotropy of BPEA and PAAE.....	69
3.4	Conclusion and Outlook.....	72
4	Experimental Part.....	74
4.1	General.....	74
4.1.1	Experimental details from chapter 2.3.6.....	76
4.1.2	Experimental details from chapter 3.3.3.....	78
4.2	Syntheses from chapter 2.....	78
4.2.1	2,7-Dibenzoyl-9,9-dimethyl-9 <i>H</i> -fluorene (FDK-DP).....	78
4.2.2	Poly[2,7-(9,9-dimethyl-9 <i>H</i> -fluorenylene)-1,2-diphenylvinylene] (PFV-DP)	79
4.2.3	4,4'-Biphenyldicarboxylic acid (8).....	80
4.2.4	4,4'-Dibenzoylbiphenyl (BDK-DP).....	80
4.2.5	Poly[4,4'-biphenyldiyl-1,2-diphenylvinylene] (PBV-DP)	81
4.2.6	9-Benzoylanthracene.....	82
4.2.7	9,10-Dibenzoylanthracene (ADK-DP)	83
4.2.8	Poly[9,10-anthrylene-1,2-diphenylvinylene] (PAV-DP).....	84
4.2.9	2,5-Dibenzoylthiophene (TDK-DP).....	85
4.2.10	Poly[2,5-thiophenylene-1,2-diphenylvinylene] (PTV-DP)	85
4.2.11	1,4-Bis(2-(9,9-dimethyl-9 <i>H</i> -fluorenyl))benzene (PDK-DF)	86
4.2.12	Poly[1,4-phenylene-1,2-bis(2-(9,9-dimethyl-9 <i>H</i> -fluorenyl))vinylene] (PPV-DF)	87
4.2.13	1,4-Bis(2-naphthoyl)benzene (PDK-DN)	88
4.2.14	Poly[1,4-phenylene-1,2-bis(2-naphthyl)vinylene] (PPV-DN).....	89
4.2.15	4,4'-Bis(<i>tert</i> -butyl)terephthalophenone (PDK-DPtBu)	90
4.2.16	Poly[1,4-phenylene-1,2-bis(4- <i>tert</i> -butylphenyl)vinylene] (PPV-DPtBu)	90
4.2.17	3,3',5,5'-Tetrakis(<i>tert</i> -butyl)terephthalophenone (PDK-DPDtBu)	92
4.2.18	Poly[1,4-phenylene-1,2-bis(3,5-di- <i>tert</i> -butylphenyl)vinylene] (PPV-DPDtBu) .	93
4.2.19	4,4'-Bis(<i>tert</i> -pentyl)terephthalophenone (PDK-DPtPent)	94

4.2.20	Poly[1,4-phenylene-1,2-bis(4- <i>tert</i> -pentylphenyl)vinylene] (PPV-DPtPent)	95
4.2.21	4,4'-Dibromoterephthalophenone (11)	96
4.2.22	4,4'-Bis(4''- <i>tert</i> -butylphenyl)terephthalophenone (PDK-DBtBu)	96
4.2.23	Poly[1,4-phenylene-1,2-bis(4-(4'- <i>tert</i> -butyl)biphenyl)vinylene] (PPV-DBtBu)	97
4.2.24	2,7-(4-(<i>tert</i> -Butyl)benzoyl)-9,9-dimethyl-9 <i>H</i> -fluorene (FDK-DPtBu).....	98
4.2.25	Poly[2,7-(9,9-dimethyl-9 <i>H</i> -fluorenylene)-1,2-bis(4- <i>tert</i> -butylphenyl)vinylene] (PFV-DPtBu)	99
4.2.26	4,4'-Bis(4- <i>tert</i> -butylbenzoyl)biphenyl (BDK-DPtBu).....	100
4.2.27	Poly[4,4'-biphenyldiyl-1,2-bis(4- <i>tert</i> -butylphenyl)vinylene] (PBV-DPtBu)	101
4.2.28	2,5-(4- <i>tert</i> -Butylbenzoyl)thiophene (TDK-DPtBu).....	102
4.2.29	Poly[2,5-thiophenylene-1,2-bis(4- <i>tert</i> -butylphenyl)vinylene] (PTV-DPtBu) ...	103
4.2.30	4,4'-Bis(<i>tert</i> -butyl)isophthalophenone (mPDK-DPtBu).....	104
4.2.31	Poly[1,3-phenylene-1,2-bis(4- <i>tert</i> -butylphenyl)vinylene] (PmPV-DPtBu)	104
4.2.32	1,3-Bis(2-naphthoyl)benzene (mPDK-DN)	105
4.2.33	Poly[1,3-phenylene-1,2-bis(2-naphthyl)vinylene] (PmPV-DN)	106
4.2.34	1-Benzoyl-4- <i>tert</i> -butylbenzene (17)	107
4.2.35	<i>E</i> -1,2-Bis(4- <i>tert</i> -butylphenyl)-1,2-diphenylethylene (TPE-DtBu)	108
4.2.36	2-Benzoylnaphthalene.....	108
4.2.37	<i>E</i> -1,2-Bis(2-naphthenyl)-1,2-diphenylethylene (DPE-DN).....	109
4.2.38	4,4'-Bis(9-carbazoyl)terephthalophenone (PDK-DPC).....	110
4.2.39	Poly[1,4-phenylene-1,2-bis(4-(9-carbazoyl)phenyl)vinylene] (PPV-DPC)	111
4.2.40	Network N1	112
4.3	Syntheses from chapter 3	112
4.3.1	2,6-Dibromoanthraquinone (30)	112
4.3.2	9-Methyleneheptadecane (32).....	113
4.3.3	2,6-Bis(2-octyldecyl)anthraquinone (33).....	114
4.3.4	9,10-Bis(dibromomethylene)-2,6-bis(2-otyldecyl)-9,10-dihydroanthracene (28).....	114

4.3.5	Poly[2,6-(2-octyldecyl)anthrylene-9,10-ethynylene] (PAAE)	115
5	Appendix.....	117
5.1	List of Abbreviations	117
5.2	References	121
5.3	Acknowledgements	128

1 General introduction

Since the 20th century, conjugated polymers have been an ever-growing field of research, based on the number of publications per year. The optical and electronic properties in combination with a superior processability predestine for a multitude of applications, such as organic field-effect transistors (OFET)¹, organic light emitting diodes (OLED)²⁻⁴, biological applications^{5,6}, sensors⁷, and photovoltaics.⁸

Two of the main classes of conjugated polymers are poly(*para*-phenylene vinylene)s (**PPV**) and poly(*para*-phenylene ethynylene)s (**PPE**).³ The general structures shown in Figure 1 can be modified in various ways to fit the needs of the diverse applications. Side chains can be attached to the phenylene units as well as to the double bonds in the case of the **PPV**. Further, the phenylenes can be exchanged by other (hetero)aromatic groups, creating infinite structural possibilities to fine tune the polymer properties.³



Figure 1 Structures of poly(*para*-phenylene vinylene) (**PPV**) and poly(*para*-phenylene ethynylene) (**PPE**).

Poly(arylene vinylene)s (PAV) as well as poly(arylene ethynylene)s (PAE) typically display high solution-state photoluminescence quantum yields.^{9,10} PAEs feature wider band gaps than PAVs which results in a blue-shifted emission in comparison to the normally yellow to red emitting PAVs.⁹ PAEs can show a higher photostability, while PAV derivatives provide a greater structural versatility, making both classes highly interesting for applications while meeting different requirements.¹¹

Plenty of these applications, like OLEDs or fluorescence sensors, require high photoluminescence quantum yields (PLQY). A major drawback in this field has been the well-known aggregation-caused quenching effect of which both polymer classes may suffer.^{12,13}

1.1 Aggregation-caused quenching

Fluorescent materials typically contain extended aromatic systems resulting in planar structures.¹⁴ While highly fluorescent in dilute solutions, these molecules experience strong

intermolecular interactions when in concentrated solution or solid state.¹⁵ Amongst others, these interactions can lead to the formation of excimers or exciplexes that cause fluorescence quenching.¹⁴ Further possible quenching mechanisms are different types of electron transfer, as Förster resonance energy transfer, and electron exchange.⁷ These effects are often discussed as concentration quenching or aggregation-caused quenching (ACQ). It is a severe limitation of the applicability of such molecules as light emitting materials in devices like OLEDs or sensors, since the materials are used in the solid state.^{2,7} Biological applications on the other hand often demand aqueous solutions of the dyes which cause hydrophobic molecules to aggregate.⁶ Many different chemical^{16,17} or physical^{18,19} attempts have been made to prevent the ACQ effect. Aggregation of PPEs for example can be hindered by introducing long linear or branched alkyl chains increasing the solid state quantum yield.^{17,20} An especially attractive solution to the ACQ problem is to utilize the opposite effect called aggregation-induced emission (AIE). Both effects are displayed in Figure 2 with the aid of two typical representatives, perylene (displays ACQ) and tetraphenylethylene (TPE) (displays AIE). The AIE effect and AIE based materials will be discussed in detail in the following chapter.

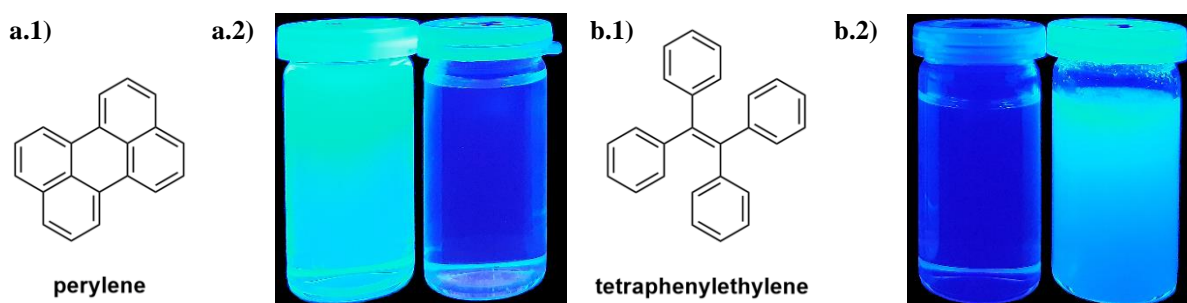


Figure 2 a.1) Chemical structure of perylene a.2) ACQ effect of perylene: perylene in pure THF (left) and THF:water 1:9 mixture (right) under UV irradiation b.1) Chemical structure of tetraphenylethylene b.2) AIE effect of tetraphenylethylene: tetraphenylethylene in pure THF (left) and THF/water 1:9 mixture (right) under UV irradiation.

2 Poly(arylene vinylene)s with AIE characteristics and enhanced surface for explosive detection

2.1 Introduction

Poly(arylene vinylene)s typically display high solution-state quantum yields.⁹ By introduction of aryl side chains to the vinylene unit, the class is able to obtain AIE characteristics and, therefore, high solid state PLQYs. Simultaneously, the solubility is increased,⁹ allowing a widely extended applicability.²¹ By now numerous aggregation-induced emission luminogens (AIEgen) are known with solid state quantum yields up to unity,^{22,23} for applications like OLEDs,⁴ lasers,²⁴ solar concentrators²⁵ or sensing devices²⁶. Therefore, the main focus is now to find new and promising combinations of attractive properties to increase overall performance.

Polymers themselves display some advantages over small molecules in terms of easy processability, cost-effectiveness, and greater tunability of structure, topology, and morphology.²⁷ Integrating AIE characteristics into fully conjugated polymers leads to extended exciton transfer pathways that increase the detection sensitivity.²⁷ The highest detection sensitivity can be obtained by porous AIE polymers due to the increased surface area and the possibility of the analyte penetrating the polymer film through the pores.⁷ The known porous polymers typically obtain their properties by rigidification of the structure that creates defined pores but decreases the solubility and therefore limits the processability.²⁷

2.1.1 Aggregation-induced emission (AIE)

AIE molecules are weakly emissive in dilute solution but display an intense emission in the aggregated or solid state.¹⁶ This phenomenon has been well known since the 19th century, but only when Tang and co-workers began to work in this field in 2001, AIE molecules became subject of intensive research. Huge progress has been made ever since.^{16,28,29}

The AIE phenomenon is widely accepted to be caused by the restriction of intramolecular motions (RIM).^{30,31} Figure 3 displays the mechanism on hand of the restriction of intramolecular rotations of the tetraphenylethylene (**TPE**) compared to the π - π stacking ACQ mechanism of perylene. In dilute solution the AIEgen converts irradiated energy to intramolecular motions like rotations or vibrations. In aggregated state those motions are restricted favouring the

radiative decay.³¹ Therefore, many of the AIE-active molecules contain a rotatable residue, but there are also known examples of molecules that display AIE only by restriction of vibrational movements.³¹

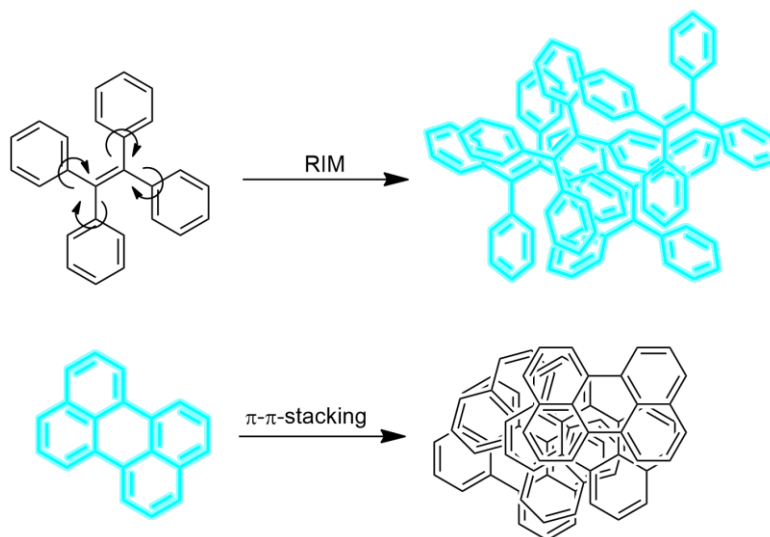


Figure 3 Schematic illustration of the AIE mechanism on hand of tetraphenylethylene compared to the ACQ mechanism of perylene.

The previously shown TPE is one of the most prominent examples for AIE molecules. It displays a distinct AIE effect on its own, and can be incorporated into larger monomeric compounds or polymers for tuned properties.^{26,32-34} There are different approaches to incorporate an AIEgen into a polymer as displayed in Figure 4. The first differentiation has to be made whether the luminogen is a building block of the main chain or attached as a side chain. The main chain can either be completely made up of the AIEgen (Figure 4a)³⁵ or be a copolymer of AIEgens and other monomers (Figure 4b).^{27,36} Another possibility is to incorporate the AIEgen at the terminals of the polymers (Figure 4c).^{27,37} As a side chain the luminogen can be attached to every repeat unit (Figure 4d)^{34,38} or only to one of the different repeat units of a copolymer (Figure 4e).^{27,39}

The PPV derivative poly(1,4-phenylene-1,2-diphenylvinylene) (**PPV-DP**) shown in Figure 5 can be regarded as a linear chain of **TPE** units. The polymer was first described by Hörhold *et al.*³⁵ in 1979. Later in 2000 Andersson and co-workers²¹ observed the expected AIE characteristics when measuring the photoluminescence quantum yields (PLQY). The quantum yields increased from 0.4% in tetrahydrofuran solution to 19 % in film.²¹

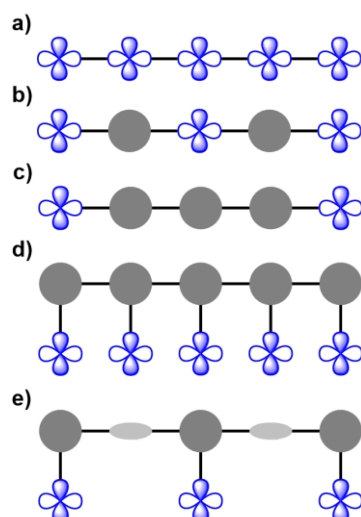


Figure 4 Schematic composition of different types of AIE polymers.²⁷

By further derivatization of **PPV-DP**, polymers with even higher PLQYs can be obtained.^{21,26,40} Baysec *et al.*²⁶ exchanged the main and side chains to increase the solid state PLQYs of **PPV-DP**. By introducing larger rotatable groups to the polymer, the AIE effect was increased. They were able to achieve quantum yields up to 73% by attaching phenoxy groups to the phenyl side chains as shown in Figure 5.²⁶ Due to the high PLQY, the resulting polymer showed a promising sensing sensitivity towards nitroaromatic explosives.

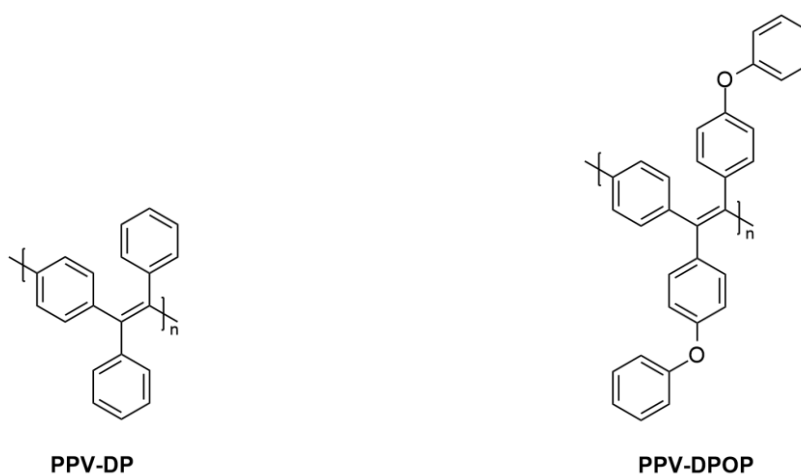


Figure 5 Structure of poly(1,4-phenylene-1,2-diphenylvinylene) (**PPV-DP**) and poly(1,4-phenylene-1,2-di((4-phenoxy)phenyl)vinylene) (**PPV-DPOP**).²⁶

2.1.2 Application of AIE molecules in explosive detection

Detection of explosives is an important field of research due to its impact on the public security, this includes not only prevention of terrorism but also detection of landmines, forensic research, and inquiry of environmental pollution caused by explosives.^{7,41} Many of the common explosives are nitroaromatic compounds.⁴² These substances are extremely sensitive to physical impact and therefore are preferably detected contact-free. This requires very high sensitivity of the detector due to the low vapor pressure of these nitro organics.⁴¹ Fluorescence quenching of polymers with AIE effect is therefore one of the favoured methods of detection in current research.^{7,26,39} This is due to its increased sensitivity caused by exciton migration along the polymer chain, convenience, and potentially low cost.⁷

Fluorescence quenching can be attributed to photoinduced electron transfer, Förster resonance energy transfer or other types of electron transfer.¹⁴ In case of the detection of nitro-compounds with fluorescent sensors, photoinduced electron transfer can be regarded as the main mechanism.⁷ An electron deficient nitroaromatic compound can bind to an electron rich fluorescent polymer via donor-acceptor interactions. The excited fluorophore can donate an electron from its lowest unoccupied molecular orbital (LUMO) to the LUMO of the acceptor. The driving force for this process is the energy offset between the LUMOs.⁷ This mechanism is depicted in Figure 6.

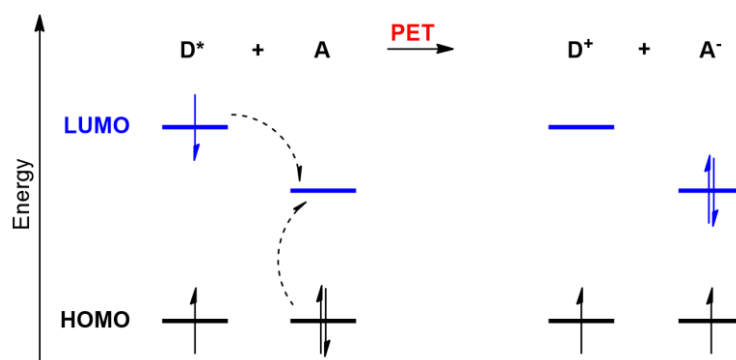
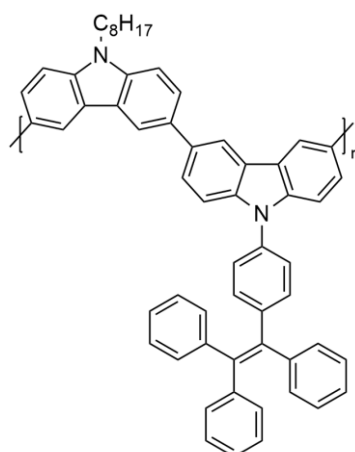


Figure 6 Molecular orbital schematic illustration of the photoinduced electron transfer (PET).⁷

Scherf and co-workers have been able to develop numerous, efficient linear conjugated polymers with AIE effect for explosive detection by integrating **TPE** into polymer structures.^{26,36,38,39,43} The best results for these polymers were obtained for a **TPE**-substituted polycarbazole displayed in Figure 7.³⁹



PCzTPE0.5

Figure 7 TPE-substituted AIE-active carbazole polymer **PCzTPE0.5**.³⁹

The observed maximal Stern-Volmer constant of $1.26 \times 10^6 \text{ M}^{-1}$ is amongst the highest known for AIE polymer based sensors.^{7,39,44-46} Compared to **PCzTPE0.5**, the Stern-Volmer constant of the **PPV-DPOP** polymer by Baysec *et al.*²⁶ with a value of $4.75 \times 10^3 \text{ M}^{-1}$ is considerably lower, despite the far higher solid state PLQY of 73% compared to 21% for **PCzTPE0.5**.^{26,39} The reason for this are presumably efficient donor-acceptor interactions between carbazole units and quencher molecules leading to an amplified quenching at higher quencher concentrations, shown for **PCzTPE0.5** in the Stern-Volmer plot in Figure 8b.

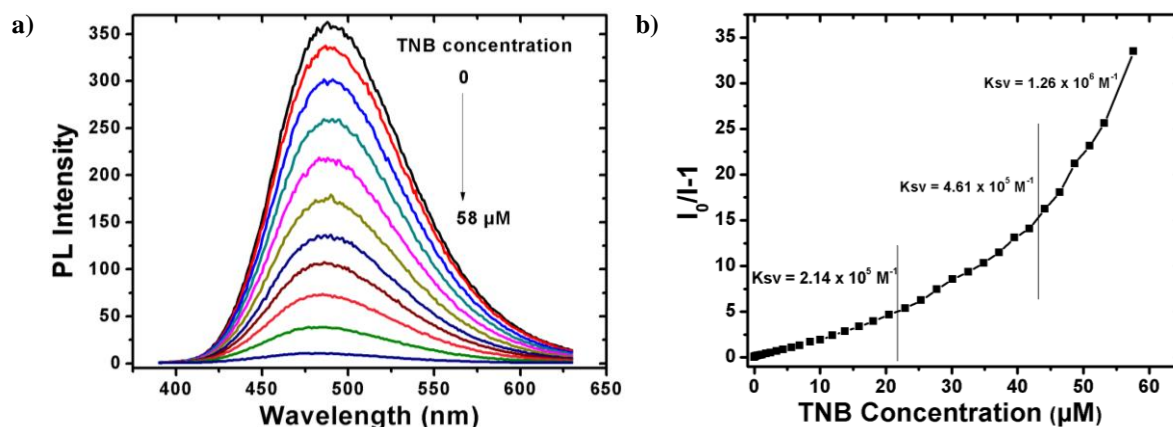


Figure 8 a) PL spectra of **PCzTPE0.5** in tetrahydrofuran:water 1:9 mixture containing different amounts of 1,3,5-Trinitrobenzene. Polymer concentration: 10^{-5} M ; $\lambda_{\text{exc.}}$: 320 nm. B) Stern-Volmer plot of **PCzTPE0.5**.³⁹

This kind of amplification occurs when an increased number of quenching sites is available at high quencher concentrations and, therefore, this behaviour can be assigned to the topology of the polymer.³⁹ This also is a common effect for microporous networks.⁴⁶ Therefore, the combination of an AIE effect with very high quantum yields, achievable by **PPV-DP** derivatives, and a microporous structure could greatly improve the sensitivity of explosives detection.

2.1.3 AIE-active, microporous polymers

Microporosity in luminescent, polymers is normally achieved in cross-linked or hyperbranched structures.⁴⁶⁻⁵⁰ The reported polymers include metal-organic frameworks,⁴⁸ amorphous microporous polymer networks^{47,49,50} and covalent organic frameworks.⁵¹ In explosive sensing experiments the combination of luminescence and porosity has proven to be very successful.⁴⁶⁻⁵¹ Still, the PLQY of these kinds of structures is often rather low. By introduction of AIE-active building blocks, the AIE effect can be transferred to the polymers increasing the quantum yields significantly.^{46,47,49}

Scherf and co-workers successfully generated a series of microporous polymer networks with high sensing efficiency, chemically^{47,52} or electrochemically.^{50,53-55} While the chemical polymerization routes are favourable when large amounts of polymer are needed, the normally insoluble polymer networks pose a problem for further processing.^{47,56} For polymer film electrodes, thin layer sensors or comparable applications an electrochemical synthesis is advantageous since a good quality film can be generated directly at the desired location.⁵⁶ Therefore, many of the networks have been electrochemically generated. This requires crosslinkable groups in the monomers, like thiophenes or carbazoles that can be electrochemically oxidized.^{57,58} Scherf and co-workers have proven that carbazole based networks are highly sensitive towards nitroaromatics.^{50,53-55}

A microporous network with comparatively high PLQYs was obtained by Preis *et al.*⁴⁷. The network, shown in Figure 9, consists of **TPE** units linked by triazine cores (**1**) and displays only a moderate surface area of 475 m²g⁻¹ but shows an AIE effect with a quantum yield of 25% and promising explosives detection behaviour.⁴⁷ This proves that the combination of AIE effect and high surface is possible and efficient.

A major drawback of these known structures is their insolubility and hence low processability.^{47,52,55} Therefore, linear conjugated polymers of intrinsic microporosity (C-PIM) have become of interest due to their solubility.⁵⁹⁻⁶² Major advances in this field have been made by Cooper and co-workers.^{59,63-65} The group published, amongst others, a series of polyacetylenes **2-5** as displayed in Figure 10.

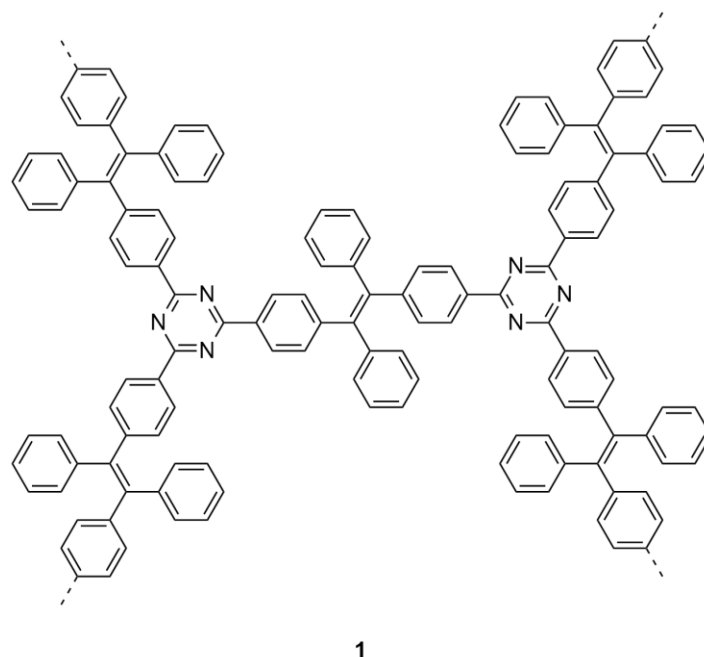


Figure 9 Idealized structure of the triazine core linked TPE network (**1**) by Preis *et al.*⁴⁷

Recently, Klein *et al.*⁶⁰ were able to synthesize novel C-PIMs based on oligocyclic monomers. The polymer **6** with the highest surface area of $757 \text{ m}^2\text{g}^{-1}$ is displayed in Figure 10. The reported PLQYs of C-PIMs are often moderate, with the highest value of 55%, offering room for improvement.^{60,61,64,65}

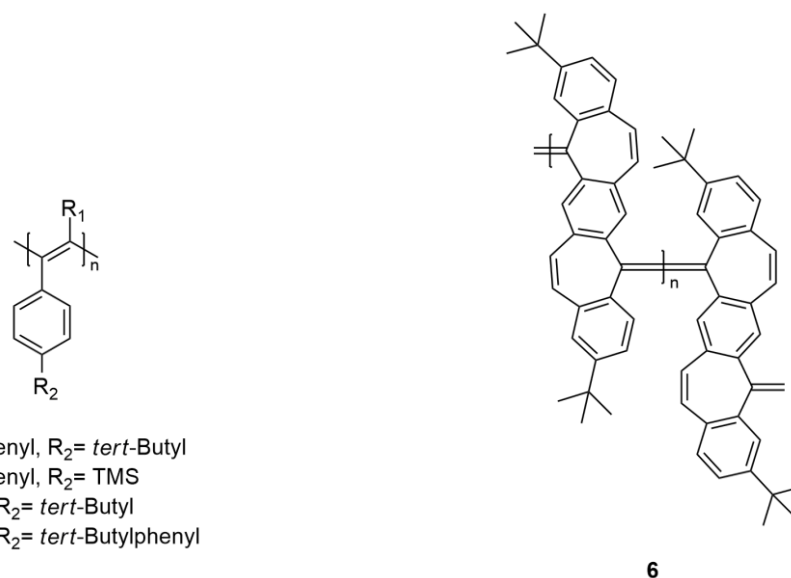


Figure 10 Structures of the C-PIMs by Cooper and co-workers⁵⁹ **2-5** and Klein *et al.*⁶⁰ **6**.

2.2 Objective and strategy

As described beforehand, a combination of AIE characteristics and high surface area can lead to efficient sensor polymers, however often at the cost of processability. Poly(arylene vinylene)s (PAV) with rotatable side chains show a pronounced AIE effect and good solubility but have a limited surface area due to the flexible polymer chain. This work focuses on the synthesis of PAVs of the general structure shown in Figure 11. The **TPE** motive should hereby lead to polymers with an AIE effect, while the structural similarities to the C-PIMs **2-6** makes this class of polymers promising candidates for the development of new, improved C-PIMs. The chosen approach to obtain porosity was to systematically vary side and main chain.

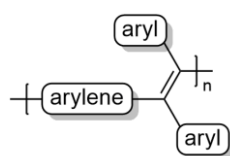


Figure 11 General structure of the poly(arylene vinylene)s with aromatic side chains.

A retrosynthetic analysis of the general structure was carried out as shown in Figure 12. The polymers will be obtained by a polyolefination reaction of bis-geminal tetrachloride monomers similar to the method described by Hörhold *et al.* in 1977.⁶⁶ The required chlorides in turn can be derived from diketones following literature procedure.⁶⁶ For the synthesis of the diketones, a suitable method is the conversion of commercially available carboxylic acids into corresponding acid chlorides followed by Friedel-Crafts acylations.⁶⁷ The obtained polymers will be fully characterized with special regard to the optical properties and S_{BET} surface areas. The most promising candidate will be tested for its ability to sense explosives.

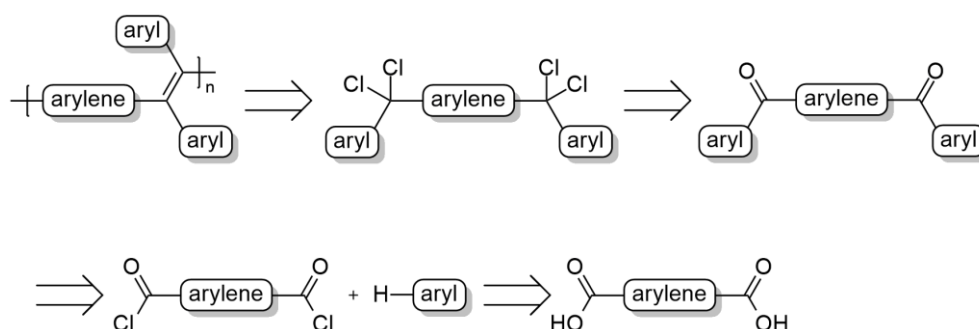


Figure 12 Retrosynthetic approach towards the desired Poly(arylene vinylene)s.

Furthermore, additional rationalization of the obtained results ought to be possible by comparison to suitable **TPE** model compounds. The model compounds can be synthesized via

reductive coupling of a ketone precursor, for example after McMurry. The precursor was obtained from a corresponding acid chloride by Friedel-Crafts acylation as shown in Figure 13.^{67,68}

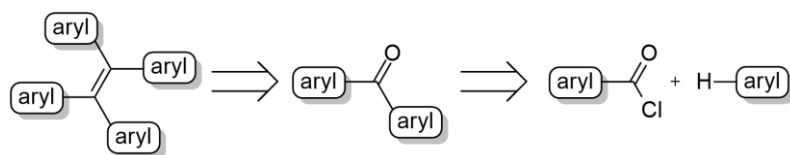


Figure 13 Retrosynthetic approach towards the model compounds.

2.3 Results and discussion

First, four poly(*para*-phenylene vinylene) derivatives with different main chains were synthesized. Thiophene, fluorene, anthracene, and biphenyl were incorporated into the main chain to receive the polymers shown in Figure 14: Poly[2,7-(9,9-dimethyl-9H-fluorenylene)-1,2-diphenylvinylene] (**PFV-DP**), poly[4,4'-biphenyldiyl-1,2-diphenylvinylene] (**PBV-DP**), poly[9,10-anthrylene-1,2-diphenylvinylene] (**PAV-DP**), and poly[2,5-thiophenylene-1,2-diphenylvinylene] (**PTV-DP**). These polymers shall be compared to the PAVs that were already synthesized, characterized and published by Baysec *et al.*²⁶, in particular poly[1,4-phenylene-1,2-diphenylvinylene] (**PPV-DP**), and poly[1,3-phenylene-1,2-diphenylvinylene] (**PmPV-DP**). In this work, only the BET surface areas of the existing polymers were supplemented to gain a deeper understanding of the effect of the structure on the S_{BET} surface area.

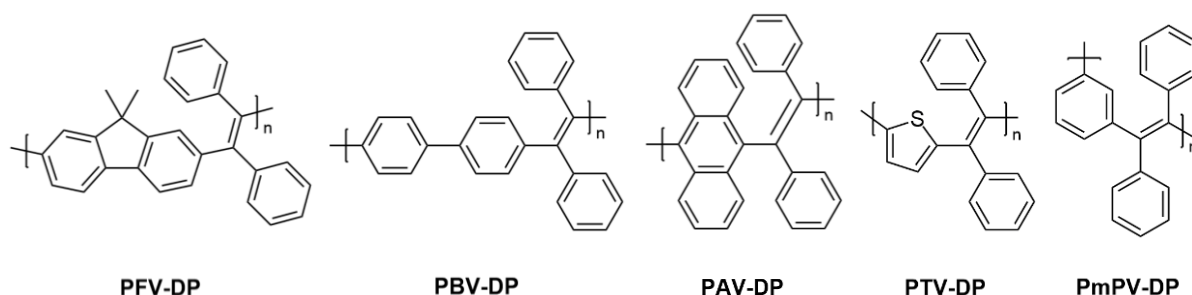


Figure 14 Structures of the poly(arylene vinylene)s with phenyl side chains.

Subsequently, seven other PPV derivatives with side chains different from phenyl were synthesized. A 9,9-dimethylated fluorene, naphthalene, three alkylated phenylenes, a *tert*-butyl biphenyl, and a 9-phenylcarbazole as substituent were introduced in polymers with a 1,4-phenylene vinylene backbone. The structures of poly[1,4-phenylene-1,2-bis(2-(9,9-dimethyl-9H-fluorenyl))vinylene] (**PPV-DF**), poly[1,4-phenylene-1,2-bis(2-naphthyl)vinylene] (**PPV-DN**), poly[1,4-phenylene-1,2-bis(4-*tert*-butylphenyl)vinylene] (**PPV-DPtBu**), poly[1,4-phenylene-

1,2-bis(3,5-di-*tert*-butylphenyl)vinylene] (**PPV-DPdBu**), poly[1,4-phenylene-1,2-bis(4-*tert*-pentylphenyl)vinylene] (**PPV-DPtPent**), poly[1,4-phenylene-1,2-bis(4-(4'-*tert*-butyl)biphenyl)vinylene] (**PPV-DBtBu**), and poly[1,4-phenylene-1,2-bis(4-(9-carbazoyl)phenyl)vinylene] (**PPV-DPC**) are displayed in Figure 15.

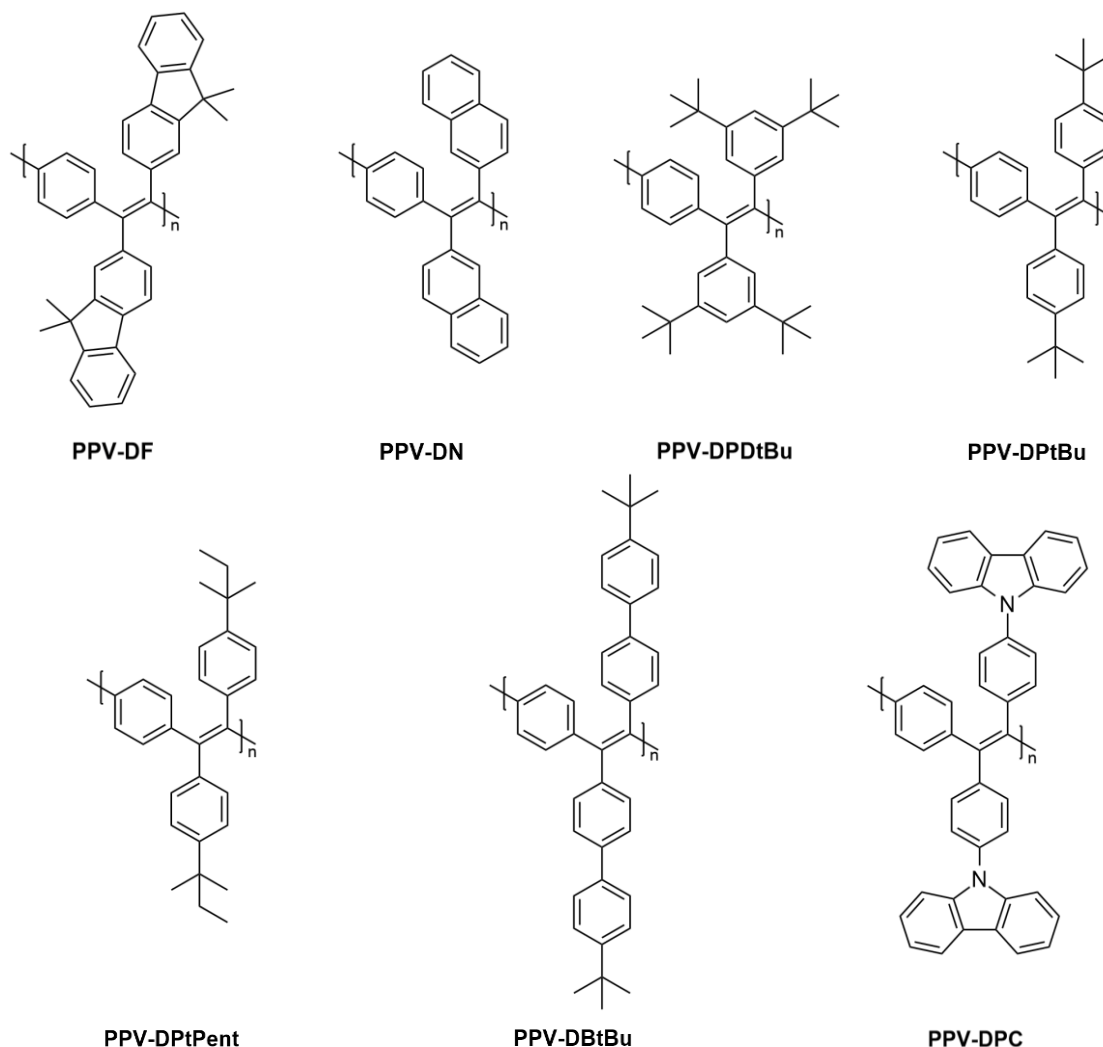


Figure 15 Structures of the poly(*para*-phenylene vinylene)s with different aryl side chains.

Lastly, PPVs with several combinations of main chain and side chain building blocks were synthesized. The structures of poly[2,7-(9,9-dimethyl-9H-fluorenylene)-1,2-bis(4-*tert*-butylphenyl)vinylene] (**PFV-DPtBu**), poly[4,4'-biphenyldiyl-1,2-bis(4-*tert*-butylphenyl)vinylene] (**PBV-DPtBu**), poly[2,5-thiophenylene-1,2-bis(4-*tert*-butylphenyl)vinylene] (**PTV-DPtBu**), poly[1,3-phenylene-1,2-bis(4-*tert*-butylphenyl)vinylene] (**PmPV-DPtBu**), and poly[1,3-phenylene-1,2-bis(2-naphthyl)vinylene] (**PmPV-DN**) are depicted in Figure 16.

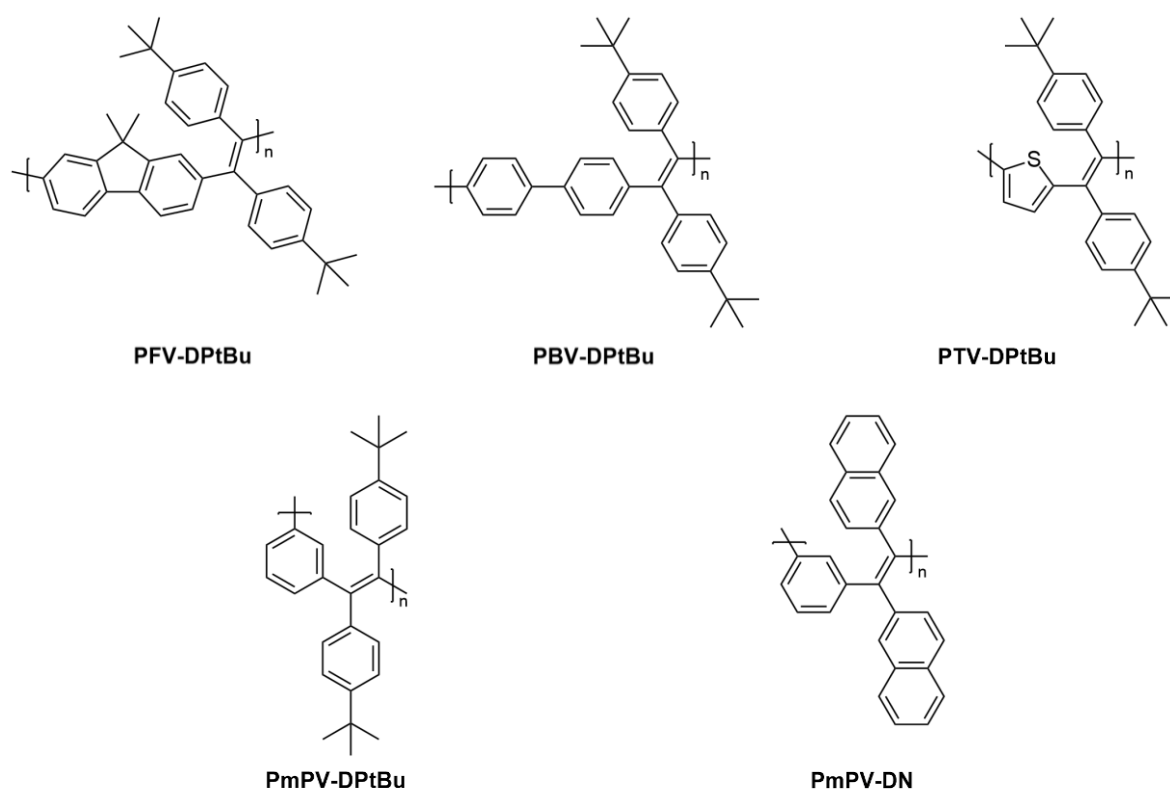


Figure 16 Structures of the poly(arylene vinylene)s with different main and side chain building block.

2.3.1 Synthesis of the diketo monomers

The desired monomers were, with one exception, obtained by Friedel-Crafts acylation using aluminium(III) chloride as Lewis acid. The monomer for **PPV-DPDtBu** synthesis is not accessible through Friedel-Crafts acylation because the electrophilic aromatic substitution is *ortho*/*para* directed by the *tert*-butyl groups. This synthesis will be discussed later. Since acylation leads to a deactivation of the arene for a second electrophilic substitution, the diketo monomers were prepared from the corresponding dicarboxylic acid chlorides.

9,9-Dimethyl-9*H*-fluorene and anthracene were the only core structures that could be disubstituted by commercial benzoyl chloride or 4-(*tert*-butyl)benzoyl chloride. Thiophene- and biphenyl-based acid chlorides were obtained from the carboxylic acids by DMF catalysed reaction with thionyl chloride and converted to the desired monomers with benzene or *tert*-butylbenzene.⁶⁹ 4,4'-Biphenyldicarboxylic acid (**8**) was obtained by homo-coupling reaction of 4-bromobenzoic acid (**7**) using a palladium(II) chloride/EDTA mixture in presence of ascorbic acid, a method developed by Ram *et al.*⁷⁰ The synthesis of 4,4'-dibenzoylbiphenyl (**BDK-DP**) is displayed in Figure 17. *meta*-Substituted phenylenes were obtained by reaction of commercially available isophthaloyl chloride and naphthalene or *tert*-butylbenzene.

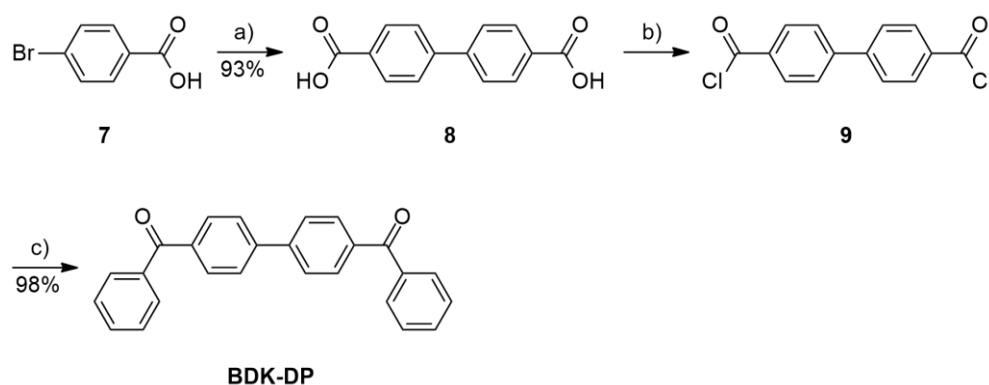


Figure 17 Synthesis of 4,4'-dibenzoylbiphenyl (**BDK-DP**): a) PdCl₂, L(+)-ascorbic acid, EDTA, K₂CO₃, EtOH/H₂O, 90 °C, 19 h; SOCl₂, DMF, 75 °C, 18 h; c) benzene, AlCl₃, 85 °C, 4 h.

The *para*-phenylene-type monomers were obtained by Friedel-Crafts reaction of commercially available terephthaloyl chloride (**10**) with fluorene, naphthalene, *tert*-butylbenzene or *tert*-pentylbenzene. For 4,4'-bis(4'-*tert*-butylphenyl)terephthalophenone (**PDK-DBtBu**), which is used as monomer for **PPV-DBtBu**, the Friedel-Crafts reaction was carried out with bromobenzene to give 4,4'-dibromoterephthalophenone (**11**). The monomer **PDK-DBtBu** was then synthesized via Suzuki-type coupling of the brominated diketone **11** with 4-*tert*-butylbenzene boronic acid, as displayed in Figure 18.⁷¹

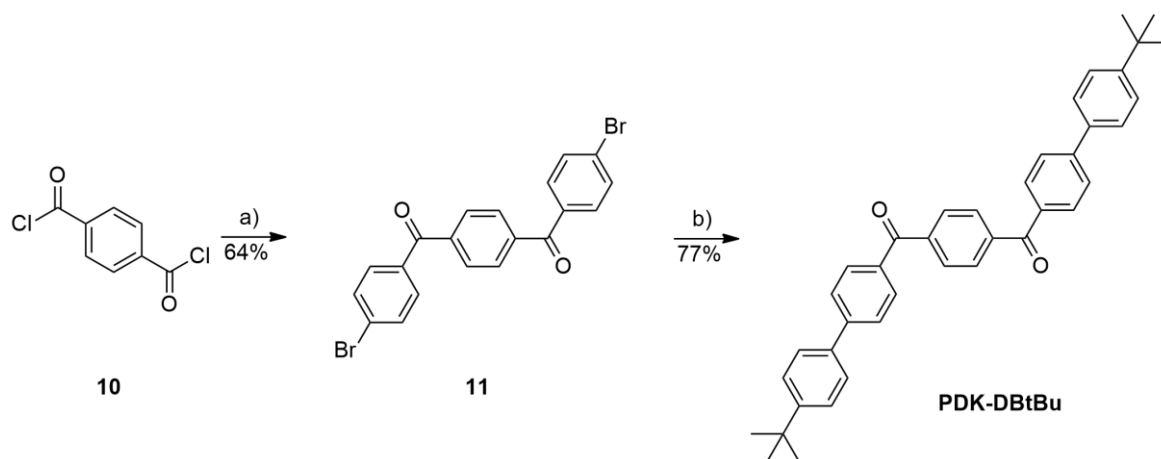


Figure 18 Synthesis of 4,4'-bis(4'-*tert*-butylphenyl)terephthalophenone (**PDK-DBtBu**): a) bromobenzene, AlCl₃, 90 °C, 18 h; b) 4-*tert*-butylbenzene boronic acid, Pd(PPh₃)₄, Na₂CO₃, Aliquat® 336, toluene, 120 °C, 48 h.

4,4'-Dibromoterephthalophenone (**11**) was also used for the monomer synthesis of **PPV-DPC**. Dibromide **11** was coupled with carbazole (**12**) in a palladium(II) acetate catalysed Buchwald–Hartwig amination reaction as displayed in Figure 19.

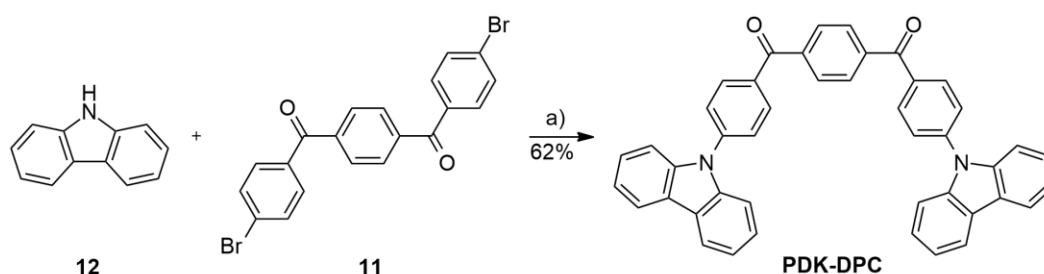


Figure 19 Synthesis of 4,4'-bis(9-carbazoyl)terephthalophenone (**PDK-DPC**): a) Pd(OAc)₂, P(*t*-Bu)₃, K₂CO₃, toluene, 120°C, 48 hours.

3,3',5,5'-Tetrakis(*tert*-butyl)terephthalophenone (**PDK-DPDtBu**) was obtained following a modified procedure by Ready and co-workers shown in Figure 20.⁷² First 1-Bromo-3,5-di-*tert*-butylbenzene (**13**) was converted to the corresponding Grignard reagent by insertion of magnesium into the carbon-halogen bond. Then, in a Grignard reaction the reagent **14** underwent a nucleophilic addition to terephthalaldehyde. The formed dialcohol **15** was oxidized to the ketone **PDK-DPDtBu** by pyridinium chlorochromate (PCC).

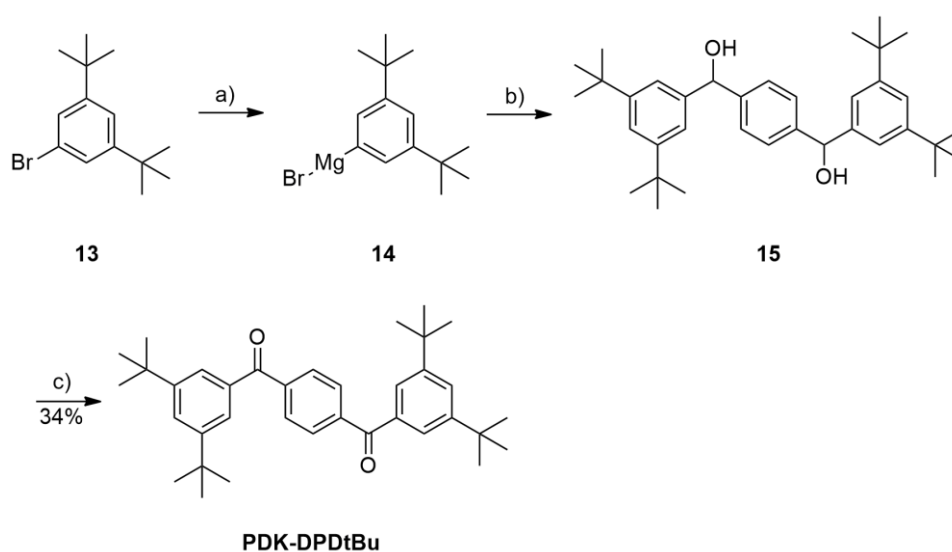


Figure 20 Synthesis of 3,3',5,5'-tetrakis(*tert*-butyl)terephthalophenone (**PDK-DPDtBu**): a) Mg, THF, rt → 65 °C, 1 h; b) terephthalaldehyde, THF, -40 °C → rt, 1 h; c) PCC, Celite®, DCM, rt, 2 h.

All diketo monomers were characterized by ¹H- and ¹³C{H}-NMR, high resolution mass, and infrared (IR) spectroscopy. Here, the results shall only be discussed exemplary on hand of 4,4'-bis(*tert*-butyl)terephthalophenone (**PDK-DPtBu**). The ¹H- and ¹³C{H}-NMR spectra of **PDK-DPtBu** are shown in Figure 21. The formation of the product can easily be confirmed in the ¹H-NMR spectrum by the appearance of the typical singlet of the symmetric 1,4-substituted phenylene core at 7.88 ppm (red), additional to the signals of the two doublets of the

unsymmetrically 1,4-substituted phenylene side chains at 7.80 ppm and 7.53 ppm (black). The *tert*-butyl groups show the expected singlet at 1.38 ppm (green). In the $^{13}\text{C}\{\text{H}\}$ -NMR spectrum the expected number of signals can be found, including six aromatic and one carbonyl carbons. The *tert*-butyl group shows two signals in the aliphatic region of the spectrum at 35.3 ppm and 31.3 ppm. The characteristic ketone signal is found at 195.9 ppm. All ketone signals of the monomers in this work appear strongly shifted downfield between 188 ppm and 200 ppm, as expected. In comparison to the corresponding acid (177.1 ppm for the dicarboxylic acid **8**), the keto signals are shifted to higher ppm values due to the presence of more electron deficient carbonyls.

The measured atmospheric pressure chemical ionization (APCI) high resolution mass to charge ratio was 399.2347 m/z compared to the calculated 399.2319 m/z .

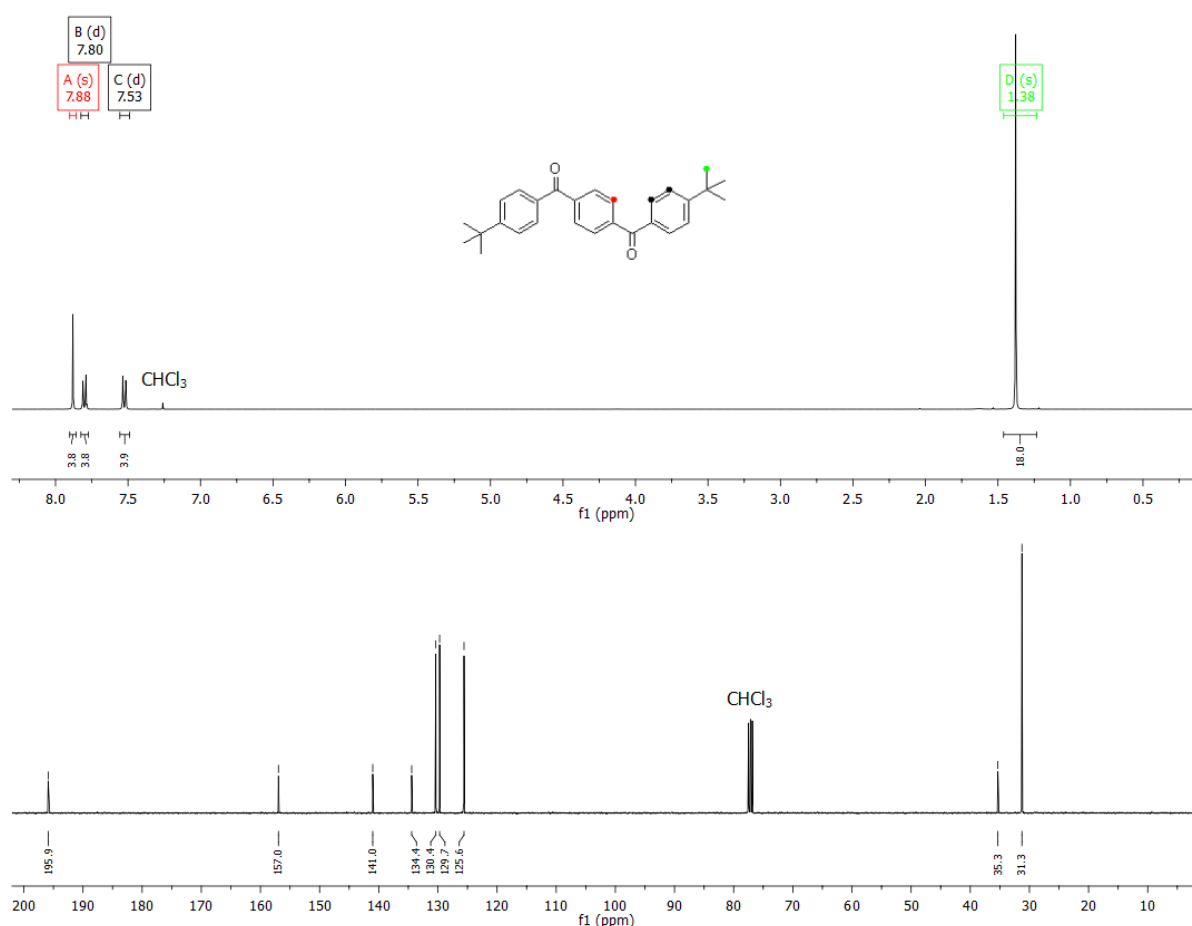


Figure 21 ^1H - and $^{13}\text{C}\{\text{H}\}$ -NMR spectra of PDK-DPtBu in CDCl_3 at room temperature.

The IR spectrum shows the weak carbon-hydrogen stretching vibrations of the aromatic groups at 3093, 3063, and 3039 cm^{-1} . The significantly stronger carbon-hydrogen stretching vibrations

of the aliphatic groups can be found at 2957, 2902, and 2867 cm^{-1} . The characteristic diarylketone signal is located at 1645 cm^{-1} , as displayed in Figure 22.

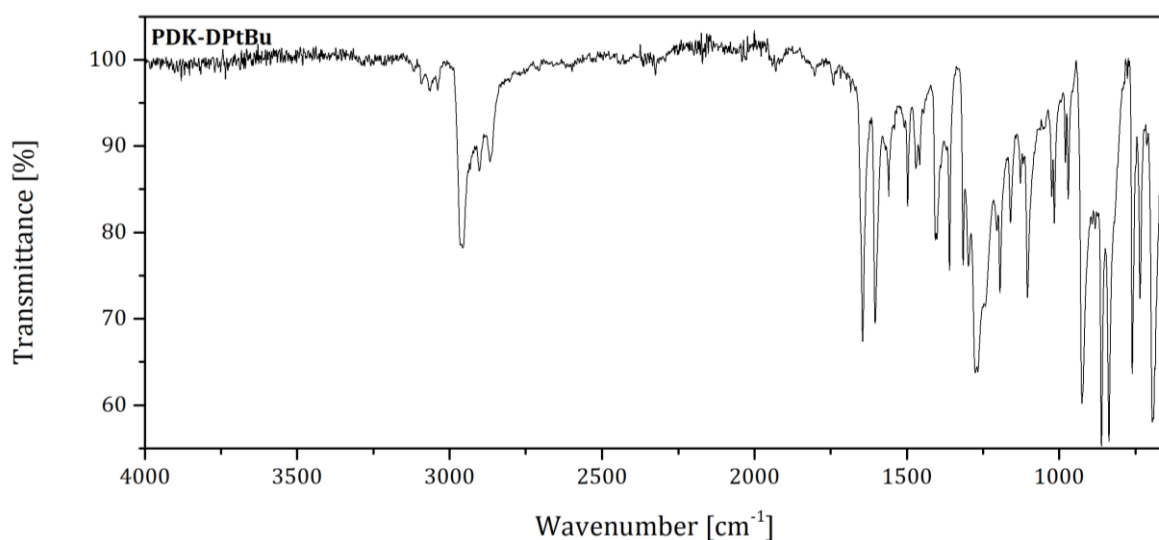


Figure 22 IR spectrum of **PDK-DPtBu**.

2.3.2 Synthesis of the poly(arylene vinylene)s

The poly(arylene vinylene)s were prepared from the diketone monomers in two steps, as shown in Figure 23 for the example of **PDK-DPtBu**.

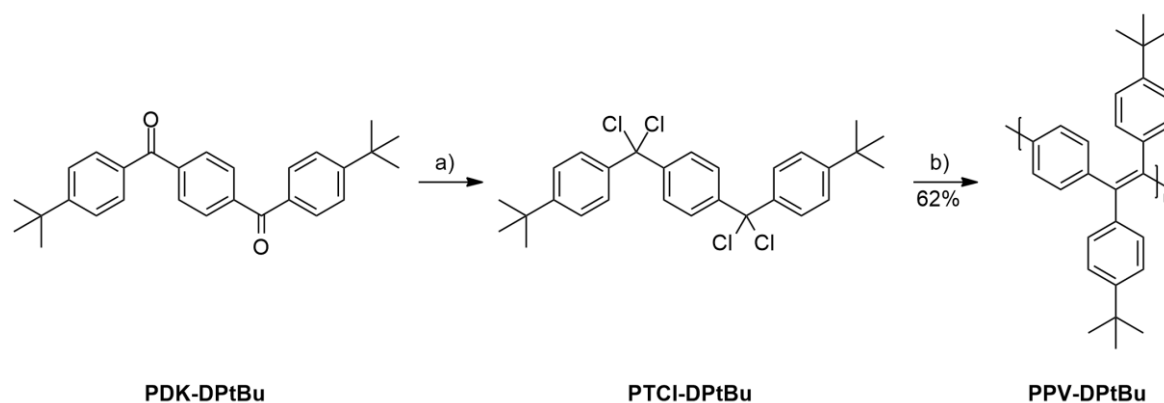


Figure 23 Synthesis of **PPV-DPtBu**: a) PCl_5 , PhCl , 120 $^\circ\text{C}$, 4 d; b) $\text{Co}_2(\text{CO})_8$, PhCl , 100 $^\circ\text{C}$, 50 min.

First the diketones were converted to geminal tetrachlorides using phosphorous pentachloride. Then the excess reagent, phosphorous oxychloride, and solvent were removed by vacuum distillation. Due to their high reactivity, the tetrachlorides were used in the next step without further purification. In a reductive polyolefination reaction, the monomers were coupled using dicobalt octacarbonyl, a method developed by Reisch *et al.*⁷³ in 1996 as a variation of the initial

procedure of Hörhold *et al.*⁶⁶, which uses chromium(II) acetate. The reagent was added to a stirred solution of the monomer in dry chlorobenzene under argon atmosphere. Then, the flask was inserted in a preheated oil bath at 100 °C and was left there for 50 minutes. Subsequently, excess reagent was disposed of by reaction with dichloroethane. The obtained polymers were precipitated into a 1:16 mixture of 2 M hydrochloric acid and methanol. The crude product was purified and fractionated by subsequent Soxhlet extraction with methanol, acetone, ethyl acetate, and chloroform. The higher molecular weight fractions were dissolved in a small amount of chloroform and reprecipitated into acidified methanol.

The here discussed choice of reagent for the polyolefination reaction was confirmed by comparison of yields and molecular weights of **PPV-DPtBu** synthesized with different reagents. Dicobalt octacarbonyl was chosen as established reagent in the Scherf group^{26,47,60,73}, chromium(II) acetate is the initial reagent used by Hörhold *et al.*⁶⁶, and vanadium(II) chloride was tested as a new, potentially interesting reagent based on the work of Slauch and Raley.⁷⁴ The results are summarized in Table 1. All methods yielded the desired product. Even though the reaction with chromium(II) acetate resulted in a higher molecular weight of the ethyl acetate fraction, the highest overall yields and molecular weights were obtained for the chloroform fraction when using the dicobalt octacarbonyl reagent. The vanadium(II) chloride-based reactions only yielded polymers with low molecular weights that equal a maximum of 16 repeating units compared to the 80 repeating units for the polymer obtained using dicobalt octacarbonyl. Based on these results, dicobalt octacarbonyl was chosen as the reducing reagent for the polyolefination reactions carried out in this work.

Table 1 Results of the reagent screening for the reductive polyolefination of **PTCl-DPtBu**.

Reagent	Ethyl acetate-fraction		Chloroform-fraction	
	Yield [%]	Molecular weights M _n /M _w [g/mol]	Yield [%]	Molecular weights M _n /M _w [g/mol]
Co₂(CO)₈	20	9900/38700	42	29300/164000
Cr₂(OAc)₄	8	18000/54400	6	22900/130000
VCl₂	<29*	5700/9400	<5*	4400/10400

* product contains impurities.

All obtained poly(arylene vinylene)s were characterized by ¹H- and ¹³C{H}-NMR spectroscopy and gel permeation chromatography (GPC). Measurements were, if possible, carried out with the chloroform fractions unless indicated otherwise. The yields, molecular weights, polydispersity indexes (PDI), and degrees of polymerization (DP) of the used fractions are summarized in

Table 2. The yields reach up to 69% for the high molecular weight fractions at overall yields of up to 89%. The lowest degrees of polymerization (DP) can be observed for the polymers with *meta*-phenylene main chain units **PmPV-DPtBu** and **PmPV-DN**, anthracene main chain units **PAV-DP**, or thiophene main chain units **PTV-DP** and **PTV-DPtBu**. In case of the thiophene-based polymers this is accompanied by a low overall yield. The most likely explanation for the poor results is an increased steric hinderance at the reaction centres caused by these building blocks due to the angled arrangement of the *meta*- or thiophene monomers. In case of the anthracene unit a steric hindrance, due to the outer rings, can be assumed. This is supported by the attempt to synthesize a poly(anthrylene vinylene) with *tert*-butylphenyl side chains at the vinylene unit that yielded no polymer under the given conditions. Another polymer with low degrees of polymerization is **PPV-DPC**, due to the insolubility of larger molecular weight fractions.

Table 2 Yields, molecular weights, polydispersity indexes (PDI), and degrees of polymerization (DP) of the poly(arylene vinylene)s.

Polymer	Fraction	Yield [%]	M _n [g/mol]	M _w [g/mol]	PDI	DP
PFV-DP	CHCl ₃	50	20600	63400	3.07	55
PBV-DP	CHCl ₃	18	14000	43200	3.08	42
PAV-DP	CHCl ₃	32	2600	4700	1.82	7
PTV-DP	CHCl ₃	2	2100	3000	1.47	7
PPV-DF	CHCl ₃	54	11400	18500	1.63	23
PPV-DN	CHCl ₃	69	11600	17800	1.54	33
PPV-DPDtBu	EA	47	12900	17800	1.38	27
PPV-DPtBu	CHCl ₃	42	29300	164000	5.62	80
PPV-DPtPent	EA	37	9900	16400	1.65	25
PPV-DBtBu	CHCl ₃	32	23100	72600	3.15	45
PPV-DPC	CHCl ₃	(67)*	5100	6100	1.20	9
PFV-DPtBu	CHCl ₃	45	15000	24200	1.61	31
PBV-DPtBu	CHCl ₃	12	26100	65700	2.51	59
PTV-DPtBu	CHCl ₃	13	6900	20300	2.93	19
PmPV-DPtBu	EA	43	7700	12800	1.67	21
PmPV-DN	CHCl ₃	65	5300	9400	1.77	15

*Contains unreacted monomeric impurities (see the discussion).

The synthesis of the carbazole polymer **PPV-DPC** faced certain challenges as the tetrachloride precursor was nearly insoluble, leading to a low conversion. Therefore, the solvent amounts were drastically increased in both reaction steps and the polyolefination was carried out in

dimethylformamide instead of chlorobenzene as solvent. In combination with a longer reaction time of four hours and an increased temperature of 160°C, the solid tetrachloride monomer visually disappeared in the reaction solution step by step. Still, the purified carbazole-polymer **PPV-DPC** showed the occurrence of some residual diketo monomer **PDK-DP**, as determined by GPC, IR, and NMR, that is formed by hydrolysis of the tetrachloride. Various attempts to accomplish a full separation by extraction, chromatography or dialysis failed due to the low and too similar solubilities of the monomer and polymer. Despite that, the polymer with trace amounts of the diketone monomer was used for an electrochemical cross-linking into polymer networks as discussed in Chapter 2.3.8.

The ^1H - and $^{13}\text{C}\{\text{H}\}$ -NMR spectra of **PPV-DPtBu** are displayed in Figure 24 exemplary for all poly(arylene vinylene)s.

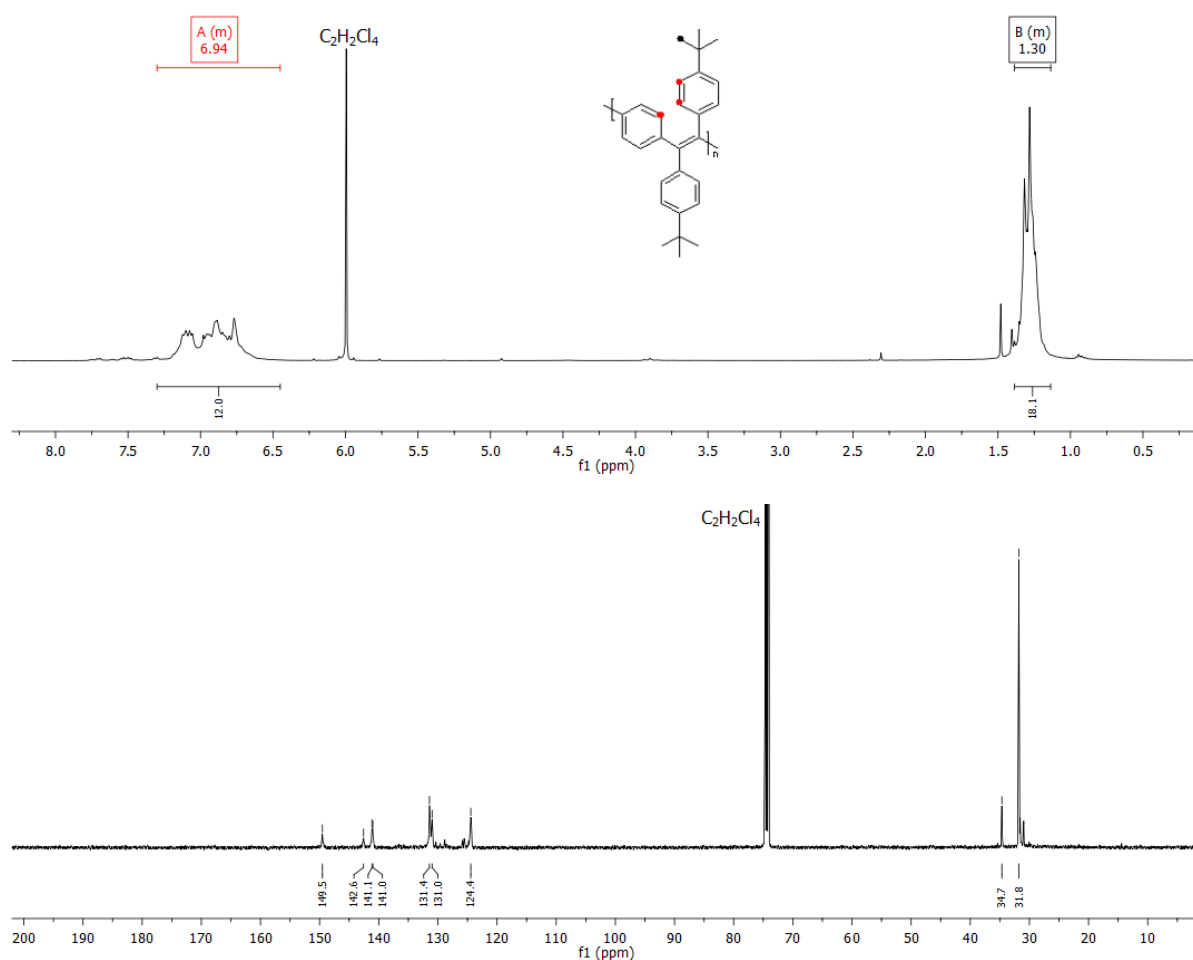


Figure 24 ^1H - and $^{13}\text{C}\{\text{H}\}$ -NMR spectra of **PPV-DPtBu** in $\text{C}_2\text{D}_2\text{Cl}_4$ at 353 K.

The polymer spectra show the expected broadening of the signals caused by the slightly different chemical environment of the repeat units. The broadening results in a weakening of the signal intensities. Therefore, the spectra were recorded at increased temperature of 353 K and for about 20 times the number of scans in comparison to the monomers. Still, the aromatic and aliphatic signals, in the most cases, merge to multiplets in the ^1H -NMR spectra. **PPV-DP_tBu** shows a multiplet from 7.30 ppm to 6.45 ppm (red) for the aromatic protons, and the aliphatic signals appear at 1.45 ppm to 1.07 ppm (black). The integrals show a proportion of 12 to 18, as expected. The *tert*-butyl group shows the characteristic $^{13}\text{C}\{\text{H}\}$ -NMR signals at 31.8 ppm and 34.7 ppm. The remaining seven aromatic and olefinic signals appear in the aromatic region of the spectrum, as expected. The ketone signal of the monomer **PDK-DP_tBu** has disappeared. A few low intensity $^{13}\text{C}\{\text{H}\}$ -NMR signals are assigned to end groups.

Furthermore, the thermal stability of **PPV-DP_tBu** was investigated by thermogravimetric analysis (TGA). The measurement was carried out under argon atmosphere in the temperature range from 35 °C to 950 °C with a heating rate of 10 °C/min. **PPV-DP_tBu** shows a good thermal stability with a weight loss of 5% at 340 °C. Possible phase transitions of the polymer were investigated by differential scanning calorimetry (DSC) in the temperature range from 25 °C to 200 °C, in an argon atmosphere with a heating rate of 10 °C/min. In this temperature range neither glass transition- nor crystallization/melting-related signals were observed.

2.3.3 Variation of the main chain structure

The polymers with different main chain units **PFV-DP**, **PBV-DP**, **PAV-DP**, and **PTV-DP**, all with phenyl side chains, were compared regarding their S_{BET} surface area and optical properties in solution and as thin films. **PPV-DP** and **PmPV-DP** shall be discussed whenever it adds to the discussion. Figure 25 displays the normalized absorption and emission spectra of **PFV-DP**, **PBV-DP**, **PAV-DP**, and **PTV-DP** in tetrahydrofuran solution. The UV-cutoff of the solvent tetrahydrofuran is at circa 212 nm, therefore the lower wavelength absorption maxima of the poly(arylene vinylene)s in this work are out of the measuring range.⁷⁵ Normally two or three maxima or shoulders at higher wavelengths can be observed. For the pure hydrocarbon polymers, the highest wavelength maximum or shoulder represents the π - π^* transitions of the conjugated systems. The thiophene-containing polymers show a similar trend with a significant red-shift of the highest absorption maximum, that can be attributed to the additionally occurring n - π^* transition of the free electrons of the thiophene sulphur. For a better overview, all

absorption and photoluminescence emission (PL) maxima of **PFV-DP**, **PBV-DP**, **PAV-DP**, and **PTV-DP** are summarized in Table 3, together with the corresponding Stokes shifts.

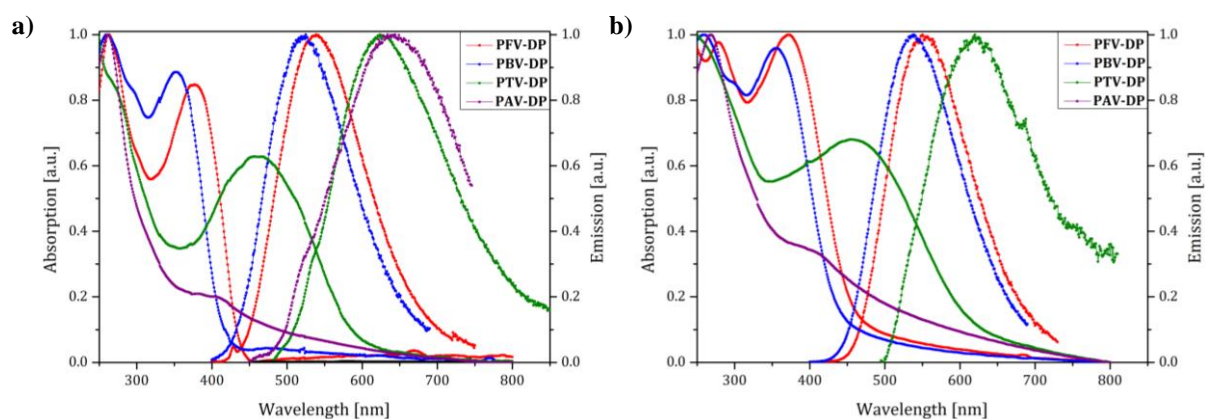


Figure 25 Normalized absorption and emission spectra of **PFV-DP**, **PBV-DP**, **PAV-DP**, and **PTV-DP**; a) in tetrahydrofuran solution, and b) as thin films.

The absorption spectra of **PFV-DP** and **PBV-DP** are very similar with slight shifts of the maxima. The highest wavelengths absorption maximum of **PFV-DP** at 377 nm shows a red-shift if compared to the 353 nm of **PBV-DP**. This bathochromic shift might be attributed to an increased effective conjugation length in the **PFV-DP** polymer. The partial planarization of the polymer backbone in the fluorene unit should result in a better overlap of the p_z -orbitals. This theory is also supported by the higher solution-state quantum yield of **PFV-DP** of 4.3% compared to the 0.5% for the biphenyl polymer, as listed in Table 4. This proves viable as it has been observed for other (partially) planarized polymers that less non-radiative pathways are available in solution.^{76,77} The anthracene polymer **PAV-DP** shows the long wavelengths absorption band at 400 nm as shoulder, likely due to the presence of the anthracene chromophore. This observation is in good agreement with results of 9,10-anthrylene containing PPVs by Yu *et al.*⁷⁸ and oligo(9,10-anthrylene)s by Müllen and co-workers.⁷⁹ The low intensity of the very broad long wavelength absorption band indicates a pronounced distortion of the electronically interacting units caused by steric hindrance.

PFV-DP and **PBV-DP** emit in the green region of the visible light range with solution-state PL maxima at 537 nm and 521 nm respectively. **PBV-DP** again shows the blue-shift that has been observed in the absorption spectra. **PTV-DP** and **PAV-DP** in contrast show bathochromically shifted orange emissions with maxima at 625 nm and 637 nm respectively.

Table 3 Absorption and emission maxima along with the Stoke shifts (Δ_{ss}) of polymers **PFV-DP**, **PBV-DP**, **PAV-DP**, and **PTV-DP** of thin films and THF solutions.

Polymer	Medium	λ^{abs} [nm]	λ^{em} [nm]	Δ_{ss} [cm ⁻¹]
PFV-DP	THF	264, 272 sh 377	537	7903
	Film	278 372	550	8700
PBV-DP	THF	261, 291 sh 353	521	9135
	Film	259, 296 sh, 355	537	9547
PAV-DP	THF	262, 400 sh	637	9301
	Film	268, 393 sh	N/A	N/A
PTV-DP	THF	262 sh, 460	625	5739
	Film	257 sh, 456	620	5801

In the solid state the absorption spectra show a similar trend as in solution state but with slightly shifted maxima. The long wavelength absorption maxima of **PFV-DP** and **PTV-DP** are slightly red-shifted and of **PBV-DP** and **PAV-DP** slightly blue-shifted, but without major changes. The very weak absorption shoulder of **PFV-DP** at previously 272 nm can no longer be observed.

The emission spectra in solid state show a red-shift of the maxima of 13 nm and 16 nm for **PFV-DP** and **PBV-DP**, respectively, compared to the solution emission maxima, while the maximum of **PTV-DP** blue shifts 5 nm. The observed red-shifts cause the Stokes shifts in thin film to be generally higher than in the solution state. The Stokes shifts of the **PTV-DP** spectra in both states are significantly lower than those of the other two polymers due to the red-shift of the absorption and emission spectra. The solid state emission of **PAV-DP** is completely quenched. This is most likely caused by π - π stacking of the rigid anthracene units.^{80,81}

Based on the photoluminescence quantum yields (PLQYs) of solutions and solid state polymers, it can be easily seen that the three polymers **PFV-DP**, **PBV-DP**, and **PTV-DP** show an increase in PLQYs in thin films and, therefore, an AIE effect or, in case of **PFV-DP**, rather an aggregation-enhanced emission (AEE) effect. This is in good agreement to the behaviour observed for the literature known polymers **PPV-DP** and **PmPV-DP**. The high PLQYs of **PBV-DP** and **PFV-DP** of 26% and 43%, respectively, are comparable to the 37% and 32% of **PPV-DP** and **PmPV-DP** in solid state. **PTV-DP** in contrast shows a very weak PLQY below 1% even in solid state. This might be connected to the tendency of thiophenes to deactivate their singlet excited states by intersystem crossing to the triplet manifold or by internal

conversion.⁸²⁻⁸⁴ The emission of **PAV-DP** in both states is below the detection limit of the spectrometer, probably due to π - π stacking interaction as discussed beforehand.

The PLQY of **PBV-DP** has previously been reported in the range from 29% to 53% depending on the *cis:trans* ratio.⁸⁵ Feast *et al.*⁸⁵ describe a decrease in PLQY efficiency of **PBV-DP** when the ratio of *cis/trans*-configured vinylene double bonds alters from 50:50. This might mean that the synthetic route of **PBV-DP** in this work favours either *cis*- or *trans*-configuration of the vinylene units. Another common reason for deviations in solid state quantum yields is connected to the morphology of the films that has a major influence on the PLQY. This has not been further investigated and it might be interesting for a future work to determine the *cis:trans* ratio of the reported polymers.

Table 4 Room temperature fluorescence quantum yields of **PFV-DP**, **PBV-DP**, **PAV-DP**, and **PTV-DP** in different media.

Polymer	PLQY (THF)	PLQY (Film)
PPV-DP ²⁶	0.008	0.37
PmPV-DP ²⁶	0.013	0.32
PFV-DP	0.043	0.43
PBV-DP	0.005	0.26
PAV-DP	N/A	N/A
PTV-DP	N/A	0.006

The specific surface areas of the polymers were determined using the Brunauer, Emmett, and Teller (BET) model.⁸⁶ The theory rationalizes the physisorption of a system in case of a multi-layer adsorption as the so called BET isotherm.⁸⁶ The isotherm in its linearized form is given in Equation 1.

$$\frac{p}{v(p_0 - p)} = \frac{1}{v_m c} + \frac{c - 1}{v_m c} \cdot \frac{p}{p_0} \quad (1)$$

where p is the pressure, p_0 is the saturation pressure of the gas, v is the total volume of gas adsorbed, v_m is the volume of gas adsorbed when the entire adsorbent surface is covered with a complete unimolecular layer, and c is a constant.⁸⁶

This equation allows the determination of v_m and c from experimental isotherms that are obtained by volumetric method.⁸⁷ The obtained isotherms can be grouped into six types by their

shapes and furthermore by the four types of hysteresis loops as shown in Figure 26.⁸⁷ The *Type I* isotherm is given by microporous solids with rather small external surfaces. The reversible *Type II* isotherm is typical for macroporous or non-porous materials. *Type IV* isotherms characteristically display a hysteresis loop that is caused by capillary condensation in mesopores. The shape of the loops can be linked to the shape of the pores.⁸⁷ The very rare *Type III* and *Type V* isotherms are adsorbate-adsorbent interaction dependent. The *Type VI* isotherm can be observed for uniform non-porous surfaces.

Type H1 hysteresis loops can be attributed to porous materials consisting of agglomerates or approximately uniform spheres creating regular arranged pores with small size distribution. *Type H2* loops arise from pore-sizes and shapes that are not well-defined. *Type H3* hysteresis loops occur in measurements of samples with plate-like particles and *Type H4* loops in samples with slit-shaped pores.⁸⁷

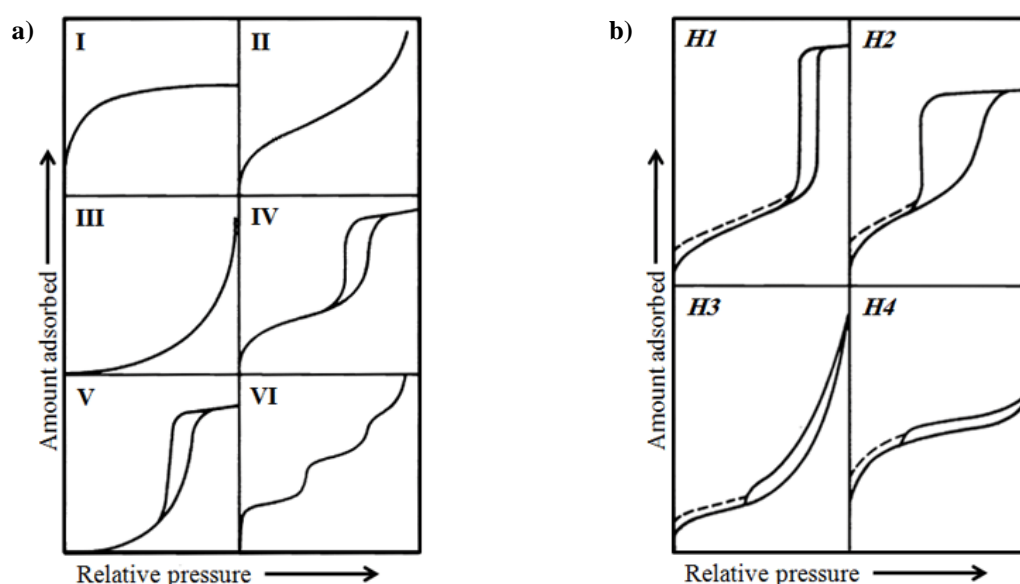


Figure 26 a) Types of physisorption isotherms. B) Types of hysteresis loops.⁸⁷

The surface areas of the polymers were determined for freshly prepared powders. Since rapidly precipitated polymers generally exhibit larger surface areas than slowly precipitated materials,⁵⁹ the polymer samples were dissolved with the minimal amount of chloroform and precipitated by dropwise addition into a cold mixture of methanol and a small amount of 2 M hydrochloric acid. The polymers were then filtered off, dried for one day, and subsequently degassed offline at $>100^{\circ}\text{C}$ for 16 hours. The BET surface areas (S_{BET}) of the polymers are summarized in Table

5. The obtained values are less reliable for lower surface areas, therefore the results are given in brackets and the corresponding polymers can be regarded as non-porous.

Additionally to the discussed polymers, a freshly precipitated sample of polymer **PPOPV-DP**, shown in Figure 27 and described by Baysec *et al.*²⁶, was measured.

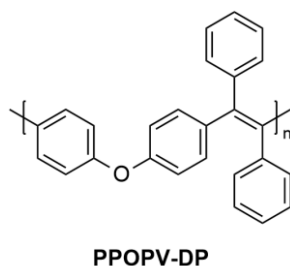


Figure 27 Structure of **PPOPV-DP**.²⁶

The surface areas of **PFV-DP**, **PPOPV-DP**, and **PAV-DP** were lower than the detection limit of the instrument. For the other polymers rather low values between 1 m²g⁻¹ and 72 m²g⁻¹ were obtained, with the highest surface area for **PBV-DP**.

Table 5 BET surface areas (S_{BET}) of the poly(arylene vinylene)s with phenyl side chains.

Polymer	PPV-DP	PmPV-DP	PFV-DP	PBV-DP	PAV-DP	PTV-DP	PPOPV-DP
S_{BET} [m ² g ⁻¹]	(41)	(29)	N/A	72	N/A	(1)	NA

All four polymers show a *Type II* shaped isotherm, indicating macroporosity, but none of the isotherms is completely reversible. Exemplary, the isotherms of **PmPV-DP** and **PBV-DP** are displayed in Figure 28. A very slight *Type H3* hysteresis, that increases with the surface area (comparison Figure 28 a) and b)), is visible in all graphs. The loops stretch over the whole p/p₀ range and do not fully close at zero pressure, a well-known behaviour for amorphous, microporous polymers.⁸⁸ One possible explanation for this observation is a swelling effect of the polymer sample.⁸⁷ Another explanation is the irregular pore topology in combination with a flexible structure leading to diffusion problems. The occurring pores can either be characterized as open or restricted access pores. The narrow entrances of the restricted access pores can only be passed under increased solvation pressure. At low relative pressures the polymer adapts a more compact conformation that blocks the restricted access pores.⁸⁸

This theory is supported by the non-uniform pore size distribution of **PBV-DP**. The distribution was calculated from the adsorption/desorption isotherms using a non-local density functional theory for slit shaped pores and is displayed in Figure 29.

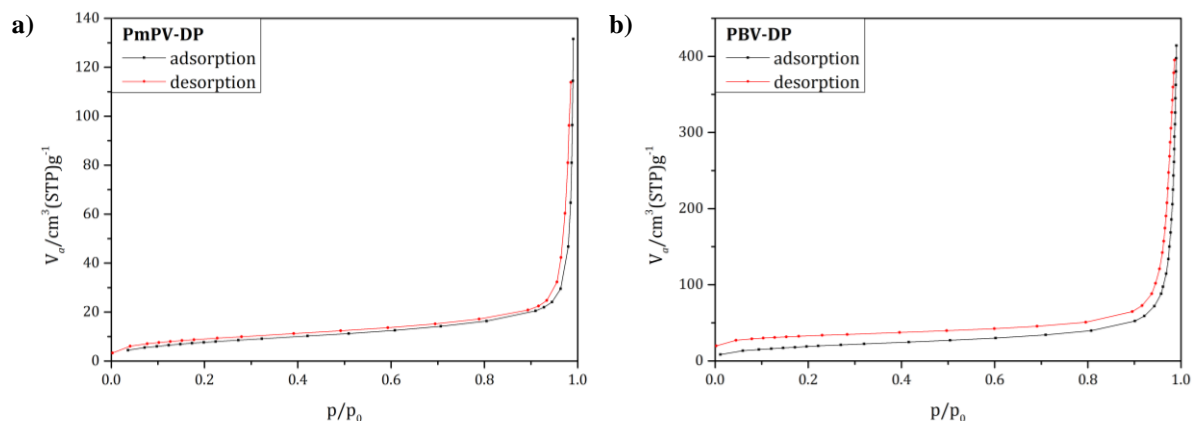


Figure 28 BET adsorption and desorption isotherms of a) **PmPV-DP** and b) **PBV-DP**.

Many peaks for the calculated pore diameters can be observed. The first peak shows the presence of the desired micropores at a diameter of circa 1.5 nm. A micropore is defined by a pore width not exceeding 2 nm.⁸⁷ The last peak represents pores larger than 92 nm. These macropores are cavities formed between the polymer chains and explain the pseudo-*Type II* isotherms of the polymers. In-between these peaks a multitude of different sized diameters in the mesopore region can be observed. The surface areas show that a pure exchange of the main chain building blocks does not suffice to obtain polymers with high intrinsic porosity. Therefore, it was investigated whether a bulkier side chain can create the desired free volume.

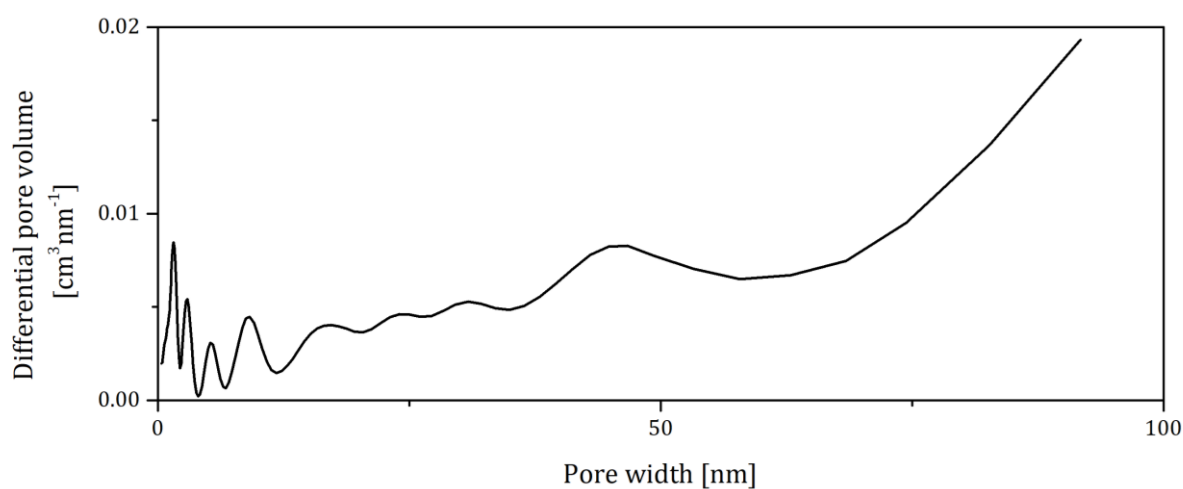


Figure 29 Pore size distribution of **PBV-DP**.

2.3.4 Variation of the side chain structure

The normalized absorption and emission spectra of **PPV-DF**, **PPV-DN**, **PPV-DP_tBu**, **PPV-DP_DtBu**, **PPV-DP_tPent**, and **PPV-DB_tBu** in tetrahydrofuran solution and as thin films are displayed in Figure 30. A detailed characterization and discussion of **PPV-DN** and **PPV-DP_tBu** will be given in Chapter 2.3.6.

The absorption spectra show the same trend as described beforehand with each polymer displaying several maxima and shoulders. All maxima are summarized in Table 6. The highest wavelength absorption maxima in solution range from 343 nm for **PPV-DN** to 391 nm for **PPV-DF**. The absorption is accompanied by PL emissions at comparatively high emission wavelengths, as example at 569 nm for **PPV-DF**. This can be attributed to the distorted, non-planar structure leading to large Stokes shifts. Upon going to the solid state the longest wavelength maxima of all polymers are slightly bathochromically shifted in comparison to the solution spectra. Two exceptions are the spectra of **PPV-DF**, which undergoes a weak hypsochromic shift, and **PPV-DB_tBu**, with the absorption remaining unchanged. The bathochromic shifts can be attributed to a slightly extended conjugation of the polymers in solid state.

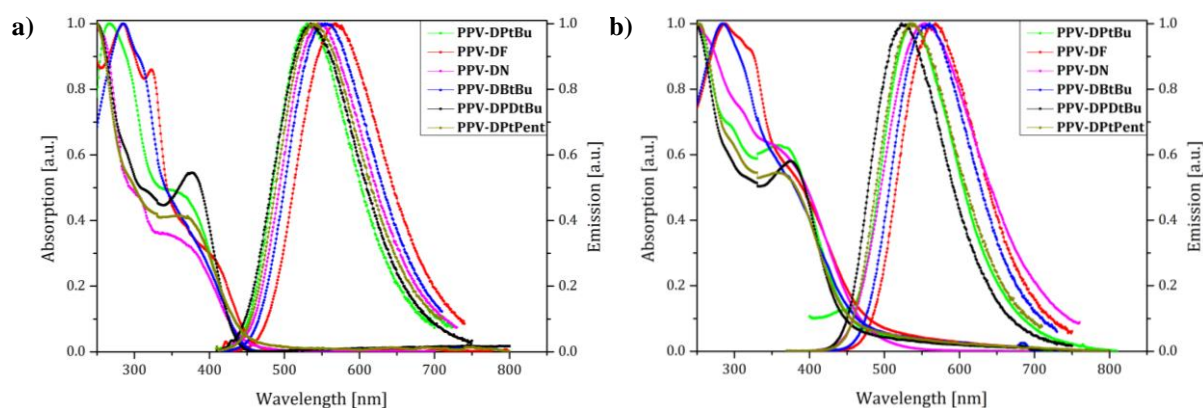


Figure 30 Normalized absorption and emission spectra of **PPV-DF**, **PPV-DN**, **PPV-DP_tBu**, **PPV-DB_tBu**, **PPV-DP_DtBu**, and **PPV-DP_tPent** in a) tetrahydrofuran solution and b) as thin films.

All polymers emit green light under UV illumination. The solution-state emission maxima vary from 530 nm to 569 nm for **PPV-DP_tBu** and **PPV-DF**, respectively, with no major differences of the peak values as expected. In solid state, the emission maxima of **PPV-DF**, **PPV-DP_DtBu**, and **PPV-DP_tPent** are slightly blue-shifted, whereas the maxima of **PPV-DN**, **PPV-DP_tBu**, and **PPV-DB_tBu** are red-shifted. The Stokes shift of **PPV-DF** and **PPV-DB_tBu** are slightly higher in the solid state than in solution, as described in the previous chapter. For the other four polymers the opposite trend is observed, likely due to an increased distortion of the interacting repeat units in the solid state, if compared to **PPV-DF** and **PPV-DB_tBu**.

Table 6 Absorption and emission maxima along with the Stoke shifts (Δ_{ss}) of polymers **PPV-DF**, **PPV-DN**, **PPV-DPtBu**, **PPV-DBtBu**, **PPV-DPDtBu**, and **PPV-DPtPent** of thin films and THF solutions.

Polymer	Medium	λ^{abs} [nm]	λ^{em} [nm]	Δ_{ss} [cm ⁻¹]
PPV-DF	THF	285, 322, 391 sh	569	8001
	Film	287, 319 sh, 375 sh	565	8968
PPV-DN^a	THF	222, 258 sh, 307 sh, 343 sh	545	10806
	Film	222, 258 sh, 307 sh, 351	553	10407
PPV-DPtBu^a	THF	267, 350	530	9704
	Film	252, 292 sh, 355	537	9547
PPV-DPDtBu	THF	249, 376	536	7939
	Film	244 sh, 375	525	7619
PPV-DPtPent	THF	242, 359 sh	539	9302
	Film	253, 292 sh, 362	537	9002
PPV-DBtBu	THF	285, 305 sh, 365 sh	554	9347
	Film	285, 307 sh, 365	557	9444

^a Experimental data from chapter 2.3.6 (measured at the University of Coimbra, Portugal).

The PLQYs of the polymers in solution and solid state are summarized in Table 7. An AIE or AEE effect can be observed for all polymers excluding **PPV-DN**. The naphthyl-substituted polymer shows an ACQ effect, similar to the anthracene polymer **PAV-DP**, of the previous chapter, probably due to π - π stacking of the naphthyl side chains, as discussed in Chapter 2.3.6. To circumvent such π - π stackings, sp³-hybridized alkyl chains were incorporated into the vinylene substituents. For **PPV-DPtBu** two differing quantum yields are given because the values measured here, as described in Chapter 4.1, did not match the previously published values of other samples of the same polymer, as described in Chapter 4.1.1. **PPV-DF** and **PPV-DPDtBu** show an already high quantum yield in solution state with an only moderate increase in intensity upon film formation. This can be explained by the sterically demanding dimethylfluorene and bis(*tert*-butyl)phenylene side chains that hinder a free rotation of the side chains already in solution. A comparison of **PPV-DPtBu** and **PPV-DPtPent** in thin films shows that an elongation of the alkyl residue (*tert*-butyl \rightarrow *tert*-pentyl) decreases the fluorescence intensity. This might be caused by a looser packing of the polymer in solid state that allows more rotations of the aryl substituents in the polymer. Furthermore, the surface area of **PPV-DPtPent** is significantly lower than that of **PPV-DPtBu**, as listed in Table 8. Therefore, the longer, more flexible

side chains probably block occurring pores. **PPV-DBtBu** shows an AEE effect with the highest solid state PLQY of 36% for all here investigated variations of side chains.

Table 7 Room temperature fluorescence quantum yields of **PPV-DF**, **PPV-DN**, **PPV-DPtBu**, **PPV-DBtBu**, **PPV-DPDtBu**, and **PPV-DPtPent** in different media.

Polymer	PLQY (THF)	PLQY (Film)
PPV-DF	0.13	0.26
PPV-DN^a	0.028	0.010
PPV-DPtBu	0.001 (0.046 ^a)	0.32 (0.64 ^a)
PPV-DPDtBu	0.18	0.27
PPV-DPtPent	0.004	0.13
PPV-DBtBu	0.074	0.36

^a Experimental values from chapter 4.1.1 (measured at the University of Coimbra, Portugal).

The S_{BET} surface areas of the polymers are summarized in Table 8. The results were compared to the surface areas of the polymers **PPV-DPOP** and **PPV-DPSP**, the structure of the latter is shown in Figure 31. For the structure of **PPV-DPOP** see page 5.

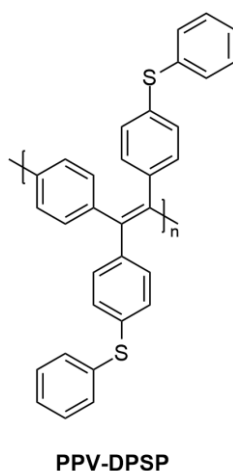


Figure 31 Structure of **PPV-DPSP**.²⁶

Only **PPV-DPtBu** shows a high S_{BET} surface area of $417 \text{ m}^2\text{g}^{-1}$, the other polymers exhibit low surface areas of $3\text{-}18 \text{ m}^2\text{g}^{-1}$. This shows that an elongation of the alkyl residue as well as an introduction of a second *tert*-butyl group at the phenyl side groups reduces the surface area. The same behaviour was observed when the phenyl side chain was elongated to a biphenyl side chain. The additional groups seem to fill the available pore space rather than creating new space. When diphenyl sulfide- **PPV-DPSP** or diphenyl ether-substituted polymers **PPV-DPOP** and **PPOP-DP** are included in the comparison, it can be assumed, that the low S_{BET} surface areas

also for these polymers are caused by the conformational flexibility of the corresponding diaryl sulfide and diaryl ether side chains.

Table 8 BET surface areas (S_{BET}) of the poly(phenylene vinylene)s with different side chains.

Polymer	PPV-DF	PPV-DN	PPV-DPtBu	PPV-DBtBu	PPV-DPDtBu	PPV-DPtPent	PPV-DPOP	PPV-DPSP
S_{BET} [m^2g^{-1}]	(3)	(14)	417	(7)	(7)	(3)	(18)	NA

The adsorption/desorption isotherms of **PPV-DPtBu** in Figure 32a are *Type IV*-shaped with a hysteresis loop stretching over the whole pressure range. The explanation for that is the same as for the previous polymers that exhibit a non-uniform pore size distribution and flexible polymer chains. When regarding the pore size distribution in Figure 33, it can be seen that the main peak is at 1.2 nm, followed by mesopore-related peaks of different size but almost no macropores. Therefore **PPV-DPtBu** displays a so-called conjugated polymer of intrinsic microporosity (C-PIM) and the occurring mesopores explain the pseudo-*Type IV* shape of the isotherm.

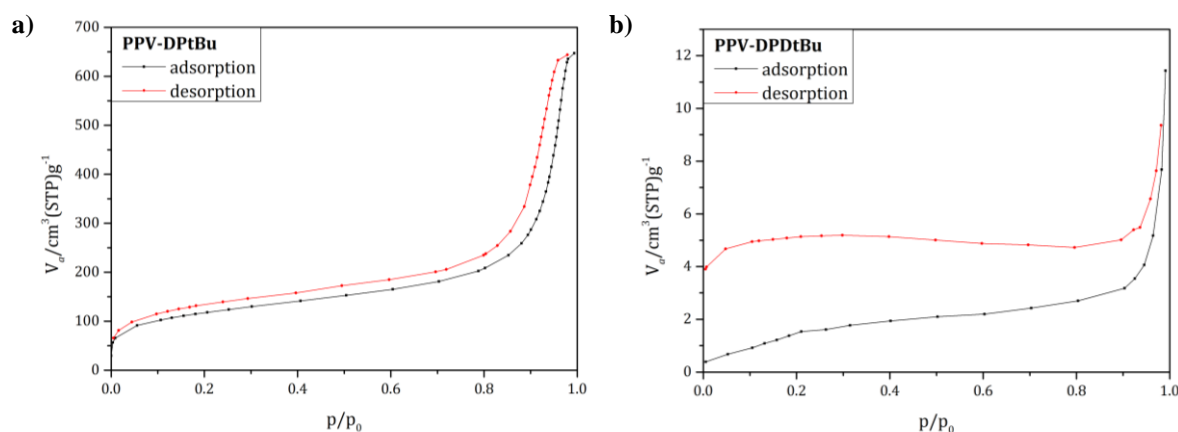


Figure 32 Adsorption/desorption isotherms of a) **PPV-DPtBu** and b) **PPV-DPDtBu**.

The isotherms of the polymers with lower surface area belong to the previously described pseudo-*Type II*. **PPV-DN** is the only polymer whose isotherms show no hysteresis loops, indicating a rigid arrangement of the polymer in the solid state that could be promoted by the occurring π - π interactions. **PPV-DPDtBu** on the other hand shows a particular large hysteresis as shown in Figure 32b.

Based on the microporosity of **PPV-DPtBu**, in the next step *tert*-butylphenyl side chains were combined with the previously tested, different backbone structures. The goal was to extract the

best combination, and to confirm whether the biphenyl-based main chains still give the highest S_{BET} surface areas, also with different side chains.

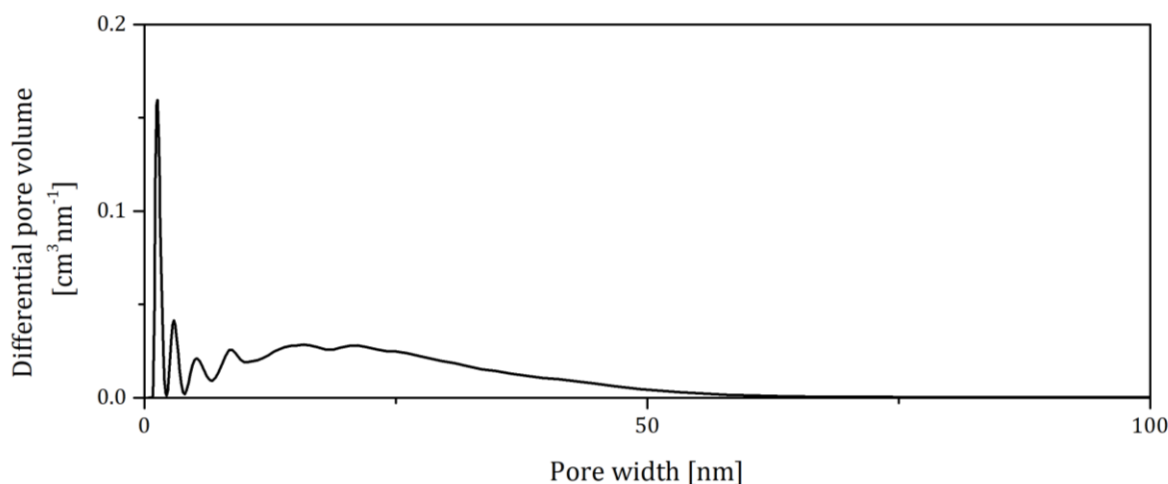


Figure 33 Pore size distribution of **PPV-DPtBu**.

2.3.5 Combinations of different side and main chains

The absorption and emission spectra of **PFV-DPtBu**, **PBV-DPtBu**, **PTV-DPtBu**, **PmPV-DPtBu**, and **PmPV-DN** in solution and solid state are depicted in Figure 34. The spectra of **PmPV-DN** will be discussed in detail in Chapter 2.3.6. This polymer was supplemented to confirm if the stacking tendency of the side chain prevails when the main chain is altered.

The absorption spectra show a similar trend as the poly(arylene vinylene)s of the previous chapters. As previously observed for **PTV-DP**, the absorption and emission spectra of **PTV-DPtBu** are red-shifted in comparison to the “pure hydrocarbon” polymers, with the exception of **PmPV-DN** in the solid state. The bathochromic shift of the maximum of **PmPV-DN** may be explained by the aggregation of the side chains, as discussed later on, and is accompanied by a strong red-shift of the emission maximum. When the absorption spectra of **PFV-DPtBu**, **PBV-DPtBu**, and **PTV-DPtBu** are directly compared to their analogues without *tert*-butyl groups, most of the maxima are found at comparable wavelengths, with exception of the highest wavelength shoulder of **PTV-DPtBu** that is blue-shifted by 50 nm and 52 nm in solution and solid state respectively. A possible explanation for this could be that the increased steric demand of the introduced *tert*-butyl group is not compatible with a planar arrangement of the polymer chain, leading to an increased distortion of the polymer, and therefore shorter effective conjugation lengths. When the solution-state absorption spectra are compared to the solid-state

spectra, the long wavelength maxima of **PFV-DPtBu**, **PmPV-DPtBu**, and **PTV-DPtBu** are slightly blue-shifted, whereas **PmPV-DN** and **PBV-DPtBu** are shifted bathochromically.

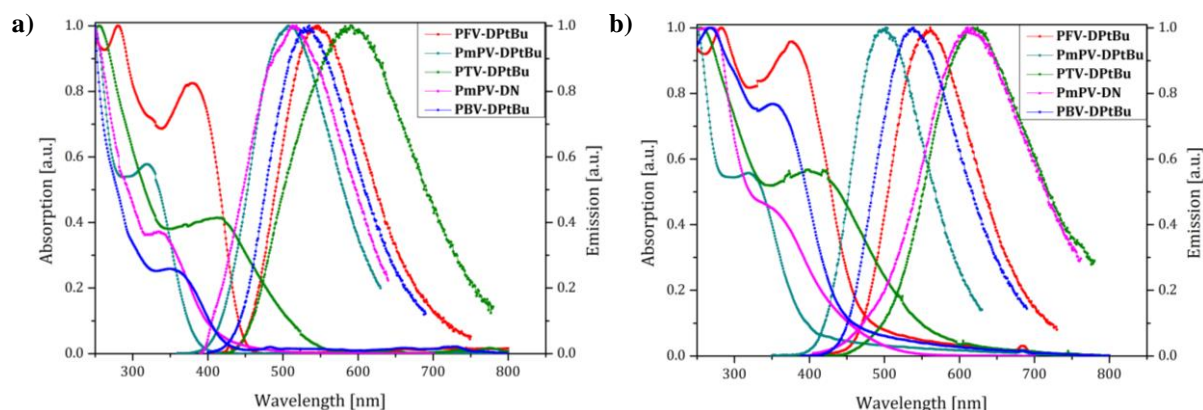


Figure 34 Normalized absorption and emission spectra of **PFV-DPtBu**, **PBV-DPtBu**, **PTV-DPtBu**, **PmPV-DPtBu**, and **PmPV-DN** in a) tetrahydrofuran solution, and b) as thin films.

The emission spectra are likewise similar to the spectra of the phenyl-substituted polymers with the same main-chain structure. Most of the polymers emit green light under UV-illumination, only **PTV-DPtBu** emits orange light, as does **PmPV-DN** in solid state. Here **PTV-DPtBu** once again shows the greatest difference in comparison to **PTV-DP** in the solution-state emission spectrum. The emission is shifted hypsochromically, by 37 nm. However, in solid state the emission appears almost at the same wavelength as that of **PTV-DP**. When solution and solid state emissions are compared all polymers except **PmPV-DPtBu** show a bathochromic shift of the peak positions in the solid state accompanied by an increased Stokes shift. **PmPV-DPtBu** shows a blue-shifted emission peak as well as a lower Stokes shift.

Table 9 Absorption and emission maxima along with the Stoke shifts (Δ_{ss}) of polymers **PFV-DPtBu**, **PBV-DPtBu**, **PTV-DPtBu**, **PmPV-DPtBu**, and **PmPV-DN** of thin films and THF solutions.

Polymer	Medium	λ^{abs} [nm]	λ^{em} [nm]	Δ_{ss} [cm ⁻¹]
PFV-DPtBu	THF	280, 380	545	7967
	Film	282, 379	559	8496
PBV-DPtBu	THF	270 sh, 349	532	9856
	Film	268, 351	538	9903
PTV-DPtBu	THF	256, 410	588	7383
	Film	254, 404	619	8597
PmPV-DPtBu	THF	248, 319	507	11624
	Film	246, 317	498	11465
PmPV-DN^a	THF	221, 335	518	10546
	Film	268, 348	611	12369

^a Experimental data from chapter 2.3.6 (measured at the University of Coimbra, Portugal).

The PLQYs of the five polymers are summarized in Table 10. The quantum yields of **PTV-DPtBu** in solution as well as in solid state lie below the detection limit of the spectrometer. **PmPV-DN** shows a solid state PL quenching effect as previously observed for **PPV-DN**. The other three polymers show an AEE effect. The solid state quantum yields of the *tert*-butylphenyl polymers are generally lower than their phenyl counterparts with the same main chain structure. With the exception of **PPV-DPtBu** having the highest PLQY of the *tert*-butylphenyl polymers, the quantum yields decrease in the same order from the fluorene main chain to the thiophene main chain as observed for the polymers from Chapter 2.3.3.

Table 10 Room temperature fluorescence quantum yields of **PFV-DPtBu**, **PBV-DPtBu**, **PTV-DPtBu**, **PmPV-DPtBu** and **PmPV-DN** in different media.

Polymer	PLQY (THF)	PLQY (Film)
PFV-DPtBu	0.048	0.21
PBV-DPtBu	0.038	0.11
PTV-DPtBu	N/A	N/A
PmPV-DPtBu	0.036	0.13
PmPV-DN^a	0.008	0.002

^a Experimental values from chapter 2.3.6 (measured at the University of Coimbra, Portugal).

The S_{BET} surface areas of the five polymers are summarized in Table 11. It is apparent that the S_{BET} values of the different main chains either combined with phenyl (Table 5) or *tert*-butyl phenylene side chains do not follow the same trend. **PFV-DPtBu** shows a high surface area of $351 \text{ m}^2\text{g}^{-1}$. The surface area of **PBV-DPtBu** is significantly lower with a value of $85 \text{ m}^2\text{g}^{-1}$, but still increased in comparison to the thiophene polymer **PTV-DPtBu** and the *meta*-phenylene polymers **PmPV-DPtBu** and **PmPV-DN**. These last three polymers all have an angular arrangement of the bonds in the polymer backbone in common, while **PFV-DPtBu**, **PBV-DPtBu**, and **PPV-DPtBu** consist of more linear backbones. Therefore, it can be assumed that the angular monomeric units promote a non-porous conformation of the polymer chain in this kind of PAVs. In contrast to this, Cooper and co-workers reported that angular polymer backbones containing *meta*-connected phenylene linkers lead to high surface areas.^{59,64} A possible explanation could be the specific location of the side chains in the PAVs, obstructing the generation of additional free volume.

Table 11 BET surface areas (S_{BET}) of the poly(arylene vinylene)s with different side chains.

Polymer	PFV-DPtBu	PBV-DPtBu	PTV-DPtBu	PmPV-DPtBu	PmPV-DN
S_{BET} [m^2g^{-1}]	351	85	(34)	(1)	(17)

The BET isotherms again show a pseudo-*Type II* curvature with an increasing hysteresis loop for higher surface areas that is particularly strong for **PFV-DPtBu** as displayed in Figure 35.

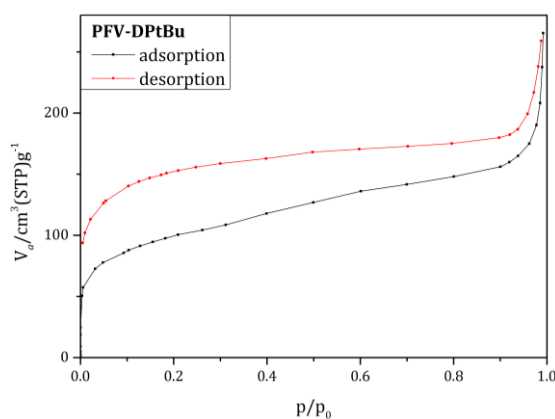


Figure 35 BET adsorption and desorption isotherms of **PFV-DPtBu**.

The pore size distributions of **PFV-DPtBu** and **PBV-DPtBu** were calculated and displayed in Figure 36. The distribution in **PBV-DPtBu** looks similar to that of **PBV-DP**, as described before, with a large micropore-related peak at 1.5 nm followed by meso- and macropore-related peaks. **PFV-DPtBu** on the other hand contains mainly smaller pores. The main peak located at 1.3 nm, as well as an intense neighbouring peak at 0.7 nm can be classified as micropores, while the third prominent peak at 3.0 nm has to be classified as mesopores. Apart from these three major maxima, only weak maxima can be observed for larger meso- or macropores. Therefore, **PFV-DPtBu** provides another AIE-active, microporous polymer. Still neither solid state PL quantum yields nor S_{BET} surface areas can compete with these of **PPV-DPtBu**.

In summary, this study for different side and main chain combinations showed that **PPV-DPtBu** is overall the most promising candidate as AIE-active, microporous polymer, and also for explosives detection studies.

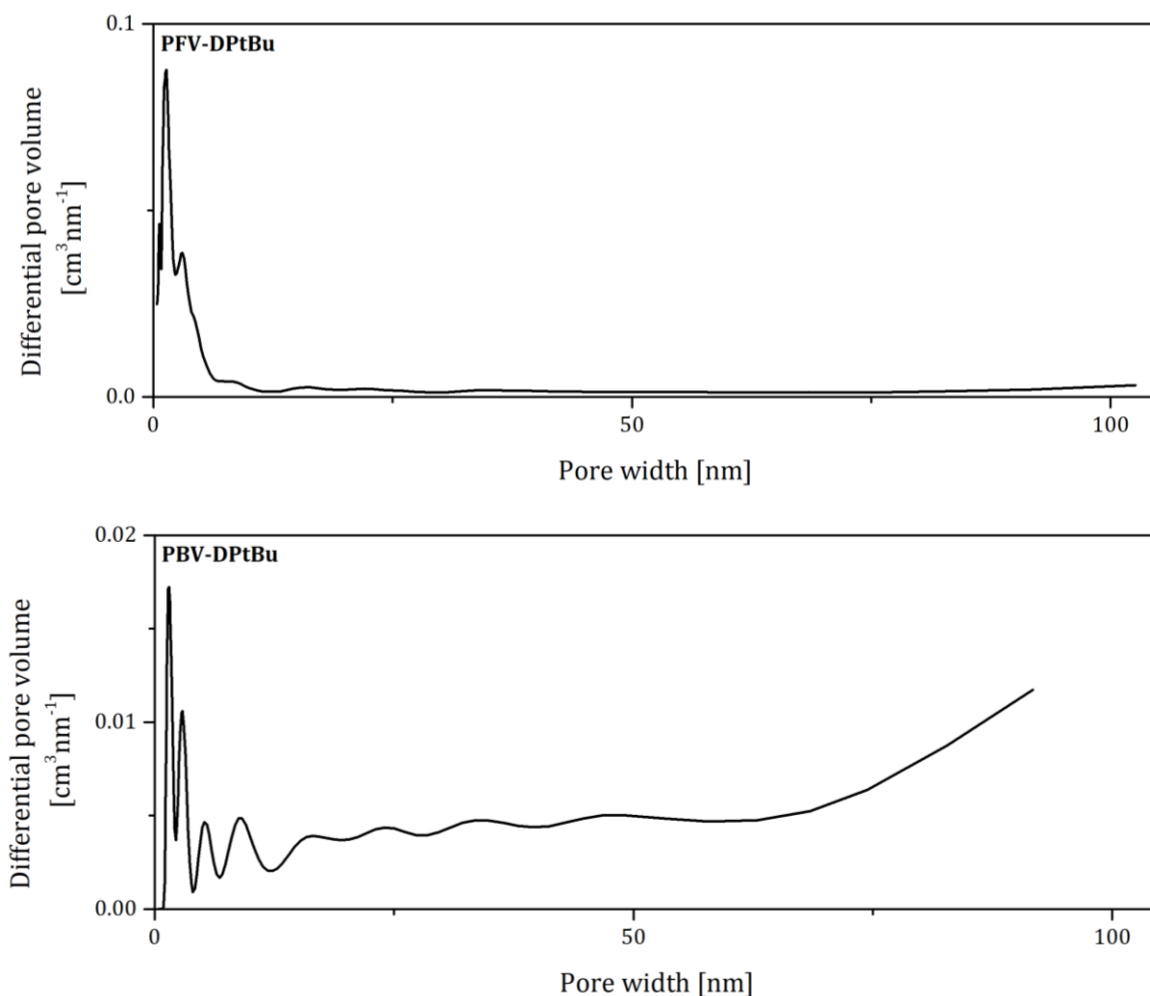


Figure 36 Pore size distributions for **PFV-DPtBu** (top) and **PBV-DPtBu** (bottom).

2.3.6 Synthesis and characterization of tetraphenylethylene model compounds

The results in this chapter were obtained and published in a collaboration with the group of Prof. Dr. J. Sérgio Seixas de Melo from the chemistry department of the University of Coimbra.⁸⁹

To gain further understanding of the polymers **PPV-DPtBu** and **PPV-DN** and accordingly **PmPV-DP**, model compounds were synthesized. The structures of *E*-1,2-bis(4-*tert*-butylphenyl)-1,2-diphenylethylene (**TPE-DtBu**) and *E*-1,2-bis(2-naphthenyl)-1,2-diphenylethylene(**DPE-DN**) are shown in Figure 37.



Figure 37 Structures of *E*-1,2-bis(4-*tert*-butylphenyl)-1,2-diphenylethylene (**TPE-DtBu**) and *E*-1,2-bis(2-naphthenyl)-1,2-diphenylethylene(**DPE-DN**).

The model compounds were synthesized as displayed in Figure 38 for **TPE-DtBu**. In the first step *tert*-butylbenzene or naphthalene were acylated via Friedel-Crafts reaction with benzoyl chloride (**16**) using aluminium(III) chloride as Lewis acid. The reaction with naphthalene yields a mixture of 1-benzoylnaphthalene and 2-benzoylnaphthalene. The regioisomers were separated by flash column chromatography. In the next step, the desired model compounds were obtained by a variant of the McMurry coupling, using a mixture of titanium(IV) chloride and zinc.⁹⁰ The reaction resulted in the expected 1:1 mixture of *E/Z*-isomers (as determined from the ¹H-NMR spectra). The isomers were separated by recrystallization from a mixture of hexane and toluene.

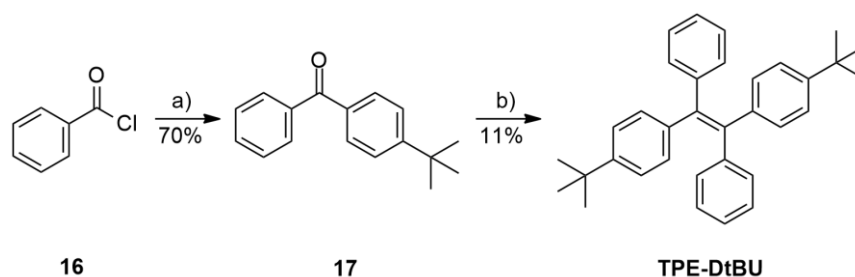


Figure 38 Synthesis of **TPE-DtBu**: a) *tert*-butylbenzene, AlCl₃, DCE, rt, 4 h; b) 1. TiCl₄, Zn, THF, 0 °C→70°C, 3.5 h, 2. **17**, THF, 70°C, 44 h.

The model compounds were characterized by ¹H- and ¹³C{H}-NMR, high resolution mass, and infrared (IR) spectroscopy. The analytics of **TPE-DtBu** shall be discussed here representatively for both compounds. The proton spectrum, shown in Figure 39, shows the singlet of the *tert*-butyl group at 1.25 ppm (green). In the aromatic region of the spectrum two multiplets at 7.10-7.07 ppm and 7.06-7.02 ppm (black) and a doublet at 6.92 ppm (black) appear. The *Z*-isomer **TPE-DtBu** shows slightly shifted signals, therefore, the easiest way to follow the separation of the isomers is to observe the aliphatic singlet. A splitting of the signal is observed for the mixture of isomers (Figure 39a), for the pure product the signal is a singlet (Figure 39b).

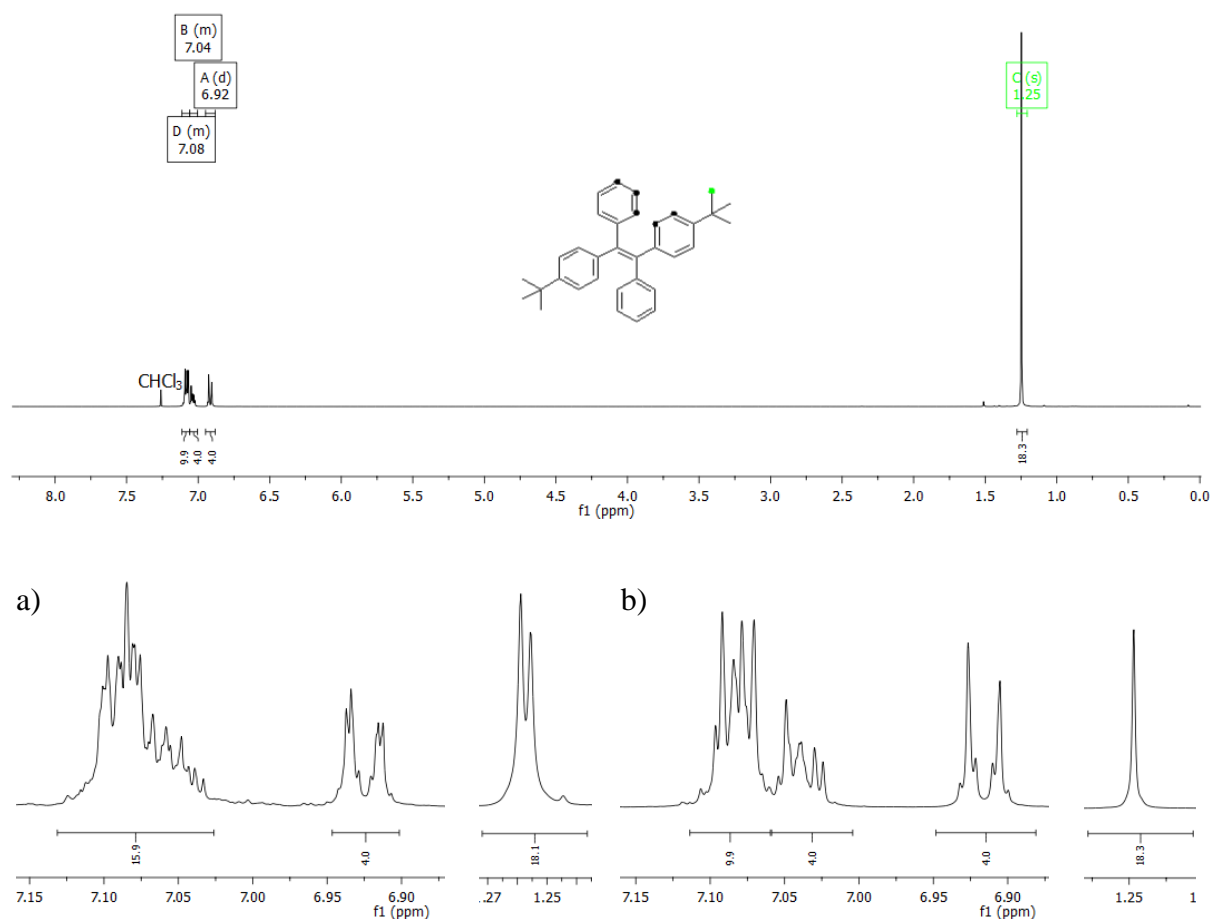


Figure 39 $^1\text{H-NMR}$ spectrum of **TPE-DtBu** in CDCl_3 at room temperature: a) detail of the $^1\text{H-NMR}$ spectrum of the mixture of isomers b) detail of the $^1\text{H-NMR}$ spectrum of the *Z*-isomer **TPE-DtBu**.

The $^{13}\text{C}\{\text{H}\}$ -NMR of **TPE-DtBu** shows the expected two aliphatic signals at 34.5 ppm and 31.5 ppm for the *tert*-butyl group. Nine signals for the two different phenyl rings and the olefinic carbon can be observed in the aromatic region of the spectrum.

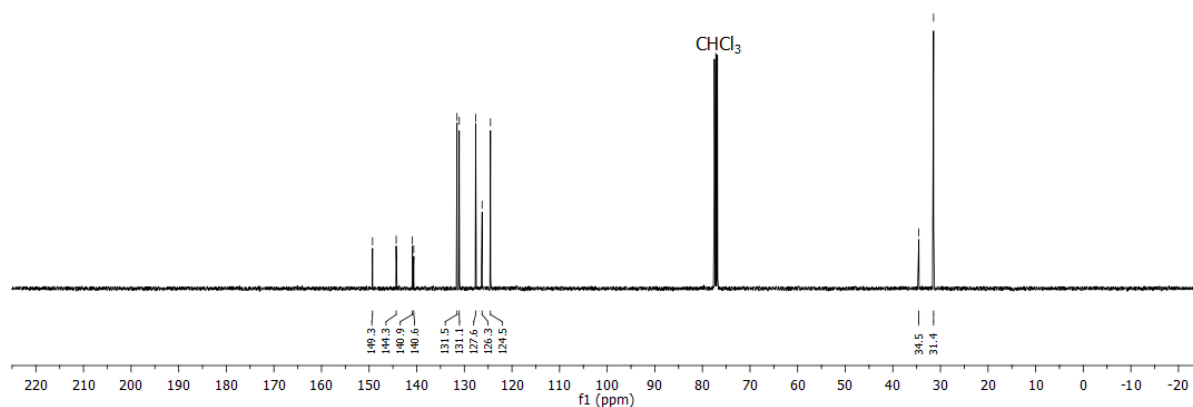


Figure 40 $^{13}\text{C}\{\text{H}\}$ -NMR spectrum of **TPE-DtBu** in CDCl_3 at room temperature.

The measured high resolution mass of the model compound **TPE-DtBu** was 467.2635 m/z compared to the calculated mass of 467.2709 m/z for the sodium salt. The IR spectrum,

displayed in Figure 41, shows the weak aromatic carbon-hydrogen valence vibrations at 3080, 3058, and 3038 cm^{-1} . The much stronger aliphatic vibration signals appear at 2962, 2901, and 2863 cm^{-1} .

The double bond-configurations of the model compounds were determined by X-ray crystallography by the group of Prof. Dr. Christian W. Lehmann at the Max-Planck-Institut für Kohlenforschung. Both crystallized model compounds adopt the desired *E*-configuration. As shown in Figure 42, the aromatic rings of both substances rotate out of the plane of the double bond in the crystalline state, creating a propeller-like conformation.

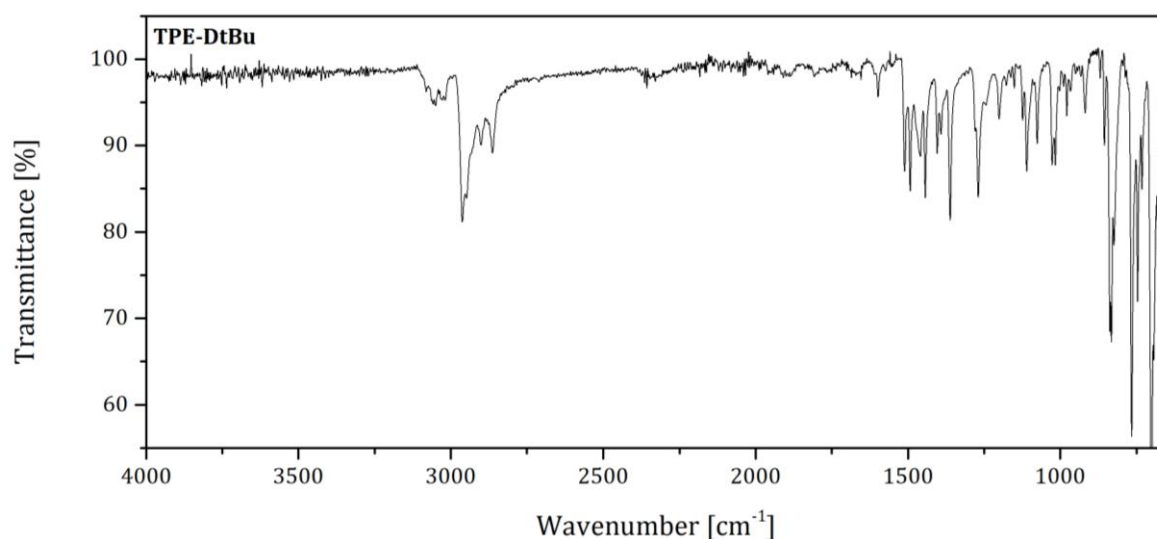


Figure 41 IR spectrum of **TPE-DtBu**.

For **TPE-DtBu** the *tert*-butylphenylene rings are rotated with dihedral angles of 38.8° and 41.1°. The phenyl rings are rotated a little further to 52.3° and 55.9°. For **DPE-DN** a twofold symmetry axis is observed, therefore, both naphthyl rings possess the same dihedral angle of 53.3°. The phenyl rings are rotated by 56.2° from the plane of the double bond. The major difference in both molecules in crystalline state becomes apparent when the intermolecular interactions are taken into account. While **TPE-DtBu** shows no π - π stacking interactions at all, the naphthyl rings of **DPE-DN** display strong π - π stacking interactions. These interactions are not limited to molecule pairs but stretched infinitely throughout the crystal along the *c*-axis. The shortest C-C distance between the rings is 3.32 Å, which is slightly shorter than graphite. The distance between the centroids of the overlapping halves of the naphthalenes is 4.8 Å. This indicates a ring slippage and therefore reduced overlap of the aromatic systems.

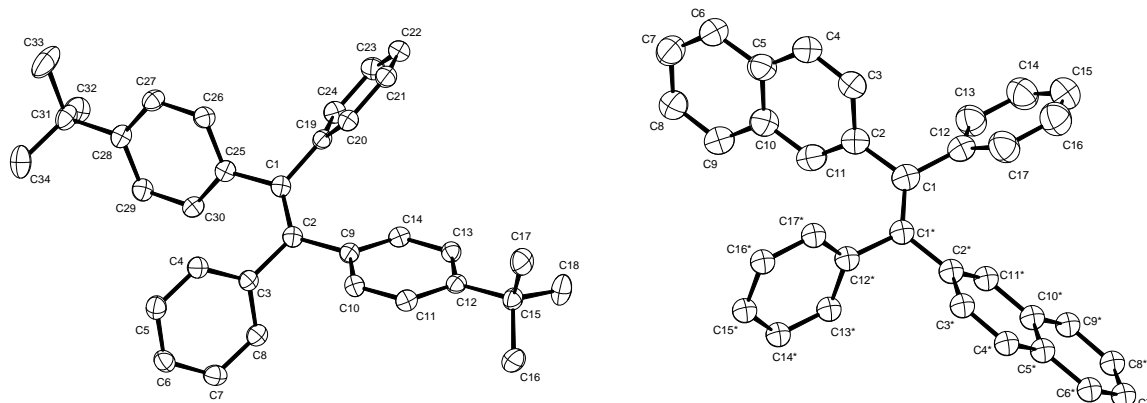


Figure 42 Molecular structures of **TPE-DtBu** and **DPE-DN** determined by single crystal X-ray crystallography.⁸⁹

This behaviour of the side groups should also be applicable in order to discuss the properties of the polymers **PPV-DPtBu**, **PPV-DN**, and **PmPV-DN**. **PPV-DPtBu** shows a significantly larger surface area than the naphthalene containing polymers, since the bulky *tert*-butyl groups create free volume between the molecules. The naphthalene side groups on the other hand tend to stack tightly in the solid state.

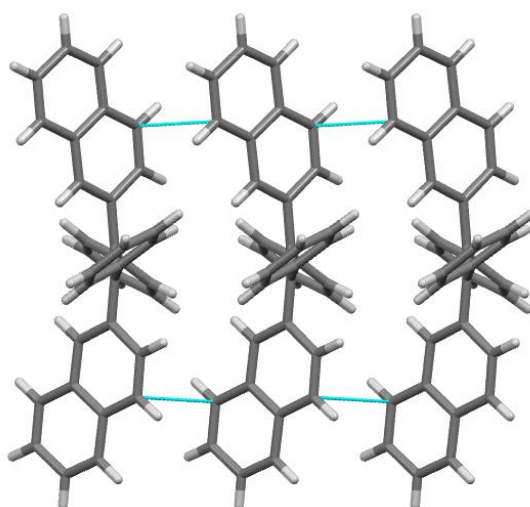


Figure 43 Crystal packaging of **DPE-DN** with short C-C distances (cyan) due to π - π stacking interactions.⁸⁹

A full comparative photophysical characterization of the model compounds **TPE-DtBu** and **DPE-DN** and the polymers **PPV-DPtBu**, **PPV-DN**, and **PmPV-DN** was carried out by the group of Prof. Dr. J. Sérgio Seixas de Melo with the major contribution coming from Ana Clara B. Rodrigues.⁸⁹ The optical properties of amorphous powders, thin films, tetrahydrofuran solutions, and solutions in mixtures of good and poor solvent (THF/water mixtures) were compared to gain insights into the effect of aggregation on the fluorescence emission. Figure 44 shows the absorption spectra of the polymers and model compounds in direct comparison to each other

and with **TPE**, in powder, film, and solution. The respective absorption and PL maxima and Stokes shifts are additionally summarized in Table 12.

A red-shift and broadening of the powder absorption and emission spectra can be observed in comparison to the THF solution spectra. This effect can be assigned to an extended conjugation of the compounds through intermolecular packing. The absorption spectra of the thin films show the same band profiles as the solutions with slightly shifted maxima. The polymer emission spectra are red-shifted due to the extended conjugation in comparison to the model compounds. The Stokes shifts of the polymers are generally higher than those of the model compounds in the same medium. This can likely be assigned to the adoption of different conformations in ground and excited state. Presumably, the polymers adopt a more planar conformation with an increased conjugation in the excited state.

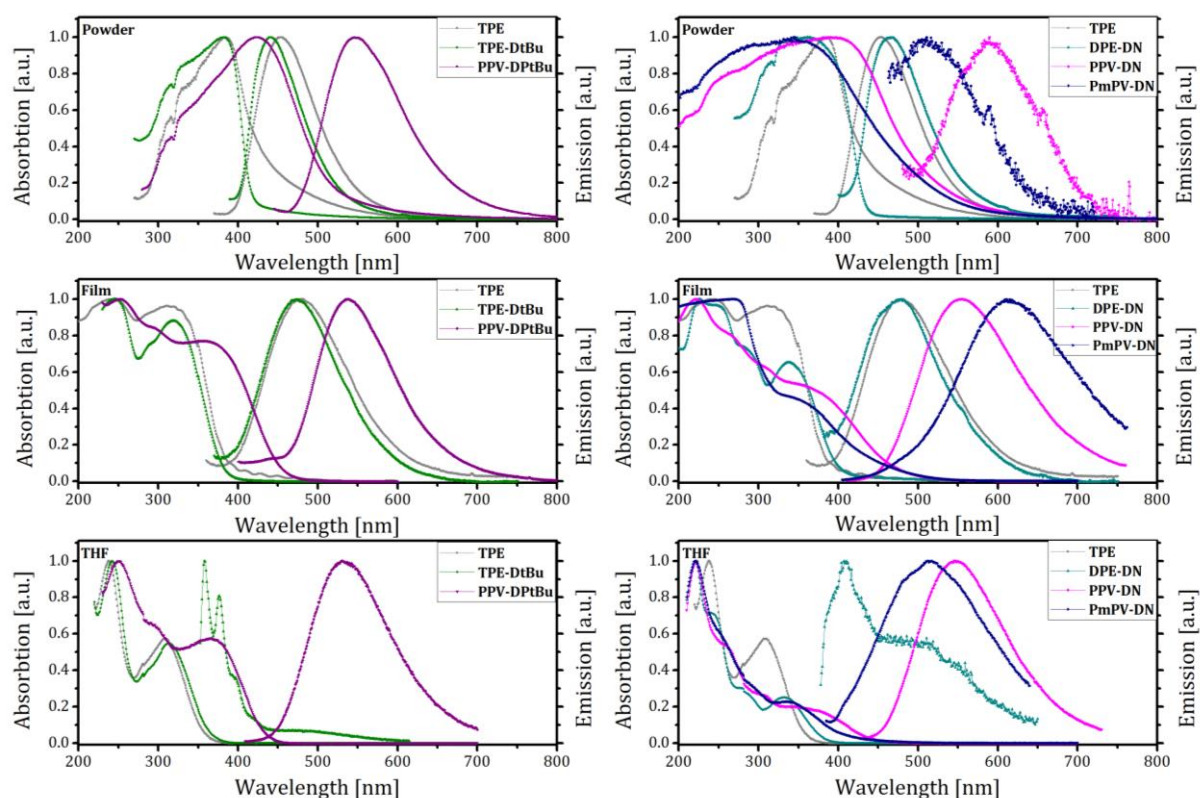


Figure 44 Normalized absorption and emission spectra of polymers and model compounds in solid state, thin film, and, THF, in comparison to TPE.⁸⁹

The solution-state emission maxima of 530 nm for **PPV-DPtBu**, 545 nm for **PPV-DN**, and 518 nm for **PmPV-DN** lie in the visible green region of the light spectrum. The higher red-shift of **PPV-DN** in comparison to **PmPV-DN** can be ascribed to a higher degree of conjugation in **PPV-DN**, given that the *meta*-substituted phenylene in **PmPV-DN** prevents a pronounced

conjugation along the polymer backbone. The opposite behaviour can be found in thin films. A significantly red-shifted maximum of 611 nm can be observed for **PmPV-DN**, while the maximum of **PPV-DN** shifts only slightly to 553 nm. This effect may be caused by an increased side chain aggregation resulting in an aggregate emission as main feature. This theory is supported by the reduced photoluminescence quantum yield ϕ_F of a **PmPV-DN** film of 0.001 versus 0.02 for **PPV-DN** as listed in Table 13.

Table 12 Main absorption and emission maxima along with the Stoke shifts (Δ_{ss}) of polymers and model compounds in solid state, thin films, and THF solutions.

Compound	Medium	λ^{abs} [nm]	λ^{em} [nm]	Δ_{ss} [cm ⁻¹]
TPE	Powder ^a	381	454	4220
	Film ^b	243, 312	482	11304
	THF ^a	238, 308	-	-
TPE-DtBu	Powder	382	441	3052
	Film ^b	245, 320	473	10108
	THF	242, 314	358, 490	3914
PPV-DPtBu	Powder	421	546	5438
	Film	252, 355	537	9547
	THF	250, 366	530	8454
DPE-DN	Powder	362	468	6257
	Film ^b	226, 337	479	8797
	THF	220, 334	407, 490 sh	5370
PPV-DN	Powder	391	590	8626
	Film	222, 351	553	10407
	THF	222, 343	545	10806
PmPV-DN	Powder	346	511	9332
	Film	268, 348	611	12369
	THF	221, 335	518	10546

^a Data from reference ³⁴. ^b Prepared using Zeonex® as polymeric matrix.

The absorption spectrum of **PPV-DPtBu** is significantly red-shifted in comparison to the model compound **TPE-DtBu**, the shifts are 39 nm for the powders, 35 nm in the films, and 52 nm in tetrahydrofuran solution. The red-shifts for **PPV-DN** are lower with 29 nm, 14 nm, and 9 nm, respectively. For the **PmPV-DN** film only a small red-shift of 9 nm can be observed, powder and solution show no red-shifts. This shows that the conjugation is limited to approximately one monomeric unit.

Table 13 Room-temperature fluorescence quantum yields of the investigated model compounds and polymers in different media.

	PLQY (THF)	PLQY (90 H₂O:10 THF)	PLQY (Powder)	PLQY (Film)
TPE	0.003	0.25	0.23 ^a	0.26 ^b
TPE-DtBu	0.024	0.20	0.14	0.46 ^b
PPV-DPtBu	0.046	0.62	0.30	0.64
TPE-DN	0.003	0.043	0.14	0.12 ^b
PPV-DN	0.028	0.011	0.012	0.010
PmPV-DN	0.008	0.003	0.004	0.002 ^c

^a Data from reference ³⁴. ^b Prepared using Zeonex® as polymeric matrix. ^c ϕ_F determined by comparison with the emission area of **PPV-DN** film, with the same absorption at the excitation wavelength.

The emission spectrum of **DPE-DN** in solution shows two maxima at 407 nm and 498 nm. This behaviour indicates the coexistence of monomeric and aggregate species. The absorption spectra of both model compounds retain the spectral absorption features of **TPE**. Since in solution, similar broad absorption bands are observed. In case of the naphthyl-substituted model compound a distinct bathochromic shift of 26 nm is observed. This shift can be attributed to the increased π -electron systems in the naphthyl units compared to the phenyls of **TPE**.³³ Regarding the emission behaviour of the model compounds in comparison to **TPE**, a clear difference can be observed. While **TPE** and **DPE-DN** are almost non-emissive in solution with a photoluminescence quantum yield of 0.003 (Table 13), the model compound **TPE-DtBu** displays fluorescence in both solution and solid state. The solution-state PLQY is, with a value of 0.024, a magnitude higher than that of **TPE**. The emission spectrum displays two bands, where the first one at 358 nm corresponds to monomer-related and the second one at 490 nm to the aggregate-related emission. The second maximum red-shifts upon water addition and increases in intensity, as shown in Figure 45. The emission maximum of **TPE-DtBu** at 441 nm in the powder state is blue-shifted compared to **TPE** at 454 nm. The PL maximum of **DPE-DN**, on the other hand, is red-shifted to 468 nm. This shift, and the rise of the PLQY upon going from solution to solid state, hints at the formation of J-aggregates.⁹¹

For further understanding of the AIE characteristics the emission of the model compounds and polymers in different non-solvent/solvent (water/tetrahydrofuran) mixtures, as shown in Figure 45, was studied. The emission of **TPE** is only detectable in mixtures with a high water content of $\geq 85\%$.

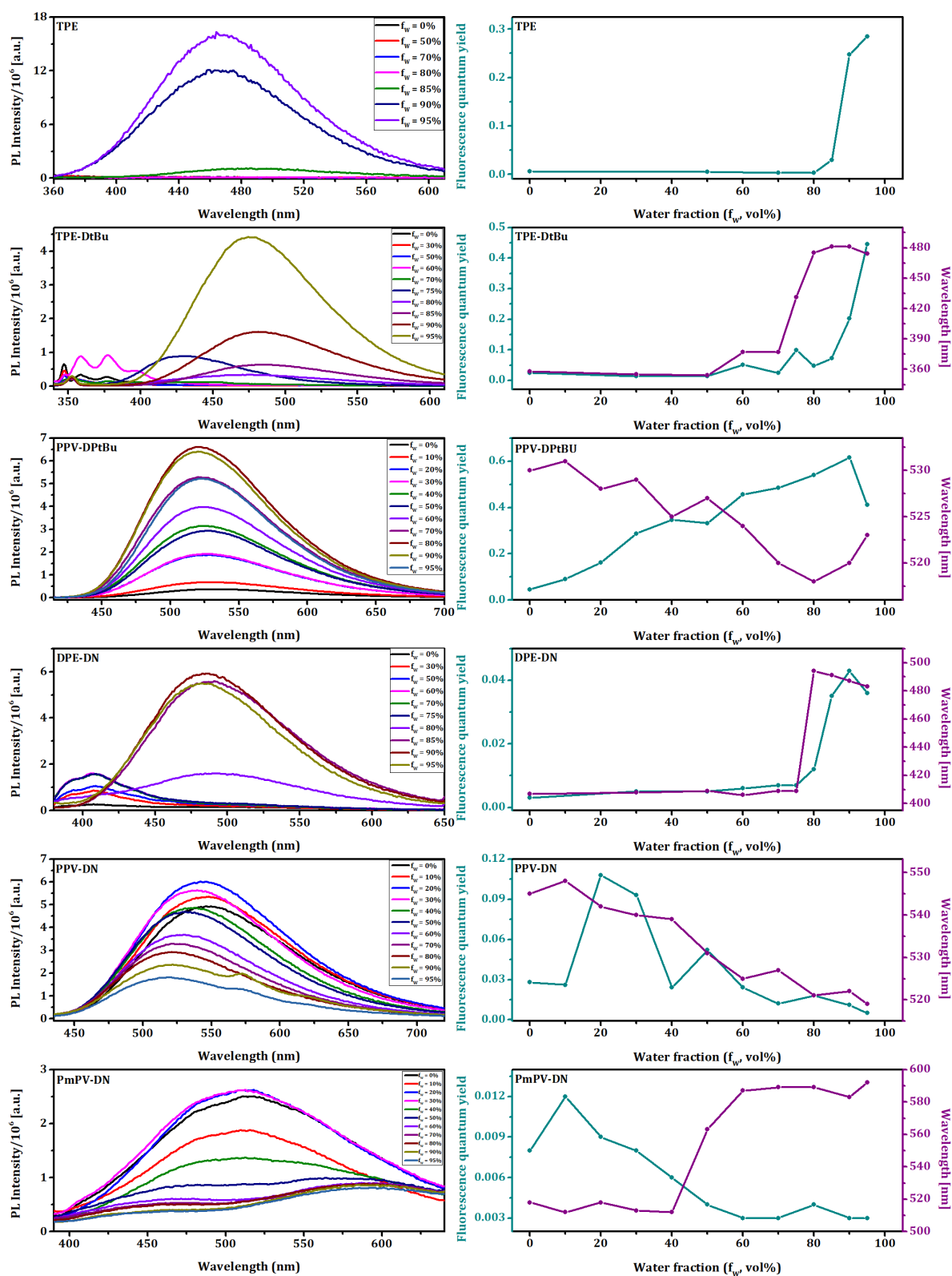


Figure 45 Photoluminescence spectra of model compounds **TPE**, **TPE-DtBu**, and **DPE-DN** and the polymers **PPV-DPtBu**, **PPV-DN**, and **PmPV-DN** in THF/water mixtures (left) and the resulting correlations of PLQYs and emission maxima with increasing water fraction $f_w = 0-95\%$ (right).⁸⁹

The emission of **TPE-DtBu** shows a structured spectrum with increasing intensity at higher water fractions up to $f_w = 45\%$. At water fractions of $f_w = 70\%$ and above the PL maximum shifts bathochromically and the PLQY rises. The highest quantum yield is reached at $f_w = 95\%$ with a value of 20%. A similar behaviour can be observed for **DPE-DN**. The structured emission at low water fractions reaches its maximal intensity at $f_w = 60\%$. Then it is almost unchanged, until at $f_w = \geq 80\%$ a red-shift appears, accompanied by an increase in PLQY, with a maximum at $f_w = 90\%$. This behaviour of the model compounds is likely to be caused by the formation of J-aggregates. Even though the naphthyl rings of **DPE-DN** may favour the formation of H-aggregates through π - π stacking, this behaviour is not observed in the spectra.

The quantum yields of **TPE** and **DPE-DN** in the film state obtained in this study are 0.24 and 0.46. These values differ from the previously reported values of 0.49 and 0.30, respectively.³³ This deviation is due to the dependence of the photophysical properties on the morphology of the films. This explanation is supported by the observation that the previously measured PLQY of **TPE** in powder of 23%³⁴ is in good agreement to the literature value of 24%.³⁰

Incorporation of an AIEgen into a polymer structure can reportedly lead to AIE-active polymers.^{26,27,34} Therefore, it was expected that the investigated polymers also display AIE behaviour. In case of **PPV-DPtBu** the expected increase of PLQYs with increased water fraction in water/tetrahydrofuran mixtures was observed, whereas both naphthyl containing polymers **PPV-DN** and **PmPV-DN** show an ACQ effect. Furthermore, **PmPV-DN** shows smaller quantum yields than **PPV-DN** in solution, solid state, and in water/tetrahydrofuran mixtures, for specific water fractions. The PL quenching for the polymers may be caused by the π - π stacking tendency of the naphthyl groups. This assumption is supported by the observed stacking in the single crystal structure of the model compound **DPE-DN**. The highest quantum yield is observed for **PPV-DPtBu** as thin film, the value of 64% is slightly higher than the value of the same polymer in aggregated state in the solvent (THF)/water mixture with $f_w = 90\%$ with a PLQY of 62%.

To gain further insight in the aggregate formation and occurring AIE effects of **PPV-DPtBu**, time resolved fluorescence decays were obtained. The fluorescence decay in water/tetrahydrofuran mixtures, with the emission observed at 525 nm, fits to a bi-exponential decay law as displayed in Figure 46, indicating the presence of two emitting species in the aggregate region. This could mean that the emissive aggregate involves two main conformers with different contributions.

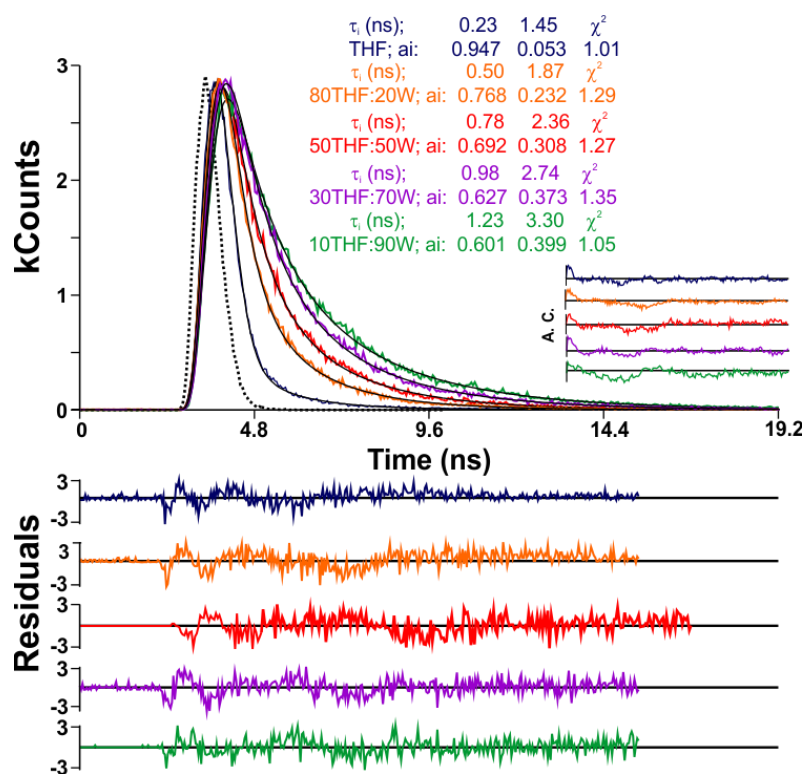


Figure 46 Room temperature fluorescence decays of **PPV-DPtBu** collected with excitation at 339 nm and emission at 525 nm in tetrahydrofuran solution and in THF/water mixtures. For a better judgement of the quality of the fit, weighted residuals (W.R.), autocorrelation function (A.C.), and χ^2 values are also presented. The dashed line corresponds to the instrumental response function.⁸⁹

Hereby, the fractional contribution (C_i), of each species is given by Equation 2. The obtained values are summarized in in Table 14.⁹²

$$C_i(\%) = \frac{a_i \tau_i}{\sum_{i=1}^n a_i \tau_i} \times 100 \quad (2)$$

C_i is the fractional contribution, a_i is the contribution of each exponential term at $t = 0$, τ_i is the associated decay time, and n is the number of exponential terms.⁹²

The decay time values and the fractional contribution of each species (C_i) at the aggregate emission wavelengths of 525 nm change with the water fraction of the mixture, as shown in Figure 47. A fast decay component τ_1 in the 0.23-1.2 ns range and a longer decay time τ_2 from 1.5 ns to 3.3 ns were found when going from 0% to 90% water content. Lifetimes, as well as PLQYs, show a similar trend of increasing values with increasing water fraction.

Table 14 Room temperature fluorescence quantum yields (ϕ_F) and lifetimes^a (τ) of **PPV-DPtbu** in selected THF/water mixtures. Furthermore, the associated pre-exponential values (a_i), fractional contribution of each decay time (% C_i), and the chi-square values (χ^2) for the judgement of the quality of the fits are listed. Radiative (k_F) and radiationless (k_{NR}) rate constants associated with the second decay component (τ_2) are also presented.

Solvent	a_1	τ_1 [ns]	a_2	τ_2 [ns]	χ^2	ϕ_F	% C_1	% C_2	k_F^b [ns ⁻¹]	k_{NR}^c [ns ⁻¹]
100% THF: 0% water	0.947	0.23	0.053	1.45	1.01	0.046	73.9	26.1	0.032	0.658
80% THF: 20% water	0.768	0.5	0.232	1.87	1.29	0.161	47.0	53.0	0.086	0.449
50% THF: 50% water	0.692	0.78	0.308	2.36	1.27	0.332	42.6	57.4	0.141	0.283
30% THF: 70% water	0.627	0.98	0.373	2.74	1.35	0.485	37.5	62.5	0.177	0.188
10% THF: 90% water	0.601	1.23	0.399	3.3	1.05	0.612	36.0	64.0	0.185	0.118

^a Experimental conditions: nanoLED $\lambda^{exc} = 339$ nm; $\lambda^{em} = 525$ nm; 48.1 ps/channel, 3 k counts. ^b $k_F = \frac{\phi_F}{\tau_F}$.

^c $k_{NR} = \frac{(1-\phi_F)}{\tau_F}$.

The determination of the rate constants shows an increase of the radiative constant k_F and a decrease of the radiationless constant k_{NR} with increasing water content. This is valid for both decay components even though only the constants for the longer decay time τ_2 are given in Table 14. The radiationless decay is dominant up to $f_w = 70\%$, whereas at higher water contents the radiative decay begins to dominate.

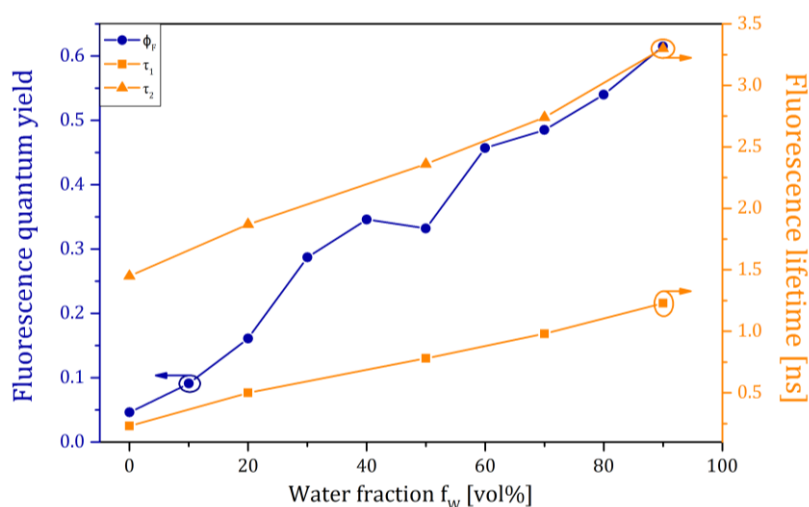


Figure 47 Correlation of fluorescence quantum yields and fluorescence decay times for **PPV-DPtbu** in THF/water mixtures with increasing water fraction.⁸⁹

2.3.7 Explosives detection with PPV-DPtBu

PPV-DPtBu was tested for its explosives sensing ability. Picric acid (TNP) was chosen as model explosive due of its commercial availability. The quenching experiments were carried out in a 10^{-6} M polymer solution based on the weight of the repeating unit in a tetrahydrofuran/water mixture with a water fraction of $f_w = 90\%$. Upon addition of increasing amounts of TNP the emission is more and more quenched, as shown in Figure 48. The results were analysed using the Stern-Volmer Equation 3.

$$\frac{I_0}{I} = 1 + K[Q] \quad (3)$$

where I_0 is the fluorescence intensity without quencher, I is the fluorescence intensity with quencher, K is the Stern-Volmer quenching constant, and $[Q]$ is the concentration of the quencher.¹⁴

The Stern-Volmer plot in Figure 48b reveals a linear trend in the low concentration region of the plot, with a quenching constant of $3.4 \times 10^4 \text{ M}^{-1}$, calculated by using Equation 3.¹⁴ With increasing concentration, a so-called super-amplification effect can be observed. The super-amplification shows itself in an upwards curvature of the Stern-Volmer plot, and stands for an increased sensitivity with increasing quencher concentration, that cannot be ascribed to the combination of static and dynamic quenching.⁴⁶ Instead, the quenching occurs purely static and the enhancement in sensitivity can be ascribed to the morphology of the polymer nanoaggregates. The super-amplification occurs in porous polymers where cavities allow the quencher molecules to enter and interact with the polymer.⁴⁶ The obtained curve can be fitted exponentially and described by Equation 4 with $A+B=1$ and $K=Ak$.⁴⁶

$$\frac{I_0}{I} = Ae^{k[Q]} + B \quad (4)$$

where I_0 is the fluorescence intensity without quencher, I is the fluorescence intensity with quencher, A and B are constants, k is the rate constant for bimolecular quenching, and $[Q]$ is the concentration of the quencher.⁴⁶

The Stern-Volmer constant obtained by Equation 4 with a value of $3.5 \times 10^4 \text{ M}^{-1}$ is in good agreement with the constant obtained by Equation 3. The first definite quenching was observed at a TNP concentration of $6.63 \times 10^{-6} \text{ M}$, this equals a detection limit of 1.5 ppm. The fluorescence is fully quenched at a concentration of $4.67 \times 10^{-4} \text{ M}$. With these values **PPV-DPtBu** shows an increased sensitive towards TNP compared to other, non-porous poly(phenylene vinylene)s

used by Baysec *et al.*²⁶, and is comparable to the values of some efficient AIE-active polymers for explosion detection.⁷

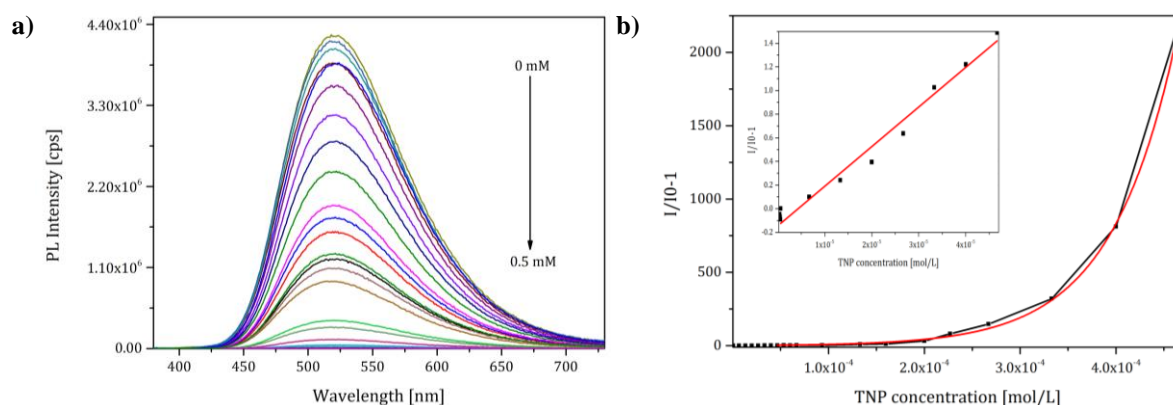


Figure 48 a) PL spectra of **PPV-DPtbu** of a 10⁻⁶ M polymer solution in a tetrahydrofuran/water mixture with a water fraction of $f_w = 90\%$ at increasing TNP concentrations, b) corresponding Stern-Volmer plot.

2.3.8 Electrochemical cross-linking of PPV-DPC as linear precursor

Carbazoles are widely applied building blocks for an oxidative coupling in electrochemistry due to their low oxidation potential of 1.16 V versus SCE.⁹³ Based on the oxidation mechanism discovered by Ambrose and Nelson⁹³, a C-C coupling between two carbazoles occurs selectively in their 3- or 6-positions. The polymeric products obtained in this way are efficient materials for sensing^{49,50,53}, OLED^{94,95}, and other optoelectronic devices in general.⁹⁶

Electrochemistry can be carried out using different setups. A commonly used setup consists of three electrodes in a solution of the reactants and a supporting electrolyte in an aprotic organic solvent, as shown in Figure 49. A working electrode, a counter electrode, and a non-polarized reference electrode, regulated by a potentiostat, are used. An electric potential is applied to working and counter electrode and the occurring current is recorded. The electropolymerization occurs on the interface between working electrode and solution. Even though the supporting electrolyte increases the conductivity of the solvent, the resistance can be high enough that the applied potential differs from the target potential. Therefore, the potentiostat measures the potential between working and reference electrode and ensures the really applied potential is correct.⁹⁷

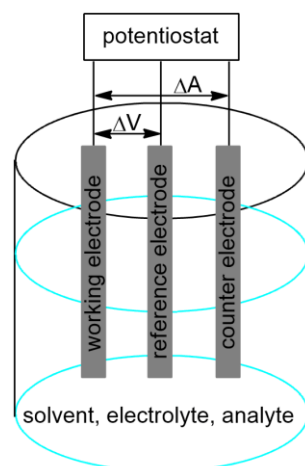


Figure 49 Schematic setup of a three electrode cell used for electrochemical measurements.

In this work the crosslinking-reactions were carried out using cyclic voltammetry. This method measures the current depending on the applied potential. Within a given potential window, the potential is increased linearly over a specific time period, followed by a decrease at the same scan rate. These cyclic scans can be repeated at will to control the conversion, for example the thickness of deposited polymer films. The conversions can be observed by a rise in the current signal with increasing potential. Reductions appear as a negative dip in the current signal with decreasing potential. Reversible electron transfer events show a pair of oxidation and reduction signals, while an irreversible chemical reaction shows only either of these signals.⁹⁷

The linear carbazole-based polymer precursor **PPV-DPC** was synthesized due to the efficient sensing abilities towards electron deficient analytes as aromatic nitro compounds of microporous carbazole-based polymer networks, as reported by Scherf and co-workers.^{50,53-55} Spacious side groups generally seemed promising to create high surface areas and pronounced AIE effects. Furthermore, the goal was to find out whether an electrochemically generated polymer network starting from **PPV-DPC** as linear polymer could maintain the AIE properties, while also producing a high surface area. When it was apparent that keto monomer leftovers were not easily removable from **PPV-DPC**, as discussed in Chapter 2.3.2, the target networks were generated from the mixture of polymer **PPV-DPC** and some leftover monomer **PDK-DPC**, named **M-PPV-DPC**.

The electrochemical behaviour of **M-PPV-DPC** was investigated by cyclic voltammetry and compared to the diketo monomer **PDK-DPC**. Both samples were measured in 10^{-6} M dichloromethane solution, for the polymer referenced to the monomeric repeat unit. Tetrabutylammonium hexafluorophosphate (TBAPF₆) was used as supporting electrolyte. The analytical cell

(5 ml) was equipped with a platinum disc electrode. For both reactants two oxidation/reduction peak couples can be observed in the potential range from 0 V to 1.5 V, as displayed in Figure 50. For **M-PPV-DPC**, in the first cycle, two reversible electron transfers can be observed. The oxidation peaks appear at 1.12 V and 1.36 V and the corresponding reduction peaks at 1.06 V and 1.18 V respectively. At potentials higher than 1.40 V the irreversible electrochemical coupling of the carbazoles occurs. This corresponds to a value of 1.06 V if a conversion factor from $\text{Ag}^+/\text{AgNO}_3$ to SCE (-343 mV) is taken into account.⁹⁸ Therefore, the oxidation occurs at a slightly lower voltage than the oxidation of pure carbazole that was reported to appear at 1.16 V.⁹³ The increase in current with every cycle indicates the formation of a conductive polymer film on the electrode.⁵⁰ The signals of the cycles two and higher consist of an overlay of the signals of the reactant and the network signals.⁹⁹

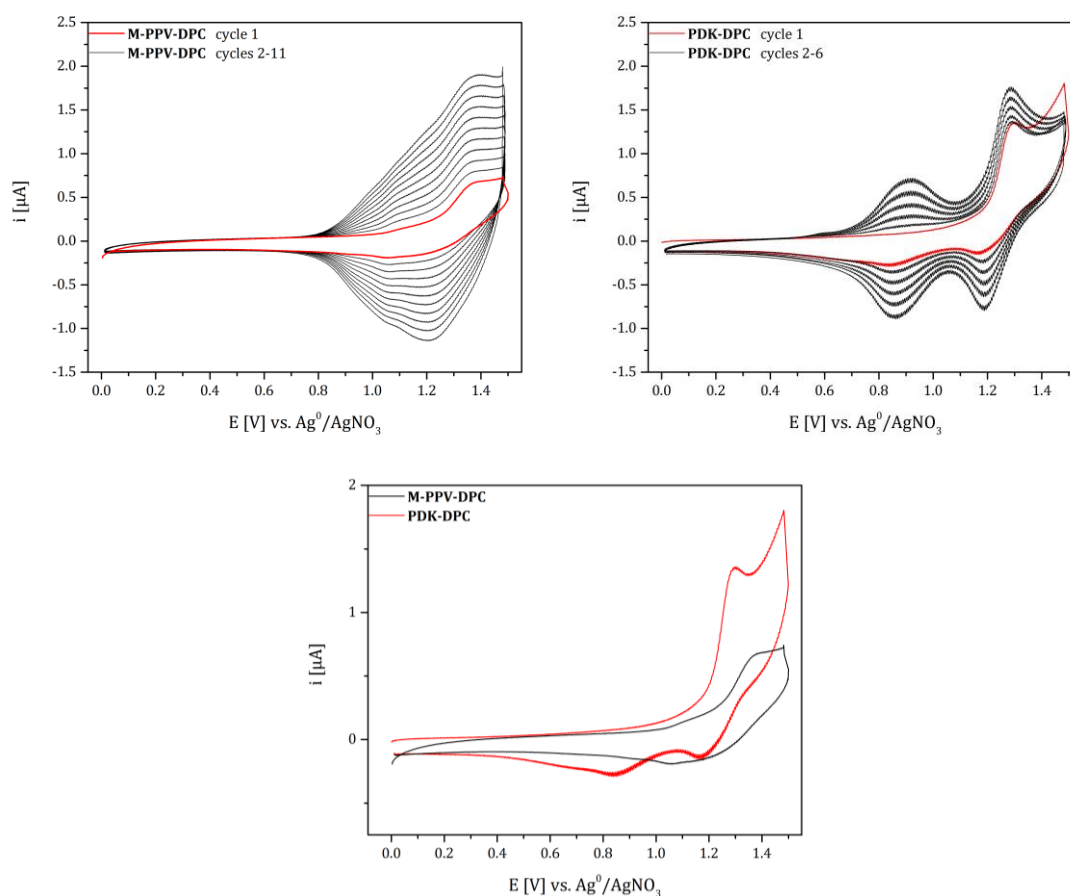


Figure 50 Cyclic voltammograms of **M-PPV-DPC** and **PDK-DPC** on a platinum disc electrode in 10^{-6} M dichloromethane solution, supporting electrolyte: 0.1 M TBAPF₆, potential range: 0-1.5 V, scan rate: 0.1 Vs⁻¹.

The keto monomer **PDK-DPC** was investigated separately, since **M-PPV-DPC** still contains leftover **PDK-DPC**. Its cyclovoltammogram shows more pronounced signals with a higher

peak current at potentials >1 V in the first cycle, presumably due to its better solubility in dichloromethane.⁵⁵ The oxidation peaks appear at 0.90 V and 1.30 V respectively, where the first peak becomes distinguishable after the second cycle. The corresponding reduction peaks are found at 1.67 V and 0.84 V. The irreversible coupling of the carbazoles starts at around 1.35 V. Interestingly, in the direct comparison it is obvious that in the cyclic voltammogram of **M-PPV-DPC** **PDK-DPC**-related signals are almost absent, this is most noticeable in potential range of 0.5-0.8 V. Therefore, it is assumed, that the monomer **PDK-DPC** does not significantly contribute in the electrochemical reaction of the mixture, and the idealized structure of the network (**N1**) obtained from **M-PPV-DPC** can be given as depicted in Figure 51, with the newly formed carbazole-carbazole connection in red.

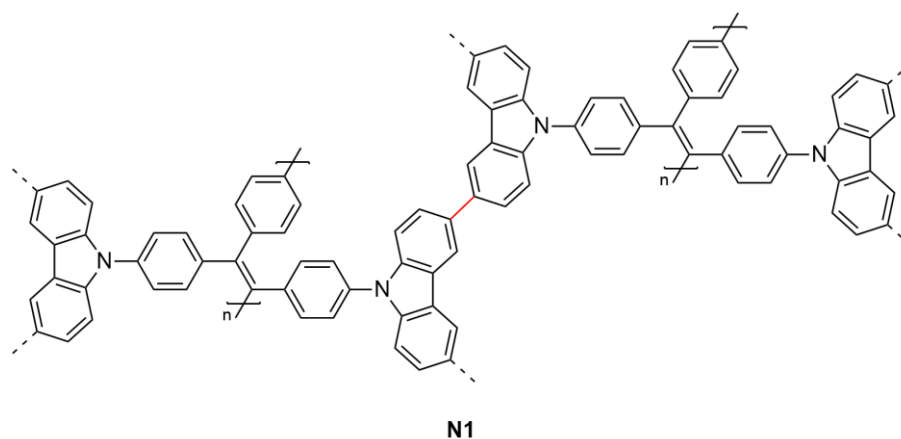


Figure 51 Idealized structure of network **N1**.

For further characterizations the network **N1** was generated on an indium tin oxide (ITO) coated quartz glass plate. The oxidation peaks on ITO are slightly shifted to higher potentials and the reduction peaks slightly to lower ones in comparison to the platinum electrode, but the working area remained the same as shown in Figure 52. At higher cycle numbers a yellow-brownish film was visible on the electrode which could be washed off if necessary.

The film formation was also characterized by an electrochemical quartz crystal microbalance (EQCM) experiment using a platinum-coated quartz crystal as electrode. In Figure 53a cycles 11-15 of the cyclic voltammogram are displayed representatively alongside the changes in the frequency of the quartz crystal caused by the increasing mass of the polymer film. Interestingly, an overlap of the frequencies can be observed between the cycles. This should be caused by charging/discharging events accompanied by the diffusion of ionic species in and out of the polymer film.¹⁰⁰ This is supported by an increasing oscillation of the mass values with increasing cycle number, displayed in Figure 53b. The mass was calculated from the frequencies using

the Sauerbrey equation with a factor of 1.068 ng/Hz .¹⁰¹ Within the 20 cycles a mass of about $1.9 \mu\text{g}$ was generated on an area of 0.165 cm^2 that equals about 94 ng per cycle.

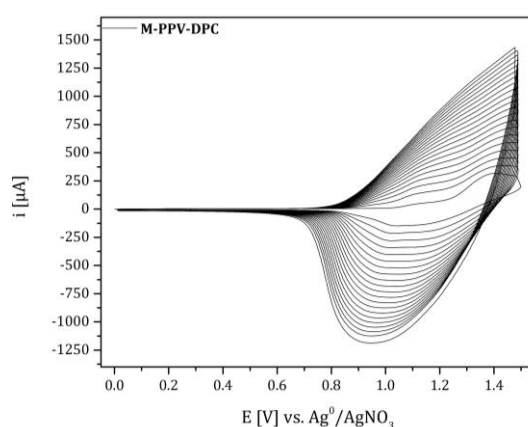


Figure 52 Cyclic voltammogram of **M-PPV-DPC** on ITO, $3 \times 10^{-6} \text{ M}$ dichloromethane solution of **M-PPV-DPC**, supporting electrolyte: 0.1 M TBAPF_6 , potential range: $0\text{-}1.5 \text{ V}$, scan rate: 0.1 Vs^{-1} .

The stability of the film was confirmed over 20 cycles by transfer of the **N1** film on the platinum coated quartz crystal electrode to a **M-PPV-DPC**-free solution. After an insignificant mass accumulation due to residual reactant, the mass is constant over several cycles, showing a stable polymer film, adhering to the working electrode.

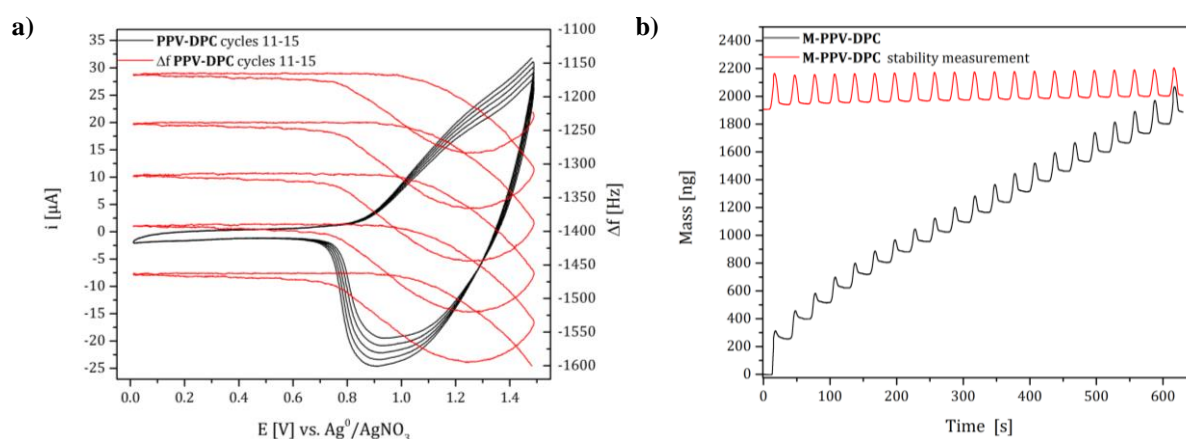


Figure 53 EQCM measurement for **M-PPV-DPC** in 10^{-6} M dichloromethane solution, supporting electrolyte: 0.1 M TBAPF_6 , potential range: $0\text{-}1.5 \text{ V}$, scan rate: 0.1 Vs^{-1} : a) cycles 11-15 of the cyclic voltammogram along with the frequency changes, and b) mass accumulation along with a stability measurement of an as-prepared polymer film in **M-PPV-DPC**-free solution.

Furthermore, the oxidation and reduction behaviour of the network **N1** on a platinum disc electrode was characterized in a reactant-free solution at different scan rates. In Figure 54 a linear correlation between signal intensity and scan rate can be observed. This indicates that the current is independent from the diffusion.⁹⁹ Two oxidation peaks with reduction peaks of about the

same intensity can be observed. This hints at a charging/discharging mechanism without a chemical reaction (doping/dedoping).

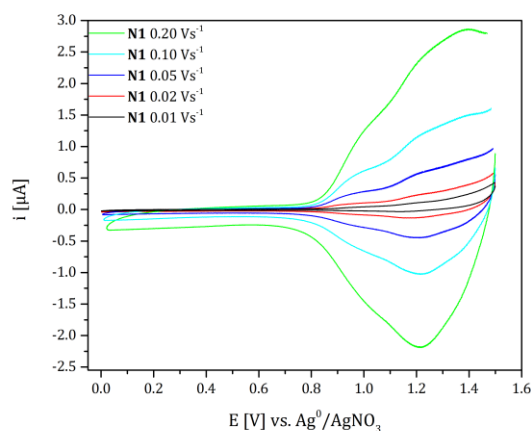


Figure 54 Cyclic voltammograms of **N1** on a platinum disc electrode at different scan rates, Supporting electrolyte: 0.01 M TBAPF_6 , potential range: 0-1.5 V.

Surface roughness and thickness of the **N1** film on ITO were measured by tapping mode atomic force microscopy (AFM). The measured film displayed an average thickness of 535 nm with an average roughness (R_q) of 45 nm. The globular morphology of the film displayed in Figure 55 is typical for electrochemically generated films. It can be explained by the generation of polymer nuclei on the electrode, followed by a spherical growth.¹⁰²

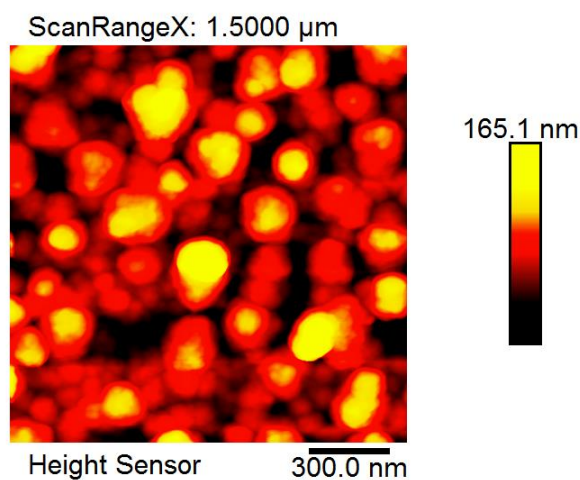


Figure 55 AFM image of network **N1** film on ITO.

The network **N1** was characterized using IR spectroscopy and compared to the IR-spectrum of reactant **M-PPV-DP**, as shown in Figure 56. First, a broadening of the signals can be observed. The aromatic C-H valence vibrations in the area of 2840-3080 cm^{-1} can be observed in both spectra. The ketone stretching vibrations of the residual monomer in **M-PPV-DP** can be observed at 1653 cm^{-1} . A similar signal can be found in **N1**, but of lower relative intensity. Since it was shown that the monomer did not react in the electropolymerization, this signal could stem from C=C stretching vibrations, or from carbonyl end groups. It has previously been reported that C=C stretching vibrations of carbazole-based networks occur at around 1600 cm^{-1} .¹⁰³

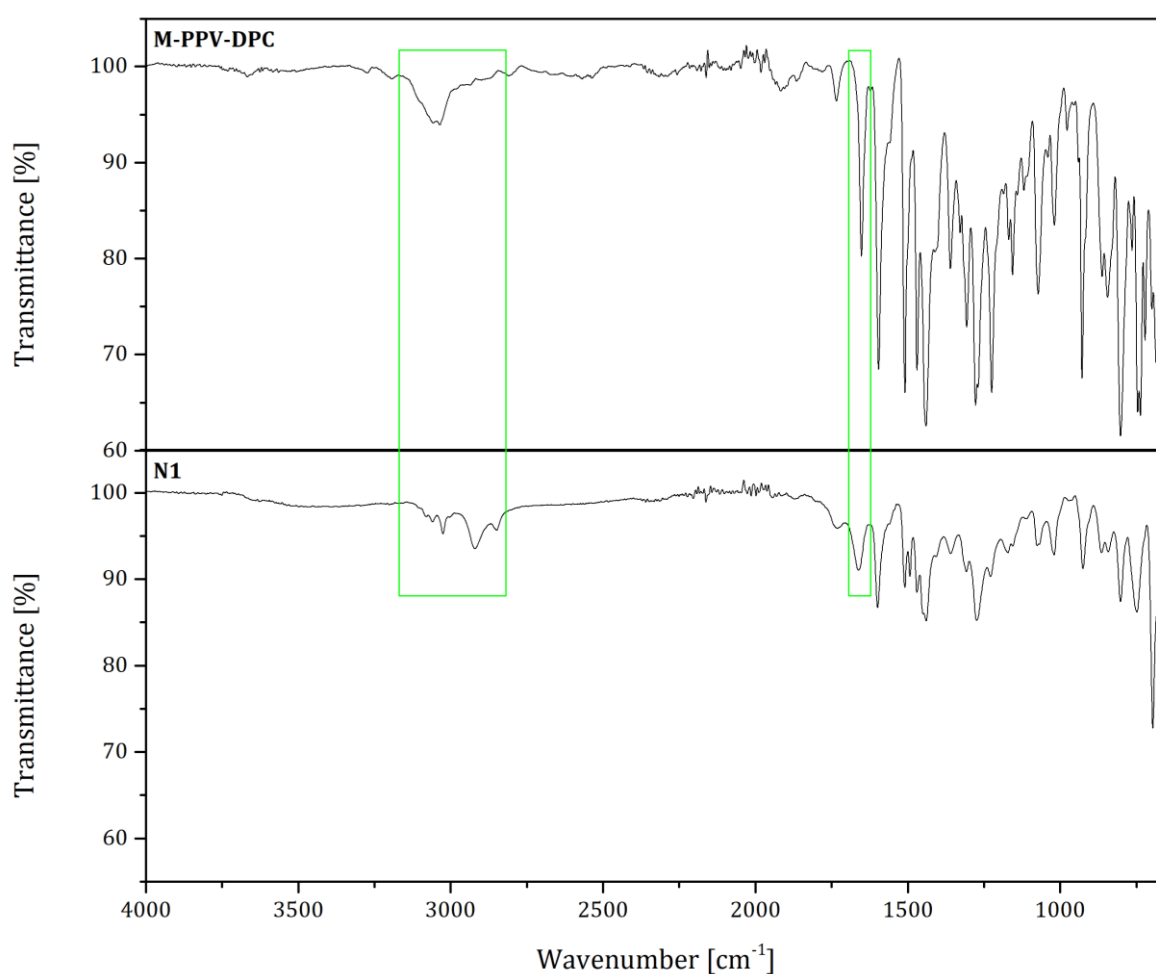


Figure 56 Room temperature IR spectra of **M-PPV-DPC** and **N1**.

The normalized absorption and emission spectra of **M-PPV-DPC** and **N1** are displayed in Figure 57. The absorption spectrum of **M-PPV-DPC** in tetrahydrofuran solution shows three maxima at 237, 291, and 349 nm. In the thin film state, the lower wavelength maxima shift bathochromically by 12 and 13 nm, respectively. The relevant long wavelength maximum remains

unchanged. Due to the smaller measurement range on ITO, only two absorption maxima of **N1** can be observed. The absolute maximum is found at 300 nm accompanied by a long wavelength shoulder at 349 nm. **N1** emits green light with a PL maximum wavelength of 533 nm. The PL maxima of **M-PPV-DPC** appear at only slightly higher wavelength of 539 nm in solid state, and 545 nm in solution. These almost identical spectra of solid **M-PPV-DPC** and **N1** show a similar amount of effective conjugation, and suggest that the conformations of linear polymer and polymer network are rather similar. A BET analysis provides that **N1** with its surface of only $5 \text{ m}^2\text{g}^{-1}$ is non-porous just like **M-PPV-DPC** with a surface area of $20 \text{ m}^2\text{g}^{-1}$. Regarding the PLQYs, **M-PPV-DPC** showed a pronounced AIE effect with an increase from 5% to 40% upon going from solution to the solid state. This effect could not be maintained upon network generation. **N1** displayed a solid state quantum yield below 1%.

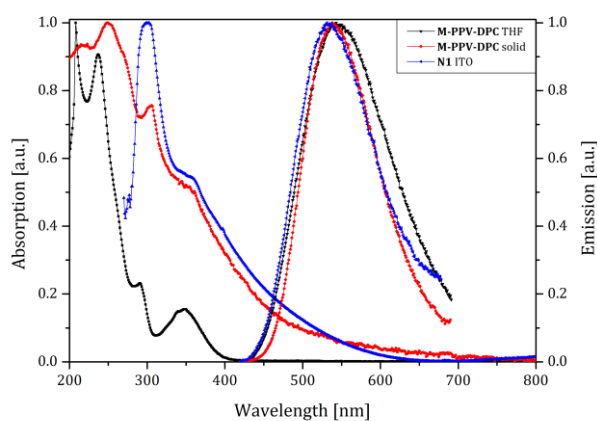


Figure 57 Absorption and emission spectra of **M-PPV-DPC** in tetrahydrofuran solution and as thin films on quartz glass, compared to **N1** on ITO.

2.4 Conclusions and Outlook

A systematic screening of poly(arylene vinylene)s with different side and main chain structures has been carried out. A series of 16 soluble PAVs have been synthesized by reductive polyolefination of bis-geminal tetrachloride monomers using dicobalt octacarbonyl as reducing agent. The choice of reagent was confirmed by comparison to chromium(II) acetate and vanadium (II) chloride. Yields up to 89% and chain lengths up to 80 repeat units could be obtained. It was shown that linear core segments in the monomers benefit the degrees of polymerization and yields compared to angled backbone segments. Furthermore, two model compounds were synthesized to further rationalize the obtained results.

Optical characterization of the polymers in solution and solid state gave rather similar spectra for all of the polymers with large Stokes shifts and green light emission. The possibility of $n-\pi^*$ transitions in the thiophene polymers allowed for a bathochromically shifted absorption and emission, shifted into the orange region. Both thiophene polymers proved to be unsuitable as light emitting polymers due to their low quantum yields, presumably caused by intersystem crossing or internal conversion.⁸²⁻⁸⁴ Furthermore, it was shown that anthracene main chain units as well as naphthyl side chains have a stacking tendency that hinders the occurrence of the AIE effect as well as the generation of permanent free volume. The suspected $\pi-\pi$ -stacking of the naphthyl groups was confirmed in a comparison to the single crystal structure of a corresponding model compound. It was concluded that it is necessary to add sp^3 -hybridized alkyl side groups to bulky but rigid aromatic side chains to prevent this stacking. This allowed for an AIE or AEE effect in several polymers. The solid state quantum yields reached values up to 43% for **PFV-DP** when only the values of the same spectrometer are taken into account. The PLQY of **PPV-DPtBu** was measured on two different spectrometers with different results of 32% and 64%, respectively.

Regarding the S_{BET} surface areas, it was shown that the variation of the main chain has an effect on the porosity, but that it is not directly transferable to other side chains. Therefore, promising side chains have to be tested for the best side chain/main chain combination. Generally, angled arrangements of the main chain again seemed to be disadvantageous in comparison to linearly connected core segments. Also, flexible core or side chain structures resulted in low surface areas. Regarding the side chains, the *tert*-butylphenyl side chain showed by far the best results. Enlarging of the group either at the alkyl part or at the aryl part as well as introduction of another *tert*-butyl group reduced the surface area. The calculated pore size distributions confirmed the intrinsic microporosity of **PPV-DPtBu** and **PFV-DPtBu**, which showed the two highest S_{BET} surface areas, but also showed a non-uniform pore diameter distribution with occurring meso- or macropores.

Of the polymers with high surface area and AIE-activity, **PPV-DPtBu** gave the best combination of properties, with a high quantum yield of 32% (or 64%) and the highest surface area of $417\text{ m}^2\text{g}^{-1}$ and was put through additional testing. TGA measurement showed a good thermal stability up to 340°C . Via time resolved fluorescence decay measurements it was possible to show that the emission origins from two different emitting species. Explosive detection experiments carried out with picric acid showed a Stern-Volmer quenching constant of 3.4×10^4 -

$3.5 \times 10^4 \text{ M}^{-1}$ and a super-amplification effect with increasing quencher concentration. The low detection limit of 1.5 ppm for picric acid shows an excellent efficiency.

For a polymer with carbazole side chains **PPV-DPC** it was shown that it is possible to electrochemically crosslink the linear polymer. In presence of not-removable impurities of the keto monomer **PDK-DPC** only the polymer reacts selectively. The non-porous reactant **M-PPV-DPC** is, thereby, converted into a likewise non-porous polymer network **N1**. Furthermore, the pronounced AIE effect of **M-PPV-DPC** vanished upon network generation.

In future works it might be interesting to synthesize **PPV-DPtBu** with a defined *cis:trans* ratio, as this has been reported to influence quantum yields.⁸⁵ Furthermore, the resulting morphological changes should also influence surface areas.

Another interesting approach would be to investigate PAVs with alternating side chains similar to the arrangement in C-PIMs **2-5**, for example polymers **18** and **22** in Figure 58. This could create additional pores and, possibly, increase the surface area, considering that the polymers **PFV-DPtBu** and **PBV-DPtBu** showed promising S_{BET} surface areas.

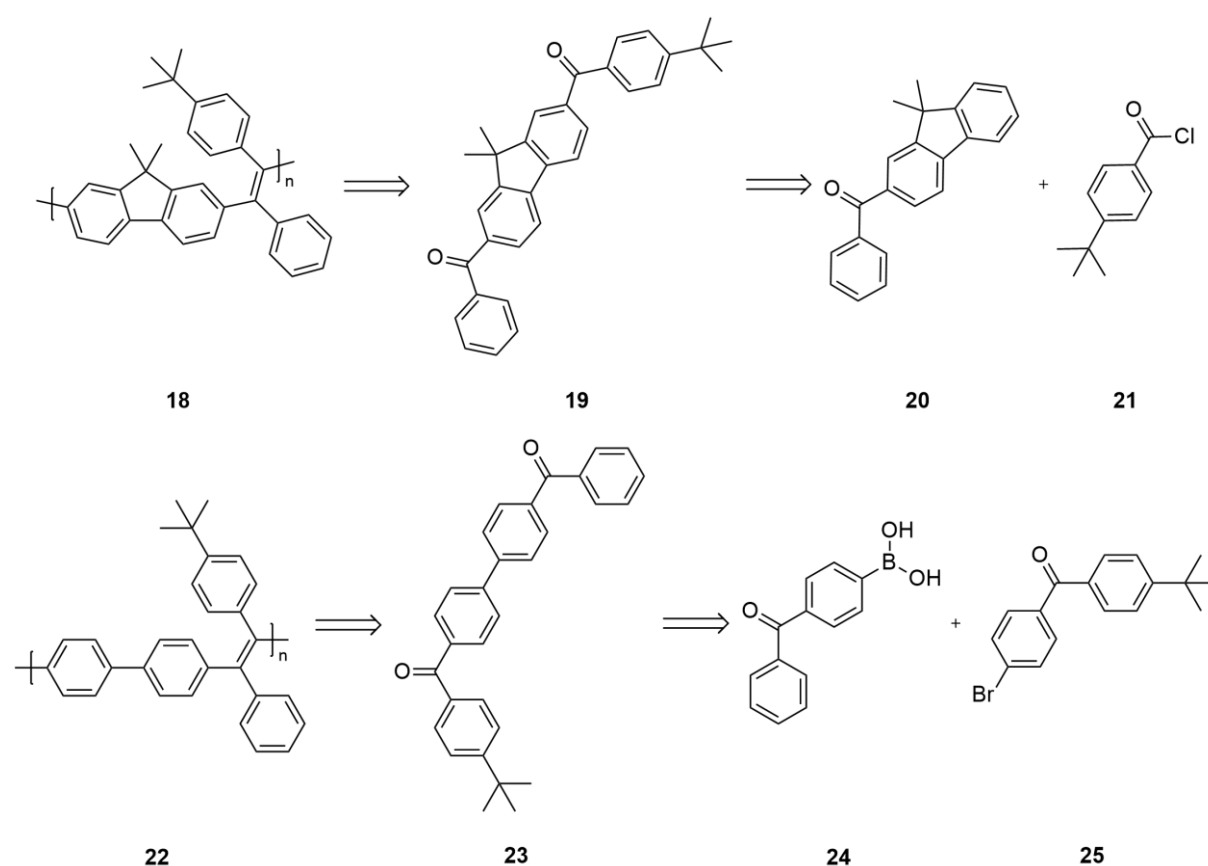


Figure 58 Retrosynthetic approach towards asymmetric PAVs.

Unsymmetrically substituted monomers should be easy to synthesize. For example, alternating phenylene and 4-*tert*-butylphenylene side chains could be introduced by the routes displayed in Figure 58. Monosubstituted fluorene is accessible by Friedel-Crafts acylation using equimolar ratios of fluorene and acid chloride.¹⁰⁴ The second acylation is likewise achievable by Friedel-Crafts reaction, as described previously. Unsymmetric biphenyl monomers can be obtained by Suzuki-Miyaura cross-coupling of facile building blocks.¹⁰⁵ The depicted boronic acid **24** is commercially available, while the bromide **25** can be obtained by Friedel-Crafts acylation.¹⁰⁶

3 Synthesis and Characterization of a Poly(anthrylene ethynylene)

3.1 Introduction

Poly(arylene ethynylene)s (PAE) as well as monomeric anthracene are known for their high emission efficiency, therefore, the combination of both structures has attracted academical interest.^{10,107-109} A polymer with very high PLQYs should be expected if the stacking can be prevented. Nevertheless, no soluble poly(anthrylene ethynylene) has been published up to now. The known polymers are limited to either structures with alternately introduced non-anthracene linkers, lowering the anthracene concentration per polymer, or to insoluble polymers. Two examples are depicted in Figure 59: Copolymer **26** by Yang *et al.*¹⁰⁷ and the on-surface synthesized poly(anthrylene ethynylene) **27** by Sánchez-Grande *et al.*^{107,109}

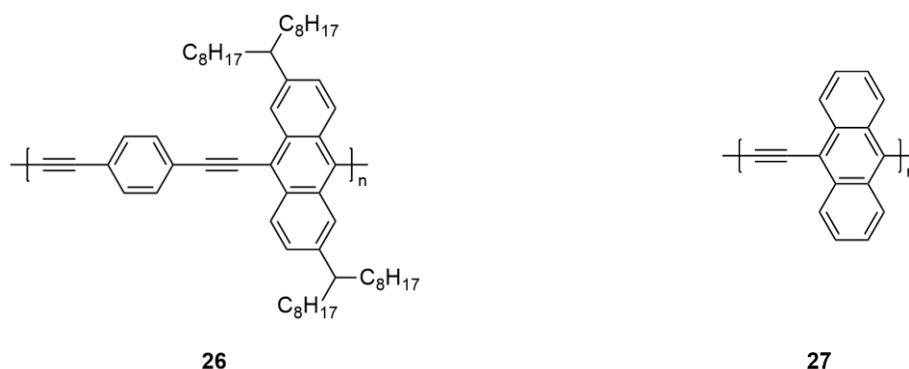


Figure 59 (Anthrylene ethynylene)-(phenylene ethynylene) copolymer **26**, and poly(anthrylene ethynylene) **27**.^{107,109}

3.1.1 Anthracene as chromophoric building block

Anthracene is a promising building block for conjugated polymers due to its unique features such as electron donor-acceptor properties, relatively high PL quantum yield, and good electrical properties.^{108,110-112} The continuous pattern of conjugated double bonds bestows properties on the molecule that are well suited for photoluminescent devices. Anthracene has, for example, been extensively studied for OLEDs due to its strong blue emission.^{107,113-115} However, easy photo-oxidation of the anthracene in ambient conditions requires a structural design that increases stability. One way to reduce photo-oxidation is lowering the reactivity through electron-accepting substituents.¹¹⁶ Therefore, a poly(anthrylene ethynylene) could provide a combination of the unique anthracene-related properties, advantages of polymeric structures, and an increased photostability all in once.

Another interesting advantage of anthracene can be observed in single crystals. The ordered molecules emit polarized light upon excitation due to their fluorescence anisotropy.¹¹⁷ The corresponding transition dipole moment is fixed to the short molecular axis (or y-axis) of anthracene as shown in Figure 60.^{14,118,119}

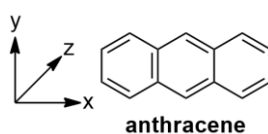


Figure 60 Structure of anthracene with assignment of the axes.

Molecules with polarized emission have the potential to reduce the brightness losses caused by the use of polarizers in polarized 3D systems and, therefore, lower energy consumption.¹²⁰ Furthermore, deployment of these materials in polarized OLEDs has been investigated.¹²¹ Hereby it has been shown that defined orientation of the dipole moment in OLED materials can increase the light outcoupling efficiency.^{122,123}

3.1.2 Fluorescence anisotropy

Upon excitation of a fluorophore, a change in the distribution of the electron density can be observed. The transition from ground state to excited state can be described by the transition dipole moment.¹⁴ The transition moment corresponds to the ability to absorb electromagnetic radiation and is fixed to a defined axis of the molecule. Fluorophores preferentially absorb light when the electric vectors are aligned parallel to the transition dipole.¹⁴ The fluorescence is

likewise fixed to an axis of the molecule. Therefore, when a sample is excited with polarized light, a photoselection of the randomly orientated fluorophores occurs, as sketched in Figure 61. Only the fluorophores with the transition dipole moment parallel to the light vector are excited which leads to a polarized emission.¹⁴ In practice, the anisotropy reached by this method is lower than in theory due to varying effects, the main cause being rotational diffusion during the lifetime of the excited state. For a small molecule in non-viscous solution, this effect is so strong that the anisotropy is normally near zero. Another randomizing factor can be the transfer of excitations.¹⁴

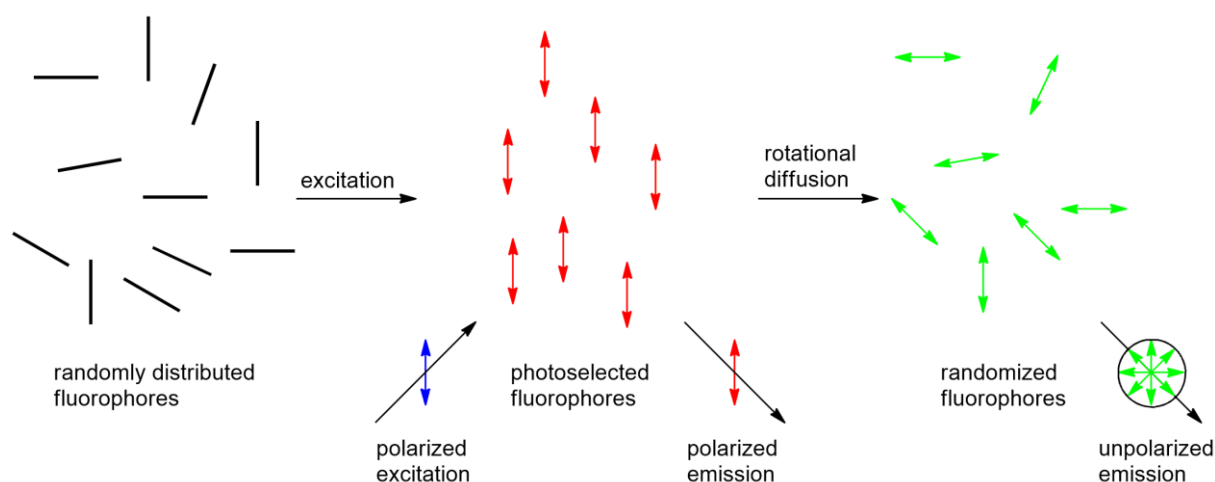


Figure 61 Effect of polarized excitation and rotational diffusion on the fluorescence anisotropy.

3.2 Objective and strategy

The anthracene-based, ethynylene polymer, poly[2,6-(2-octyldecyl)anthrylene-9,10-ethynylene] (**PAAE**), depicted in Figure 62, shall be synthesized and characterized. The specific alkyl chains in this positions were chosen based on the work of Yang *et al.*¹⁰⁷ to prevent stacking without inducing torsion of the polymer backbone. The polymer shall be compared to a monomeric reference compound regarding the fluorescence anisotropy. As representative of a monomeric unit the commercially available 9,10-bis(phenylethynyl)anthracene (**BPEA**) shall be used as reference material.

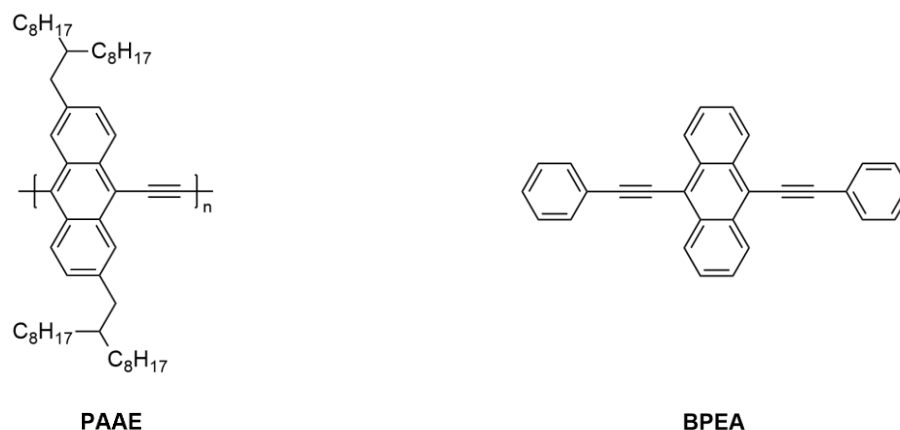


Figure 62 Structure of poly[2,6-(2-octyldecyl)anthrylene-9,10-ethynylene] (**PAAE**) and of the model compound **BPEA**.

3.3 Results and discussion

The general synthetic strategy towards **PAAE**, depicted in Figure 63, was developed on basis of the work of Sánchez-Grande *et al.*¹⁰⁹. The literature on-surface synthesis of a poly(anthrylene ethynylene) was adapted to solution-state synthesis by adding alkyl chains to the monomer for an improved solubility and to prevent an ACQ effect.^{17,20,107} Furthermore, the reduction by thermal annealing on an Au(111) surface had to be replaced by a suitable reducing agent. The polymer is shown as both possible electron isomers, a cumulene and the, expectantly better stabilized, PAE-type structure. It is expected that the dibromomethylene end-groups corresponding to the cumulene-type structure are hydrolysed upon work up. Upon addition to the water/methanol mixture the olefinic end groups should be converted to single-bonded end groups corresponding to the **PAAE** structure. The formed end groups are expected to contain carbonyl groups like carboxylic acids, esters or aldehydes.

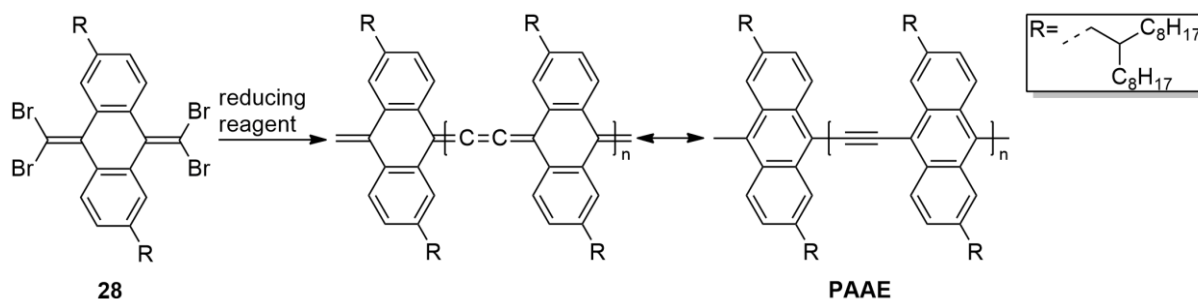


Figure 63 General synthetic strategy towards **PAAE**.

3.3.1 Synthesis of the bis-geminal tetrabromide monomer

Figure 64 depicts the synthetic pathway for the synthesis of the 9,10-bis(dibromomethylene)-2,6-bis(2-otyldecyl)-9,10-dihydroanthracene (**28**) monomer starting from commercially available 2,6-diaminoanthraquinone (**29**).

2,6-Diaminoanthraquinone (**29**) was brominated in a twofold Sandmeyer-type reaction as described by Seidel *et al.*¹²⁴. Hereby, the amines react with *tert*-butyl nitrite to diazonium salts that undergo a radical-nucleophilic aromatic substitution reaction with *in situ* generated copper(I) bromide. 2,6-Dibromoanthraquinone (**30**) was obtained in 88% yield. The formation of the product can be confirmed by the absence of amine proton-related signals in the ¹H-NMR spectrum of **30** below 5 ppm, in combination with a molar mass, obtained by high-resolution mass spectrometry of 363.8816 m/z, corresponding to the calculated mass of the product.

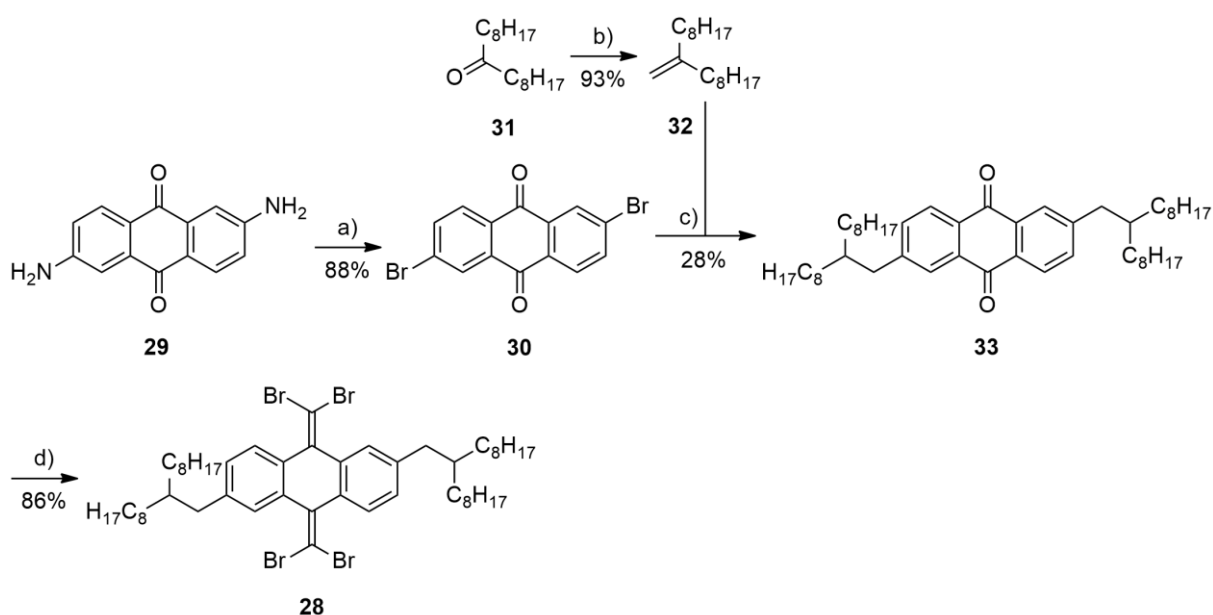


Figure 64 Synthesis of monomer **28** a) *t*-BuNO₂, CuBr₂, ACN, 85 °C, 4 h; b) NaH, Ph₃PMeBr, DMSO, rt, 20 h; c) 1.) 9-BBN, THF, rt, 23 h, 2.) Pd(PPh₃)₄, K₂CO₃, 75 °C, 23 h; d) CBr₄, PPh₃, toluene, 80 °C, 24 h.

The alkyl chains were introduced following a method by Yang *et al.*¹⁰⁷. First, 9-methyleneheptadecane (**32**) was obtained from commercially available 9-heptadecanone (**31**) by Wittig reaction. An ylide was generated by deprotonation of methyltriphenylphosphonium bromide by sodium hydride. The ylide adds to the ketone in a [2+2] cycloaddition. Driven by the oxophilicity of the phosphor, the oxaphosphetane quickly reacts to the 9-methyleneheptadecane (**32**) in 93% yield. The product shows an additional singlet for the two new protons at 4.69 ppm in the ¹H-

NMR spectrum. In the $^{13}\text{C}\{\text{H}\}$ -NMR spectrum it shows two signals for the double bond carbons at 150.6 ppm and 108.5 ppm instead of one strongly downfield shifted carbon of the ketone in the starting material. In the next step, the alkylethylene **32** was hydroborated by the sterically demanding 9-borabicyclo[3.3.1]nonane (9-BBN) to the anti-Markovnikov product. In a one pot reaction the obtained terminal boronic ester was Suzuki-coupled using tetrakis(triphenylphosphine)palladium(0) as catalyst and potassium carbonate as base. The alkylated anthraquinone **33** was obtained in 28% yield as confirmed by the appearance of the expected aliphatic and aromatic signals in the ^1H -NMR spectrum and the correct integral ratio. In the last step, the anthraquinone **33** was converted to the desired monomer **28** in a Corey-Fuchs reaction as described by Pola *et al.*¹²⁵. Triphenylphosphine and carbon tetrabromide react to a phosphorous ylide that undergoes a Wittig reaction with the ketones to yield the dibromomethylene compound **28** in 86% yield. The product shows an additional $^{13}\text{C}\{\text{H}\}$ -NMR signal at 89.4 ppm for the dibromomethylene groups. The carbon signal of the former ketone carbon of the starting material at 183.6 ppm is strongly upfield shifted. Figure 65 shows the ^1H - and $^{13}\text{C}\{\text{H}\}$ -NMR spectra of the monomer **28**.

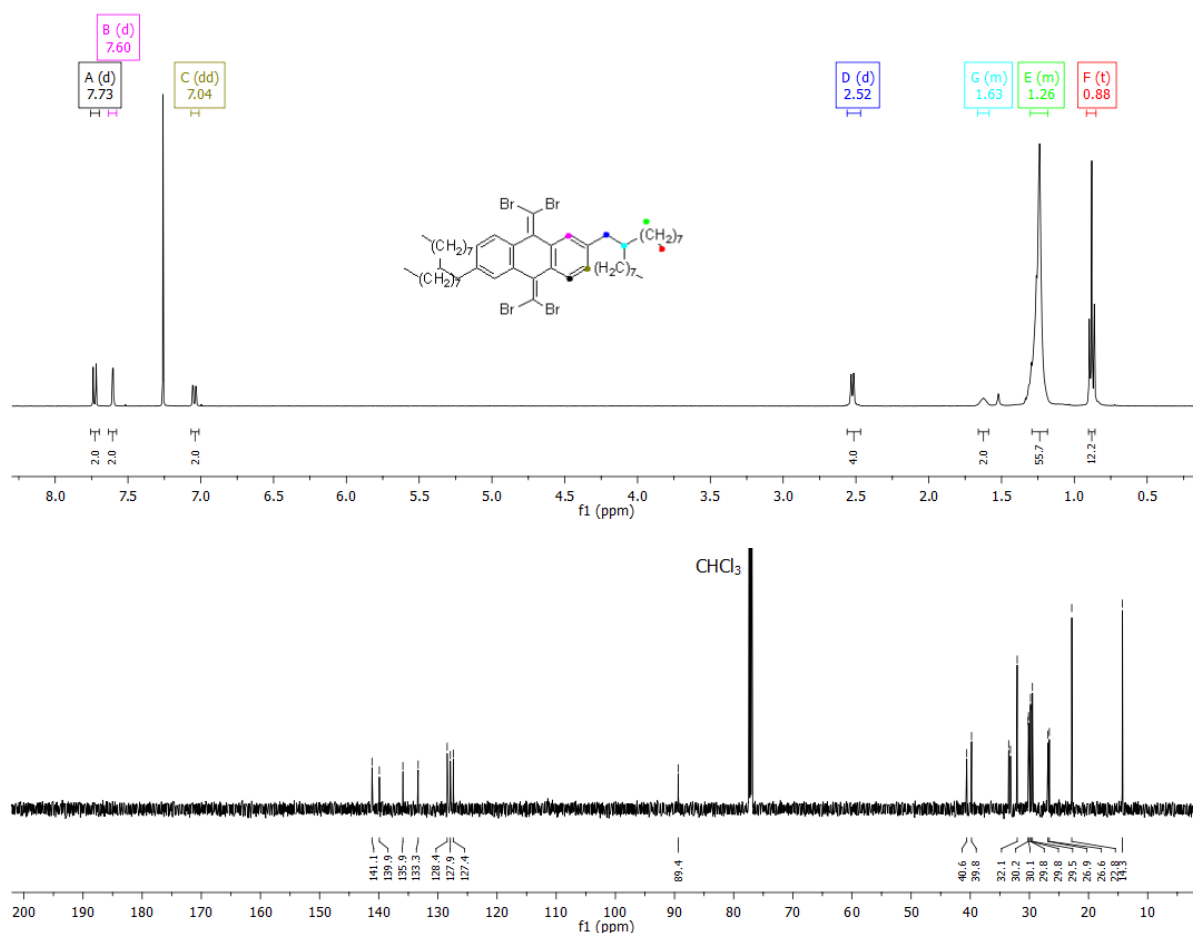


Figure 65 ^1H - and $^{13}\text{C}\{\text{H}\}$ -NMR spectra of monomer **28** in CDCl_3 at room temperature.

In the aromatic region of the $^1\text{H-NMR}$ spectrum the three signals of the anthracene core can be found at 7.73 ppm (black), 7.60 ppm (magenta), and 7.04 ppm (dark yellow). Additional to the coupling of the directly neighbouring protons a 4J -coupling (1.5/1.7 Hz) of signals at 7.60 ppm and 7.04 ppm can be observed. In the aliphatic region of the spectrum the typical signals of the branched alkyl chain can be observed. The doublet of the methylene unit that is directly connected to the aromatic ring (blue) is shifted downfield (2.52 ppm) in comparison to the other alkyl signals.

3.3.2 Synthesis and Characterization of PAAE

For the synthesis of PAAE in solution the method by Sánchez-Grande *et al.*¹⁰⁹ cannot be used. Instead of thermal annealing of the monomer on a gold surface used for the on-surface synthesis, a suitable reducing reagent had to be found for a polycondensation reaction in solution as depicted in Figure 63.

Also based on procedures described in Chapter 2.3.2, different reagents were tested. The results are summarized in Table 15. The first attempt was to couple the tetrabromide monomer **29** using the conditions applied for the polycondensation of the tetrachlorides in Chapter 2.3.2. The dicobalt octacarbonyl reagent gave the desired product as oligomers in rather low yields. Next, chromium(II) acetate was used according to the method by Hörhold *et al.*⁶⁶. This did not yield product formation, neither did bis(cycloocta-1,5-diene)nickel or bis(triphenylphosphine)dicarbonylnickel that were introduced by Reisch *et al.*⁷³ for C-C coupling of dibenzylic, geminal dichloro compounds, as described earlier. Additionally, metallic copper and zinc as well as a mixture of zinc and copper(I) chloride were tested in reference to the synthesis of tetraphenylethylene from diphenyldichloromethane without success.^{126,127} The final approach was to use a butyllithium and copper(I) cyanide mixture based on a work of Iyoda *et al.*¹²⁸ describing the formation of butatriene derivatives under these conditions. This method produced the desired polymer in 53% yield with a mean average molar mass of $M_n=7100$ g/mol (ethyl acetate fraction), and a small larger molecular weight fraction with a M_n of 13000 g/mol (chloroform fraction).

Table 15 Results of the reagent screening for the synthesis of **PAAE**.

Reagent	Ethyl acetate fraction		Chloroform fraction	
	Yield [%]	Molecular weights M_n/M_w [g/mol]	Yield [%]	Molecular weights M_n/M_w [g/mol]
Co₂(CO)₈	0.4	5500/7300	0.3	5300/8000
Cr₂(OAc)₄	-	-	-	-
Ni(COD)₂	-	-	-	-
Ni(PPh₃)(CO)₂	-	-	-	-
Cu	-	-	-	-
Zn	-	-	-	-
Zn, CuCl	-	-	-	-
<i>n</i>-BuLi, CuCN	53	7100/16600	0.5	13000/44400

Further characterization was carried out with the ethyl acetate fraction of the polymer. The fraction has a PDI of 2.33 and a degree of polymerization of circa 10. The ¹H- and ¹³C{H}-NMR spectra are shown in Figure 66.

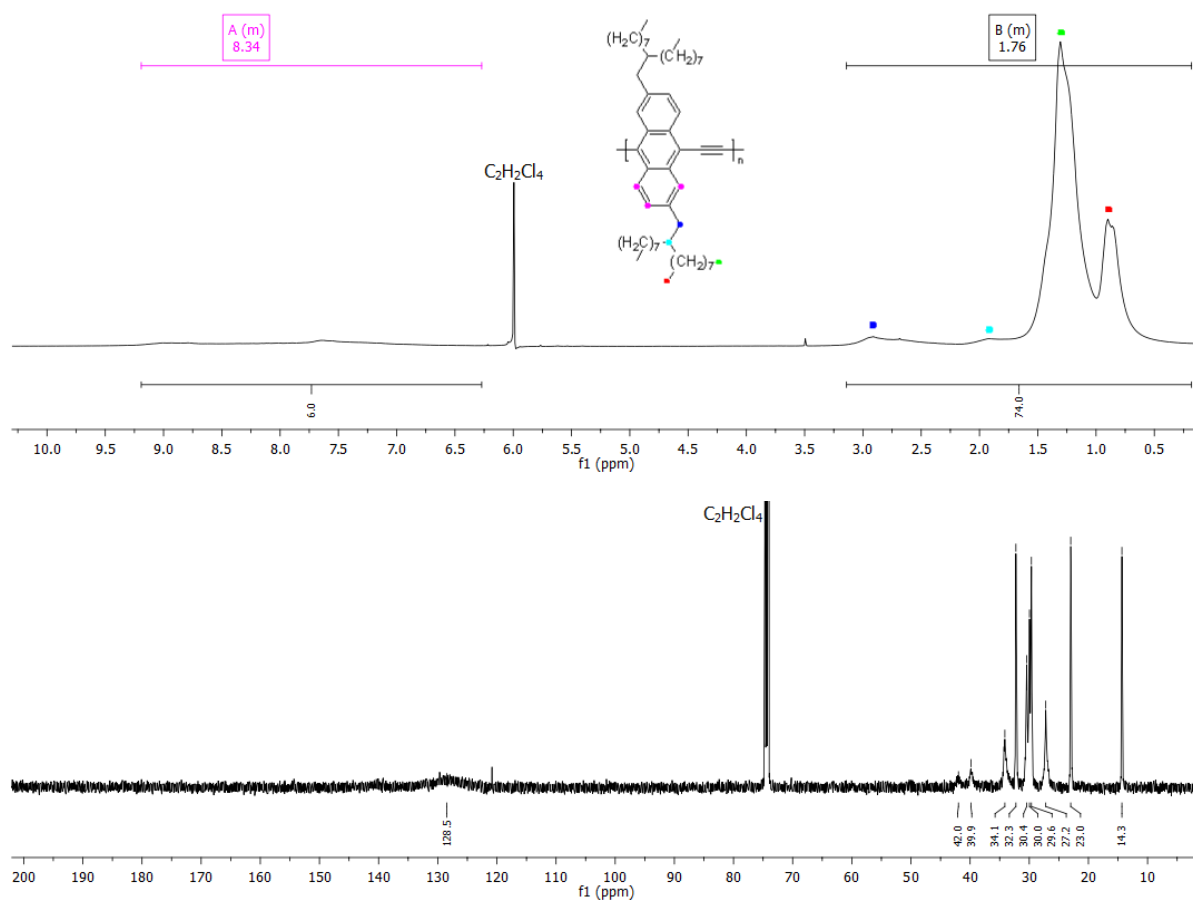


Figure 66 ¹H- and ¹³C{H}-NMR spectra of polymer **PAAE** in C₂D₂Cl₄ at 353 K.

In the $^1\text{H-NMR}$ spectrum the aromatic protons show a broad multiplet from 9.21 ppm to 6.48 ppm and the aliphatic protons from 3.25 ppm to 0.25 ppm. Even though there is no clear separation, the four characteristic signals of the alkyl chain are still discernible. In the $^{13}\text{C}\{\text{H}\}$ -NMR spectrum the aromatic carbons appear as broad multiplet from 134.9 to 122.0 ppm. The alkyl chains show the expected ten signals in the upfield region.

The IR spectrum of **PAAE**, displayed in Figure 67, shows three strong, aliphatic C-H vibration bands at 2954, 2923, and 2847 cm^{-1} . The carbonyl stretching vibration bands of the expected end-groups are found at 1778, 1727, 1675, 1626, and 1612 cm^{-1} . This hints at the presence of different end groups. A definite assignment of the signals is difficult due to the strong aliphatic C-H vibration bands that could superimpose O-H or C-H stretching bands of carboxylic acids or aldehydes.

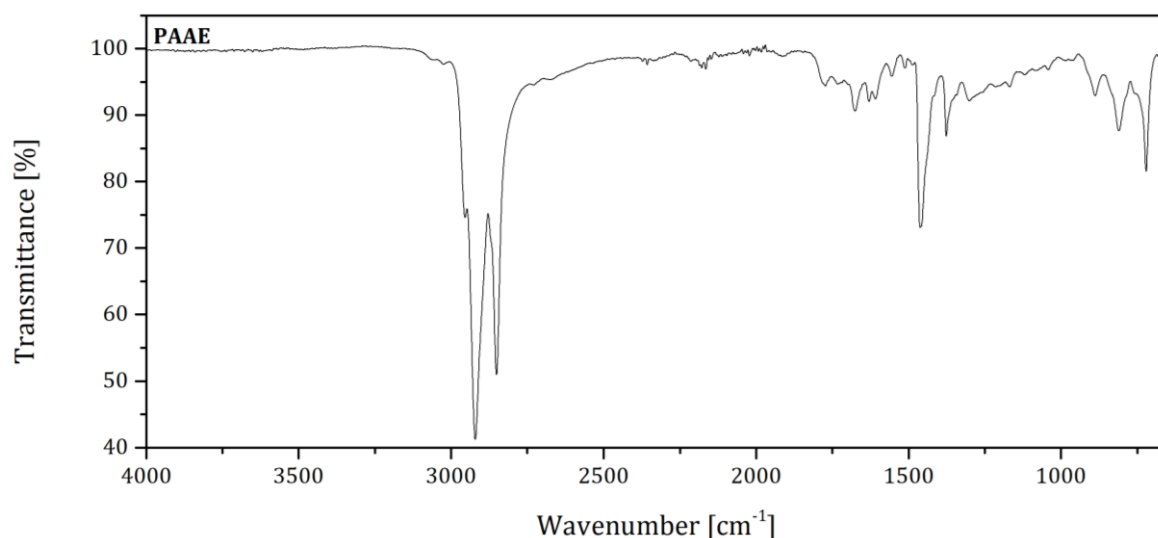


Figure 67 IR spectrum of **PAAE**.

Thermogravimetric analysis (TGA) was carried out in the temperature range from 35 °C to 950 °C with a heating rate of 10 °C/min. The polymer **PAAE** shows a good thermal stability with a weight loss of 5% at 279 °C. Phase transitions of the polymer were investigated via differential scanning calorimetry (DSC) in a temperature range from -20 °C to 150 °C in an argon atmosphere and a heating rate of 10 °C/min. In this temperature range neither glass transition nor crystallization/melting signals were observed.

Figure 68 displays the absorption and emission spectra of **PAAE** in chloroform solution and solid state also compared to the model monomer **BPEA**. A thin film of **BPEA** was obtained using polystyrene as polymer matrix. The absorption spectrum of **PAAE** in solution shows a

broad maximum at 502 nm. There is an additional weak maximum at 385 nm. This can be attributed to the absorption of localized anthracene chromophores because it is similar to one of those of pure anthracene.¹⁰⁷ In the solid state the absorption spectrum shows a very similar trend with a maximum at 506 nm. The additional maximum is less pronounced in film than in the solution spectrum where it appears as slight shoulder. The absorption spectra, especially in solution, are rather broad. This can be explained by the increased torsion angles of the PPE backbone in solution.¹⁰ This is furthermore supported by the reported distortion of neighbouring 9,10-anthrylene units in dianthrylacetylene dimers and broad unstructured absorption bands occurring in related trimers.¹²⁹⁻¹³¹ The orange/red emission maximum of **PAAE** shifts bathochromically from 611 nm in solution to 687 nm in thin film.

The absorption spectrum of the less flexible **BPEA** shows the expected narrow peak with the maxima at 437 and 459 nm in chloroform solution. They are shifted hypsochromically in comparison to the polymer due to the limited conjugation length in the monomeric compound. Upon going to a thin film, a slight bathochromic shift of the absorption maxima to 447 nm and 470 nm is observed. However, the emission peak strongly shifts from a defined, narrow peak at 475 nm with shoulders at 508 and 536 nm to one broad maximum at 568 nm. These results can be attributed to the stronger intermolecular interactions in solid state with a dominating aggregate emission.

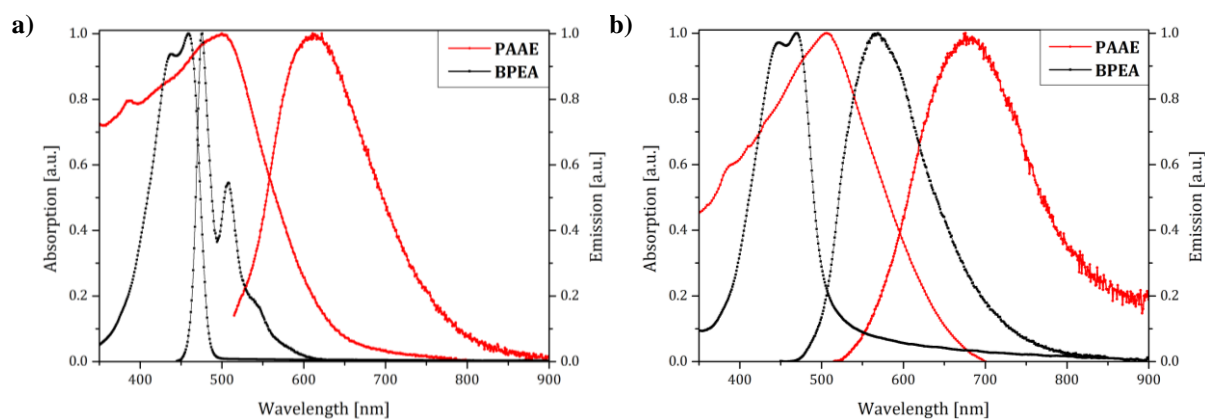


Figure 68 Absorption and emission spectra of polymer **PAAE** and model compound **BPEA** a) in chloroform solution and b) as film on quartz glass.

This is emphasized by the strong ACQ effect seen in the photoluminescence quantum yields summarized in Table 16. The quantum yield of the **BPEA** film is almost five times lower than in solution state. The PLQY in solution of 93% is near unity and in good agreement to literature.¹³² **PAAE** on the other hand shows a much lower PLQY of 7.2% in solution and despite substitution with the bulky alkyl chains an ACQ effect can be observed.

The Stokes shift of **BPEA** with a value of 734 cm^{-1} in solution is very low, as expected for a rigid structure, but absorption and emission spectra are no mirror images. This is caused by the adaption of different conformations of the rotating phenyl rings of **BPEA** while the emission is mostly contributed by a planar conformation.¹³³ The increased distortion of the polymer chain leads to a greater Stokes shift of 3554 cm^{-1} for **PAAE** in solution. In solid state both Stokes shifts of **BPEA** and **PAAE** increase significantly to 3671 cm^{-1} and 5207 cm^{-1} , respectively, due to the occurrence of bathochromically shifted aggregate emissions.

Table 16 Room temperature PLQYs of polymer **PAAE** and model compound **BPEA**.

Compound	CHCl ₃	Film
PAAE	0.072	0.038
BPEA	0.93	0.19 ^a

^a Prepared by using a polystyrene matrix

The highest occupied molecular orbital (HOMO) energy level of **PAAE** with a value of $E_{\text{HOMO}} = -5.49\text{ eV}$ was determined by photoemission spectroscopy. The LUMO energy was obtained by subtracting the onset absorption energy derived from the solid state absorption spectrum. The energy of the absorption onset ($E_g^{\text{opt}} = 2.24\text{ eV}$) was determined by Equation 5.¹³⁴

$$E_g^{\text{opt}} = \frac{1243.125\text{ nm} \cdot \text{eV}}{\lambda_g} + 0.3\text{ eV} \quad (5)$$

where E_g^{opt} is the optical bandgap, $1243.125\text{ nm} \cdot \text{eV}$ equals the product of Planck constant and speed of light, λ_g is the wavelength of the absorption onset, and 0.3 eV is a correction for the average exciton binding energy.¹³⁴

The energy of the LUMO level was calculated to be $E_{\text{LUMO}} = -3.25\text{ eV}$.

3.3.3 Fluorescence anisotropy of **BPEA** and **PAAE**

The following results were obtained in cooperation with the group of Prof. Dr. John Lupton from the physics department of the University of Regensburg with the main contribution by Jakob Schedlbauer who carried out the measurements.

The low quantum yields of **PAAE** did not allow for reliable results in single molecule measurements, therefore anisotropy measurements were carried out in toluene solution. The fluorescence anisotropy (r) is defined by Equation 6.¹⁴

$$r = \frac{I_{\parallel} - I_{\perp}}{I_{\parallel} + 2I_{\perp}} \quad (6)$$

where I_{\parallel} and I_{\perp} are the fluorescence intensities of the vertically (\parallel) and horizontally (\perp) polarized emission, when the sample is excited with vertically polarized light.

First, the anisotropy of the model compound **BPEA** was measured for two different excitation wavelengths at the absorption maxima displayed in Figure 69. On a time scale the expected anisotropy can be observed directly after the excitation, followed by a decrease due to the rotation of the molecules in solution. A dependence of the excitation wavelength cannot be observed.

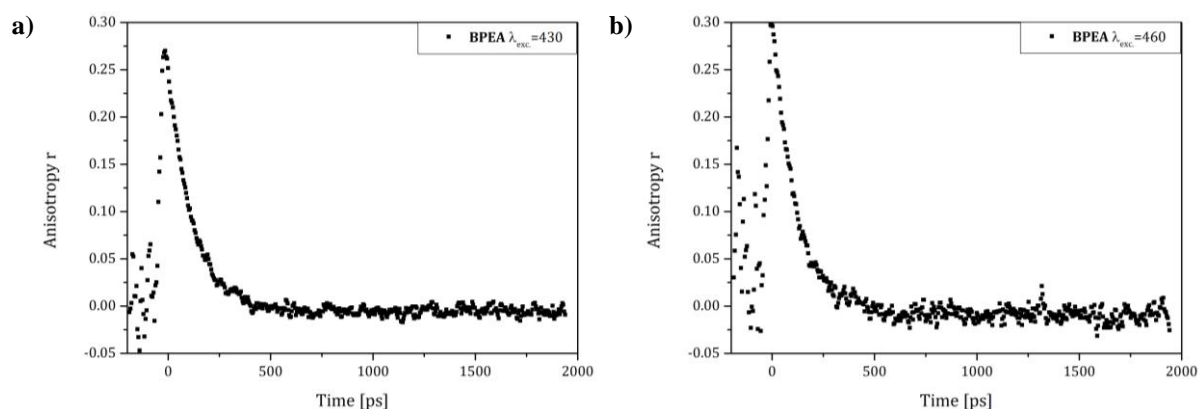


Figure 69 Time dependence of the fluorescence anisotropy of **BPEA** at different excitation wavelengths (detection: 470 nm-550 nm.).

Subsequently, the anisotropy was observed at a defined time after excitation over the whole emission spectrum, as shown in Figure 70. It is apparent that the anisotropy is wavelength independent regarding excitation as well as emission wavelength. These results show that the model compound has a well-defined transition dipole moment.

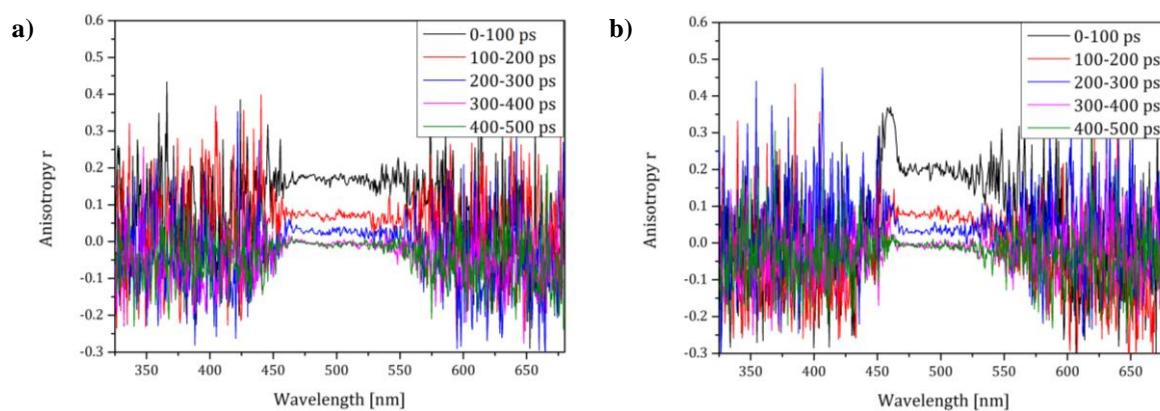


Figure 70 Wavelength dependency of the fluorescence anisotropy of **BPEA** at an excitation wavelength of a) 430 nm and b) 460 nm.

For the polymer **PAAE** the same measurements were carried out at four different wavelengths, as displayed in Figure 71. For **PAAE** a fluorescence anisotropy can be observed that dissipates slower than that of the model compound **BPEA**. The reason for this is the higher molecular weight that is accompanied by slower rotation of the polymer in solution. With decreasing excitation wavelength a decreasing maximal anisotropy can be observed, indicating that the transition dipole moment is not clearly defined. This is confirmed by the measurement of the fluorescence anisotropy over the whole emission wavelength range. The graphs were recorded in the time window from 100 ps to 300 ps, this equals the starting, maximal value of the anisotropy. It can be observed that the anisotropy decreases with an increasing emission wavelength and is close to zero in the higher wavelength region of the spectrum for all excitation wavelengths. For the lower excitation wavelength, this is even stronger than for 460 nm and 490 nm. This observation confirms the absence of a clearly defined transition dipole moment. The reason could be the vertical incorporation of the anthracenes into the polymer structure. Even though the dipole moment of pure anthracene is located along the short molecule axis, it is possible that by substitution the transition moment partly changes towards the long axis. This would result in different dipole moments for the anthracene units and the main polymer backbone. To confirm this theory further investigations would be required. Furthermore, the four different excitation wavelength graphs are spectrally shifted relative to each other along the wavelength axis, the reason most likely being the high PDI of the sample. Due to the relatively short length of the polymer a change of molecular weight has a large effect on the emission spectra, meaning that different wavelengths excite different subpopulations unequally. This could also partially cause the occurrence of the broad absorption and emission bands of **PAAE**.

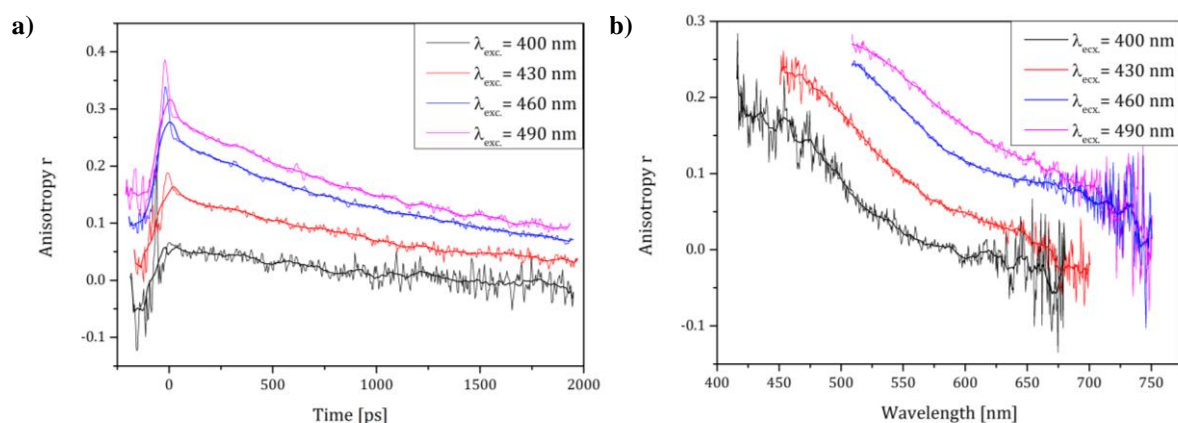


Figure 71 a) Time dependency of the fluorescence anisotropy (detection: 500 nm-550 nm) and b) wavelength dependency of the fluorescence anisotropy of **PAAE** in the time window of 100-300 ps.

3.4 Conclusion and Outlook

The poly(anthrylene ethynylene) **PAAE** was synthesized for the first time from the tetrabromide **28** in a newly developed synthesis route. Using a *n*-butyllithium/copper cyanide mixture as reducing agent **PAAE** was obtained in a yield of 53% with a mean average molecular weight of $M_n=7100$ g/mol.

The obtained polymer showed a good thermal stability with a weight loss of 5% at 279 °C and an optical bandgap of $E_g^{opt} = 2.24$ eV. Absorption and emission spectra of **PAAE** were surprisingly broad, which is most likely caused by the high PDI of the sample and a highly distorted conformation of the polymer backbone. The orange/red emission maximum of **PAAE** appears at 611 nm in solution, and at 687 nm in thin film. Despite the introduction of the bulky alkyl side chains an ACQ effect could not be prevented. Therefore, the maximal quantum yield of 7% is measured in solution.

Fluorescence anisotropy measurements showed PL anisotropies for the model compound **BPEA** as well as for the polymer **PAAE**. While the commercially available model compound **BPEA** displays a clearly defined transition dipole moment, in **PAAE** the anisotropy is wavelength dependent. Therefore, it can be concluded that the transition moment of **PAAE** is not clearly defined. Additionally, the high PDI of the sample resulted in an excitation wavelength dependency of the anisotropy, by exciting of different subpopulations of the polymer chains.

In a future work a screening of different side chains including linear alkyl chains or alkoxy chains could possibly lead to poly(anthrylene ethynylene)s without ACQ, and lead to efficiently red emitting polymers. A higher PLQY would also allow single molecule anisotropy measurements, for a deeper understanding of the already obtained data.

The developed synthesis method could, furthermore, be applied to other, elongated acenediones as tetracenedione or pentacenedione, to obtain, for example, the polymers depicted in Figure 72. The required bromo-substituted diones can be obtained by literature procedure.^{135,136}

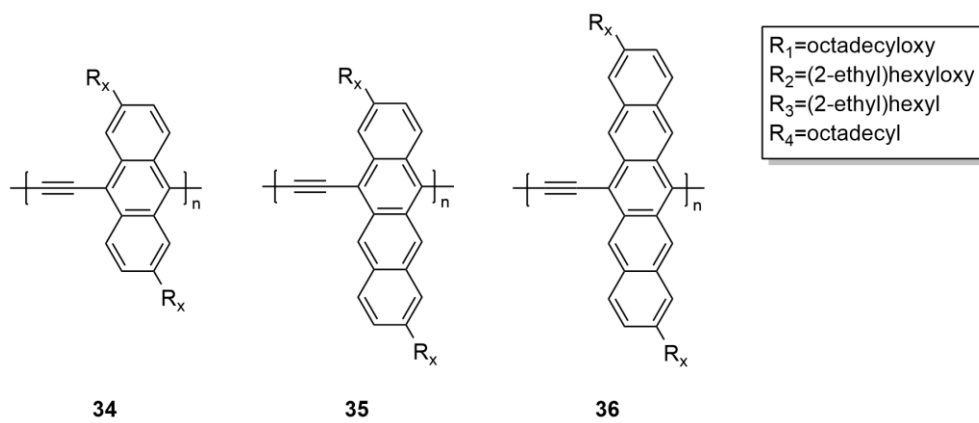


Figure 72 General structures of PAEs 35-37.

4 Experimental Part

4.1 General

All commercially available **chemicals and solvents** including dried solvents were obtained from the suppliers Fisher Scientific, Sigma-Aldrich Co., ABCR GmbH, VWR International GmbH, TCI Deutschland GmbH, chemPUR GmbH, Carl Roth GmbH + Co. KG, Santa Cruz Biotechnology Inc., and Merck KGaA and used without further purification. Acetonitrile was dried over calcium hydride and stored over molecular sieve 3 Å.

Reactions under **argon atmosphere** were carried out using standard Schlenk techniques and flame dried glassware.

Reactions were monitored by **thin-layer chromatography** using ALUGRAM® SIL G/UV 254 silica gel plates from Macherey-Nagel with a thickness of 0.2 mm. The visualization was carried out using an UV lamp at 254 nm and 365 nm or common staining reagents.

Flash column chromatography was carried out using a system by Biotage (Isolera™ One) with pre-packed silica gel columns by Büchi Labortechnik GmbH.

¹H- and ¹³C{H}-NMR spectra were recorded on Bruker AVANCE 400 MHz- or AVANCE III 600 MHz-NMR spectrometers using deuterated solvents. All spectra were referenced to the residual solvent signal. Spin multiplicities were given as follows: s (singlet), d (doublet), t (triplet), q (quartet), m (multiplet), dd (doublet of doublet). Assignment of the signals was supported by COSY- and HSQC-correlation spectra when necessary.

APCI (Atmospheric Pressure Chemical Ionization) and ESI (electrospray ionisation) **mass spectrometry** (MS) was carried out on a Bruker Daltronik micrOTOF system. For APCI an APCI unit with corona discharge needle was used. FD (field desorption) mass spectra were obtained from a JEOL AccuTOF-GCX spectrometer.

Gel permeation chromatography (GPC) measurements were carried out on a PSS/Agilent SEcURITY GPC system equipped with a diode array detector (G1362A) and a refractive index detector (G1362A). Separation was carried out on a set of two PSS SDV Linear S columns (8 x 300 mm, particle size 5 µm) and a PSS SDV precolumn (8 x 300 mm, particle size 5 µm) at room temperature using chloroform or THF as the eluent. The flow rate was 1 ml/min and the molar masses were referenced to a polystyrene standard.

High temperature GPCs were carried out at the Max-Planck-Institut für Polymerforschung in Mainz on a GPC system equipped with a refractive index detector model Agilent PL220. Separation was carried out on a PSS SDV (8.0 mm x 50 mm, particle size 10 μm) and three PSS SDV (8.0 mm x 300 mm, particle size 10 μm) columns at 160°C using 1,2,4-trichlorobenzene (TCB) as eluent. The flow rate was 1 ml/min and the molar masses were referenced to an internal polystyrene standard.

Infrared spectroscopy was carried out on a Jasco FT/IR-4200 Fourier-Transform spectrometer equipped with an ATR unit.

UV/VIS absorption spectra were obtained on a Jasco V-670 spectrometer.

Photoluminescence spectra were measured on a Horiba Scientific FluoroMax-4 spectrometer at room temperature. Quantum yields were obtained in an integrating sphere accessory (QuantaPhi).

Spin coated polymer films were obtained from 7 mg/ml chloroform solutions on quartz glass using a Süss MicroTec **Spin-Coater** at a rotational speed of 1000 rpm. 20 mg polystyrene was added to the solution of BPEA as polymer matrix.

HOMO energy levels were determined by **photoemission spectroscopy**. Measurements were carried out on a Riken Keiki (AC-2) spectrometer.

Nitrogen **adsorption-desorption isotherms** were recorded on a BEL Japan Inc Belsorp-max system at 77 K. The surface areas were calculated using the BET model in the pressure range p/p_0 from 0.05–0.25. All samples were degassed offline at >100 °C for 16 hours under a vacuum. Krypton measurements were carried out on the same system after washing with overcritical CO_2 .

Thermogravimetric analysis and **Differential Scanning Calorimetry** were carried out in a Mettler Toledo TGA/DSC1 STAR-System under an argon stream of 50 ml/min and a heating rate of 10 K/min.

Atomic force microscopy (AFM) was carried out on a diInnova by Bruker. The measurements were carried out as films on an ITO coated quartz glass, in the intermittent modus. To determine the thickness of the layer the film was cut with the help of a diamond cutter.

Analytical and preparative **electrochemistry** were carried out in a VersaSTAT4 potentiostat from Princeton applied research. Gravimetric measurements were obtained using a quartz crystal microbalance QCM922A system by Princeton applied research. Measurements were carried out with a three electrode setup at 25°C using dry solvents under an argon atmosphere.

Analytical measurements were carried out in a cell with 5 ml solvent volume. The working electrode was a platinum disc of 1 mm diameter, the counter electrode a platinum wire of 0.7 mm diameter, and Ag⁰/AgNO₃ (U= 0.60 V vs. NHE, c(AgNO₃)= 0.01 mol/l, c(TBAP)= 0.01 mol/l in ACN) was used as the reference electrode.

Preparative film formation was carried out in a cell with 10 ml solvent. As working electrode an indium tin oxide coated quartz glass with a size of 12.5 mm by 40 mm by PGO GmbH was used. The counter electrode was a platinum coated gauze with a size of 10 mm by 25 mm, and the reference electrode was identical as used in the analytical measurements.

Gravimetric measurements were carried out using a platinum coated quartz crystal as working electrode with a surface area of 0.165 cm². Counter and reference electrode were the same as in the analytical measurements. The used cell had a solvent volume of 20 ml. The mass changes were detected by the changes of the frequency of the quartz crystal resonator of the microbalance. This is based on the Sauerbrey equation with an conversion factor of 1.068 ng/Hz.¹⁰¹

All electrochemical measurements were carried out in dichloromethane with tetrabutylammonium hexafluorophosphate (TBAPF₆) as supporting electrolyte. The generated networks were carefully washed with dichloromethane and, then, the polymer was removed from the ITO glass plate using acetonitrile. After 24 hours the network was collected and treated with ethanol. The ethanol was renewed three times, after 24 hours each, by decantation. Then, prior to the gas adsorption measurements, the network was washed with **supercritical CO₂** using a TousimisTM (sandri-795) apparatus. Four cycles were conducted (0.5 h, 1 h, 2.5 h, and 18 h).

4.1.1 Experimental details from chapter 2.3.6

The experimental details are cited as published.⁸⁹

Single crystal X-ray structures were obtained on a Bruker-AXS Kappa Mach3 APEX-II-diffractometer with a FR591 rotating anode, equipped with graded multilayer optics emitting

copper radiation (1.54178 Å), and measured at 100 K. For structure solution and refinement, the SHELX-package^{137,138} was used as integrated in Olex2.¹³⁹

Solutions and film preparation: An appropriate amount of powder of each compound was diluted in THF to prepare a stock solution with an optical density of 1.0 at the excitation wavelength used for the experiments. Then, 100 µL of the stock solution was diluted with the proper amount of THF or THF/water mixture to obtain the desired water fraction ($f_w = 0\text{--}95\%$, v/v) in 2 mL of final volume. Thin films from the compounds were obtained with a desktop precision spin-coating system, model P6700 series from Speedline Technologies, as described elsewhere.¹⁴⁰ Briefly, thin films from the samples were obtained by deposition of ca. 50 µL from a solution of the compounds onto a circular sapphire substrate (10 mm diameter) followed by spin-coating (2500 rpm) in a nitrogen-saturated atmosphere (2 psi). The solutions for spin-coating were prepared by adding 2 mg of the samples to 200 µL of chloroform solution, with stirring, at environment temperature, overnight. 15 mg of Zeonex® was added to the chloroform solution of the model compounds, TPE, TPE-DtBu, and DPE-DN, as a polymeric matrix to obtain thin films of these samples.

The **absorption spectra** were recorded using Shimadzu UV-2450 or Agilent Cary 5000 UV-vis-NIR spectrometers. Absorption spectra of the transparent thin films were obtained in absorption mode using a clean sapphire substrate as the reference sample. The absorption spectra of the amorphous powder samples were recorded by collecting diffuse reflectance using a Cary 5000 DRA (an integrating sphere accessory with detection in the 200–2500 nm range). Background correction was performed by collecting the baseline with 100% and 0% reflectance (using a polytetrafluoroethylene (PTFE) reference sample and a blocked beam, respectively) prior to the determination of the spectra of the solid samples. Conversion to absorption was performed assuming the Kubelka–Munk function, $F(R)$.¹⁴¹

Fluorescence spectroscopic studies were performed using a Horiba-Jobin-Yvon Fluorolog 3-22 spectrofluorometer. The fluorescence quantum yields (ϕ_F) of all compounds, in solution or in the solid state, were measured using the absolute method with a Hamamatsu Quantaurus QY absolute photoluminescence quantum yield spectrometer, model C11347 (integrating sphere). A clean sapphire substrate was used as a reference for the ϕ_F measurements of solid-state thin films.

Fluorescence decays were measured using a home-built Time-Correlated Single Photon Counting (TCSPC) apparatus described previously.¹⁴⁰ An IBH nanoLED (339 nm, 1.0 kHz)

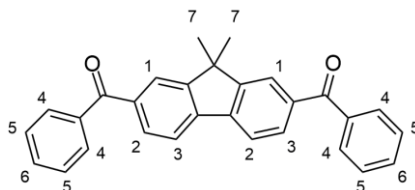
was used as the excitation source. The fluorescence decays and the instrumental response function (IRF) were collected using 1024 channels on a time scale of up to 48.8 ps per channel; alternate measurements (500 counts) of the pulse profile at the excitation wavelength and the sample emission were performed until 3000 counts at the maximum were reached. Deconvolution of the fluorescence decay curves was performed using the modulation function method in the SAND program, as previously described.¹⁴²

4.1.2 Experimental details from chapter 3.3.3

Fluorescence anisotropy measurements were carried out in toluene solution. The absorption was kept below 0.1 to avoid reabsorption. The molecules were excited using a Chameleon Ultra II frequency-doubled Ti-sapphire laser by Coherent Inc. The laser repetition rate is 80 MHz and the excitation beam operates at a quasi-continuous-wave output power of 5 mW. The measurement was carried out on a Bruker 250is c6878 spectrometer coupled with a Hamamatsu universal streak camera, c5680 series.

4.2 Syntheses from chapter 2

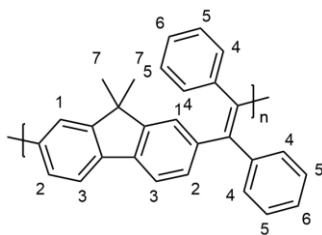
4.2.1 2,7-Dibenzoyl-9,9-dimethyl-9H-fluorene (FDK-DP)



Benzoyl chloride (2.7 ml, 23.2 mmol, 2.3 eq.) was added to 9,9-dimethyl-9H-fluorene (2.00 g, 10.3 mmol, 1.0 eq.) and aluminium chloride (3.02 g, 22.7 mmol, 2.2 eq.) in a dry flask under argon. The solution was stirred at 85 °C for 4 hours. Subsequently, a large amount of cold water was added. Then, the aqueous phase was separated, extracted with chloroform and the combined organic phases were dried over magnesium sulfate. The solvent was evaporated in vacuo, and the crude product was purified by twofold flash column chromatography (hexane/CHCl₃ 3:2) to yield a white solid (1.33 g, 10.3 mmol, 32%).

¹H-NMR (400 MHz, CDCl₃, 300 K): δ [ppm] = 7.98 (s, 2H, H₁), 7.89-7.80 (m, 8H, H₂₋₄), 7.62 (t, *J* = 7.4 Hz, 2H, H₆), 7.52 (t, *J* = 7.5 Hz, 4H, H₅), 1.57 (s, 6H, H₇). **¹³C{¹H}-NMR** (101 MHz, CDCl₃, 300 K): δ [ppm] = 196.7, 155.0, 142.3, 138.2, 137.6, 132.5, 130.3, 130.2, 128.5, 124.6, 120.6, 47.5, 27.0. **IR**: $\tilde{\nu}$ [cm⁻¹] = 3056 (C_{ar}-H), 2953+2924+2871 (C_{alkyl}-H), 1643 (C=O). **MS** (ESI): *m/z* = 403.1687 calculated for [C₂₉H₂₃O₂]⁺ = 403.1693.

4.2.2 Poly[2,7-(9,9-dimethyl-9H-fluorenylene)-1,2-diphenylvinylene] (PFV-DP)



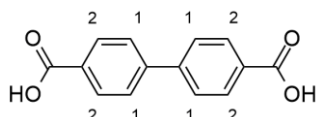
Chlorobenzene (20 ml) was added to 2,7-dibenzoyl-9,9-dimethyl-9H-fluorene (1.00 g, 2.49 mmol, 1.0 eq.) and phosphorus pentachloride (2.07 g, 9.94 mmol, 4.0 eq.) in a Schlenk tube under argon atmosphere. The solution was stirred for 24 hours at 120 °C. Subsequently, the solvent, phosphorus oxychloride, and excess phosphorus pentachloride were removed by distillation under reduced pressure. The resulting 2,7-bis(dichloro(phenyl)methyl)-9,9-dimethyl-9H-fluorene was used without further purification.

2,7-Bis(dichloro(phenyl)methyl)-9,9-dimethyl-9H-fluorene (1.27 g, 2.49 mmol, 1.0 eq.) and dicobalt octacarbonyl (2.29 g, 6.71 mmol, 2.7 eq.) were dissolved in chlorobenzene (10 ml) under argon atmosphere. The solution was heated to 100 °C for 50 minutes. Then, 1,2-dichloroethane (10 ml) was added and stirred for further 10 minutes. The polymer was precipitated into acidified (2 M HCl) cold methanol, filtrated, and washed with methanol. The crude product was purified by Soxhlet extraction (MeOH, acetone, EtOAc, CHCl₃). The ethyl acetate and chloroform fractions were redissolved in chloroform (ca. 10 ml) and reprecipitated into acidified (2 M HCl) cold methanol. The products were obtained as yellow solids (ethyl acetate fraction: 0.06 g, 0.16 mmol, 6%; chloroform fraction: 0.46 g, 1.24 mmol, 50%).

¹H-NMR (600 MHz, C₂D₂Cl₄, 353 K): δ [ppm] = 7.94-6.76 (m, 16H, H₁₋₆), 1.69-0.70 (m, 6H, H₇). **¹³C{¹H}-NMR** (151 MHz, C₂D₂Cl₄, 353 K): δ [ppm] = 153.9, 144.2, 143.2, 142.0, 139.1, 137.6, 131.9, 130.5, 128.0, 126.7, 119.4, 46.4, 27.0. **GPC** (THF) ethyl acetate fraction: *M_n* = 3100 g/mol, *M_w* = 5100 g/mol, PDI = 1.64; chloroform fraction: *M_n* = 20600 g/mol, *M_w* =

63400 g/mol, PDI = 3.07. **UV/Vis** (THF solution): λ_{\max} . [nm] = 264, 272 sh, 377; (film): λ_{\max} . [nm] = 278.372. **PL** (THF solution, λ_{exc} . [nm] = 380 nm): λ_{\max} . [nm] = 537, PLQY = 4.3%; (film, λ_{exc} . [nm] = 370 nm): λ_{\max} [nm] = 550, PLQY = 43%. **BET** (N_2 adsorption): S_{BET} [m^2/g] = N/A; Total pore volume [cm^3/g] = N/A.

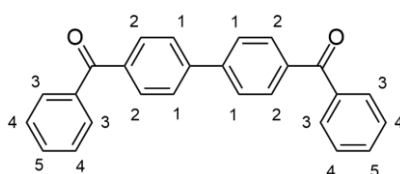
4.2.3 4,4'-Biphenyldicarboxylic acid (8)



L(+)-Ascorbic acid (8.76 g, 49.7 mmol, 1.0 eq.), 4 mM ethylenediaminetetraacetic acid aqueous solution (373 ml, 1.50 mmol, 0.03 eq.), potassium carbonate (20.7 g, 0.15 mol, 3.0 eq.), and 4-bromobenzoic acid (10.0 g, 49.7 mmol, 1.0 eq.) in ethanol (100 ml) were added to palladium(II) chloride (0.27 g, 1.50 mmol, 0.03 eq.) in water (187 ml). The mixture was heated to 90 °C for 19 hours, then cooled to room temperature, and most of the ethanol was evaporated off. The mixture was extracted with dichloromethane, the water phase was filtered and acidified with hydrochloric acid. The precipitated solid was filtered and dried in vacuo. The product was obtained as white solid (5.61 g, 23.2 mmol, 93%).

$^1\text{H-NMR}$ (400 MHz, D_2O , 300 K): δ [ppm] = 7.99 (d, J = 8.2 Hz, 4H, $\text{H}_{1/2}$), 7.77 (d, J = 8.2 Hz, 4H, $\text{H}_{1/2}$). **$^{13}\text{C}\{\text{H}\}\text{-NMR}$** (101 MHz, D_2O , 300 K): δ [ppm] = 177.1, 144.2, 137.5, 131.3, 128.7. **IR**: $\tilde{\nu}$ [cm^{-1}] = 2979+2814+2662+2543 (O-H), 1669 (C=O). **MS** (MALDI): m/z = 242.046 calculated for $[\text{C}_{14}\text{H}_{10}\text{O}_4]^+ = 242.058$.

4.2.4 4,4'-Dibenzoylbiphenyl (BDK-DP)



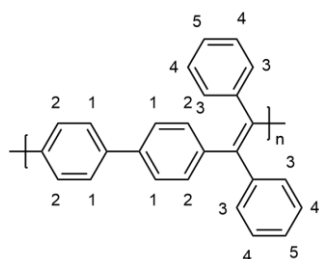
Thionyl chloride (6.0 ml, 82.2 mmol, 10 eq.) and dry dimethylformamide (0.13 ml, 1.68 mmol, 0.2 eq.) were added to 4,4'-biphenyldicarboxylic acid (2.00 g, 8.26 mmol, 1.0 eq.) under argon atmosphere. The solution was heated to 75 °C for 18 hours. Then, the solvent and excess thionyl

chloride were removed under reduced pressure. The resulting 4,4'-biphenyldicarbonyl chloride was used without further purification.

Benzene (30 ml, 334 mmol, 75 eq.) was added to 4,4'-biphenyldicarbonyl chloride (1.25 g, 4.48 mmol, 1.0 eq.) and aluminium chloride (1.50 g, 11.3 mmol, 2.5 eq.) under argon atmosphere. The solution was stirred at 85 °C for 4 hours. Subsequently, a large amount of cold water was added. The mixture was extracted with chloroform, the organic phase dried over magnesium sulfate, and the solvent removed by evaporation. The crude product was purified by column chromatography (hexane:CHCl₃ 6:4). The product was obtained as white solid (1.60 g, 4.41 mmol, 98%).

¹H-NMR (600 MHz, CDCl₃, 323 K): δ [ppm] = 7.91 (d, *J* = 8.2 Hz, 4H, H_{1/2}), 7.85 (d, *J* = 7.5 Hz, 4H, H₃), 7.76 (d, *J* = 8.2 Hz, 4H, H_{1/2}), 7.61 (t, *J* = 7.4 Hz, 2H, H₅), 7.51 (t, *J* = 7.7 Hz, 4H, H₄). **¹³C{¹H}-NMR** (151 MHz, CDCl₃, 323 K): δ [ppm] = 196.1, 144.1, 138.0, 137.5, 132.6, 130.9, 130.1, 128.5, 127.4. **IR**: $\tilde{\nu}$ [cm⁻¹] = 3050 (C_{ar}-H), 1641 (C=O). **MS** (ESI): *m/z* = 385.1190 calculated for [C₂₆H₁₈O₂Na]⁺ = 385.1199.

4.2.5 Poly[4,4'-biphenyldiyl-1,2-diphenylvinylene] (PBV-DP)



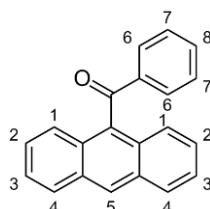
Chlorobenzene (35 ml) was added to 4,4'-dibenzoylbiphenyl (1.33 g, 3.66 mmol, 1.0 eq.) and phosphorus pentachloride (3.05 g, 14.7 mmol, 4.0 eq.) in a Schlenk tube under argon atmosphere. The solution was stirred for 4 days at 120 °C. Subsequently, the solvent, phosphorus oxychloride and excess phosphorus pentachloride were removed by distillation under reduced pressure. The resulting 4,4'-bis[dichloro(phenyl)methyl]biphenyl was used without further purification.

4,4'-Bis[dichloro(phenyl)methyl]biphenyl (1.73 g, 3.66 mmol, 1.0 eq.) and dicobalt octacarbonyl (3.11 g, 9.09 mmol, 2.5 eq.) were dissolved in chlorobenzene (10 ml) under argon atmosphere. The solution was heated to 100 °C for 50 minutes. Then, 1,2-dichloroethane (10 ml) was

added and stirred for further 10 minutes. The polymer was precipitated into acidified (2 M HCl) cold methanol, filtrated, and washed with methanol. The crude product was purified by Soxhlet extraction (MeOH, acetone, EtOAc, CHCl₃). The ethyl acetate and chloroform fractions were redissolved in chloroform (ca. 10 ml) and reprecipitated into acidified (2 M HCl) cold methanol. The products were obtained as yellow solids (ethyl acetate fraction: 0.04 g, 0.12 mmol, 3%; chloroform fraction: 0.22 g, 0.66 mmol, 18%).

¹H-NMR (600 MHz, C₂D₂Cl₄, 353 K): δ [ppm] = 7.45-7.26 (m, 4H, H₁₋₅), 7.22-6.98 (m, 14H, H₁₋₅). **¹³C{¹H}-NMR** (151 MHz, C₂D₂Cl₄, 353 K): δ [ppm] = 144.2, 144.1, 143.2, 141.2, 138.6, 138.5, 132.1, 131.7, 128.2, 128.0, 126.9, 126.3, 126.2. **GPC** (THF) ethyl acetate fraction: M_n = 3000 g/mol, M_w = 4100 g/mol, PDI = 1.34; chloroform fraction: M_n = 14000 g/mol, M_w = 43200 g/mol, PDI = 3.08. **UV/Vis** (THF solution): λ_{max} [nm] = 261, 291 sh 353; (film): λ_{max} [nm] = 259, 296 sh, 355. **PL** (THF solution, λ_{exc} [nm] = 350 nm): λ_{max} [nm] = 521, PLQY = 0.5%; (film, λ_{exc} [nm] = 350 nm): λ_{max} [nm] = 537, PLQY = 26%. **BET** (N₂ adsorption): S_{BET} [m²/g] = 72; Total pore volume [cm³/g] = 0.64.

4.2.6 9-Benzoylanthracene

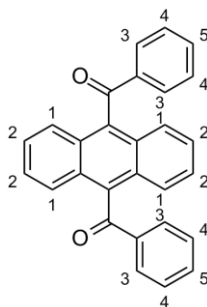


In a flame-dried flask benzoyl chloride (4.0 ml, 34.5 mmol 1.2 eq.) was added to a solution of anthracene (5.03 g, 28.2 mmol 1.0 eq.) and aluminium chloride (4.56 g, 34.2 mmol, 1.2 eq.) in dichloroethane (60 ml) under argon atmosphere. The solution was stirred for 24 hours at room temperature. Subsequently, a large amount of cold water was added and the aqueous phase was extracted with chloroform (3x), the organic phase dried over magnesium sulfate and the solvent was evaporated in vacuo. The crude product was purified by flash column chromatography (hexane/CHCl₃ 8:2 → 7:3). The product was obtained as yellow solid (5.87 g, 20.8 mmol, 74%).

¹H-NMR (600 MHz, CDCl₃, 300 K): δ [ppm] = 8.57 (s, 1H, H₅), 8.07 (d, J = 8.6 Hz, 2H, H₁), 7.85 (d, J = 7.1 Hz, 2H, H₆), 7.75 (d, J = 8.8 Hz, 2H, H₄), 7.58 (t, J = 7.4 Hz, 1H, H₈), 7.48 (m, 2H, H₂), 7.41 (dd, J = 15.7, 7.1 Hz, 4H, H_{3,7}). **¹³C{¹H}-NMR** (151 MHz, CDCl₃, 300 K):

δ [ppm] = 200.3, 138.3, 134.2, 134.1, 131.2, 130.2, 129.0, 128.8, 128.5, 126.7, 125.6, 125.5. **IR:** $\tilde{\nu}$ [cm^{-1}] = 3053 ($\text{C}_{\text{ar}}\text{-H}$), 1662+1656 ($\text{C}=\text{O}$). **MS** (APCI): m/z = 305.0952 calculated for $[\text{C}_{21}\text{H}_{14}\text{ONa}]^+$ = 305.0937.

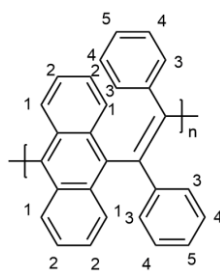
4.2.7 9,10-Dibenzoylanthracene (ADK-DP)



Benzoyl chloride (2.1 ml, 18.1 mmol, 1.2 eq.) was added to a solution of 9-benzoylanthracene (4.32 g, 15.3 mmol, 1.0 eq.) and aluminium chloride (2.45 g, 18.4 mmol, 1.2 eq.) in dichloroethane (150 ml) in a flame-dried flask protected by a drying tube. The solution was stirred at 85 °C for 11 days. Then, the reaction was allowed to cool to room temperature. Subsequently, a 2:3 mixture of concentrated, aqueous hydrochloric acid and saturated aqueous sodium chloride was added and stirred for another hour. Then, the aqueous phase was diluted with water and extracted with chloroform (3x). The combined organic layers were dried over magnesium sulfate and the solvent was evaporated in vacuo. The crude product was purified by recrystallization from acetone followed by flash column chromatography (hexane/ CHCl_3 1:1) to yield a light-yellow powder (2.89 g, 7.47 mmol, 49%).

$^1\text{H-NMR}$ (600 MHz, CDCl_3 , 300 K): δ [ppm] = 7.87 (d, J = 7.4 Hz, 4H, H_3), 7.79 (dd, J = 6.8, 3.2 Hz, 4H, $\text{H}_{1/2}$), 7.61 (t, J = 7.4 Hz, 2H, H_5), 7.45 (t, J = 7.8 Hz, 4H, H_4), 7.39 (dd, J = 6.8, 3.1 Hz, 4H, $\text{H}_{1/2}$). **$^{13}\text{C}\{\text{H}\}\text{-NMR}$** (151 MHz, CDCl_3 , 300 K): δ [ppm] = 199.8, 138.4, 136.3, 134.3, 130.3, 129.1, 128.3, 126.8, 126.0. **IR:** $\tilde{\nu}$ [cm^{-1}] = 3074 ($\text{C}_{\text{ar}}\text{-H}$), 1657 ($\text{C}=\text{O}$). **MS** (ESI): m/z = 409.1193 calculated for $[\text{C}_{28}\text{H}_{18}\text{O}_2\text{Na}]^+$ = 409.1199.

4.2.8 Poly[9,10-anthrylene-1,2-diphenylvinylene] (PAV-DP)

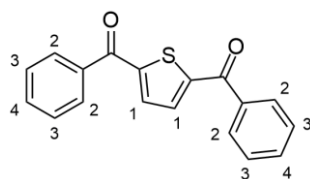


Chlorobenzene (50 ml) was added to 9,10-dibenzoylanthracene (1.91 g, 4.95 mmol, 1.0 eq.) and phosphorus pentachloride (4.13 g, 19.8 mmol, 4.0 eq.) in a Schlenk tube under argon atmosphere. The solution was stirred for 4 days at 120 °C. Subsequently, the solvent, phosphorus oxychloride, and excess phosphorus pentachloride were removed by distillation under reduced pressure. The resulting 9,10-bis[dichloro(phenyl)methyl]anthracene was used without further purification.

9,10-Bis[dichloro(phenyl)methyl]anthracene (0.80 g, 1.61 mmol, 1.0 eq.) and dicobalt octacarbonyl (1.51 g, 4.40 mmol, 2.7 eq.) were dissolved in chlorobenzene (20 ml) under argon atmosphere. The solution was heated to 100 °C for 50 minutes. Then, 1,2-dichloroethane (10 ml) was added and stirred for further 10 minutes. The polymer was precipitated into acidified (2 M HCl) cold methanol, filtrated, and washed with methanol. The crude product was purified by Soxhlet extraction (MeOH, acetone, EtOAc, CHCl₃). The ethyl acetate and chloroform fractions were redissolved in chloroform (ca. 10 ml) and reprecipitated into acidified (2 M HCl) cold methanol. The products were obtained as dark solids (ethyl acetate fraction: 0.03 g, 0.07 mmol, 4%; chloroform fraction: 0.18 g, 0.51 mmol, 32%).

¹H-NMR (600 MHz, C₂D₂Cl₄, 353 K): δ [ppm] = 9.33-6.10 (m, 18H, H₁₋₅). **¹³C{¹H}-NMR** (151 MHz, C₂D₂Cl₄, 353 K): δ [ppm] = 129.1. **GPC** (THF) ethyl acetate fraction: M_n = 1200 g/mol, M_w = 1700 g/mol, PDI = 1.51; chloroform fraction: M_n = 2600 g/mol, M_w = 4700 g/mol, PDI = 1.82. **UV/Vis** (THF solution): λ_{max}. [nm] = 262, 400 sh; (film): λ_{max}. [nm] = 268, 393 sh. **PL** (THF solution, λ_{exc}. [nm] = 380 nm): λ_{max}. [nm] = 637, PLQY = N/A; (film, λ_{exc}. [nm] = 390 nm): λ_{max} [nm] = N/A, PLQY = N/A. **BET** (N₂ adsorption): S_{BET} [m²/g] = N/A; Total pore volume [cm³/g] = N/A.

4.2.9 2,5-Dibenzoylthiophene (TDK-DP)

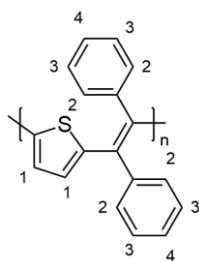


Thionyl chloride (8.5 ml, 116 mmol, 10 eq.) and dry dimethylformamide (0.20 ml, 2.58 mmol, 0.2 eq.) were added to 2,5-thiophenedicarboxylic acid (2.02 g, 11.70 mmol, 1.0 eq.) under argon atmosphere. The solution was heated to 75 °C for 2 hours. Then, the solvent and excess thionyl chloride were evaporated under reduced pressure. The resulting 2,5-thiophenedicarbonyl chloride was used without further purification.

Benzene (25 ml, 278 mmol, 24 eq.) was added to 2,5-thiophenedicarbonyl chloride (2.45 g, 11.7 mmol, 1.0 eq.) and aluminium chloride (3.43 g, 25.7 mmol, 2.2 eq.) under argon atmosphere. The solution was stirred at room temperature for 17 hours. Subsequently, a large amount of cold water was added. The mixture was extracted with chloroform, the organic phase dried over magnesium sulfate, and the solvent removed by evaporation. The crude product was purified by column chromatography (hexane/CHCl₃ 3:2). The product was obtained as orange solid (2.29 g, 7.83 mmol, 67%).

¹H-NMR (600 MHz, CDCl₃, 300 K): δ [ppm] = 7.91 (d, *J* = 7.1 Hz, 4H, H₂), 7.68 (s, 2H, H₁), 7.64 (t, *J* = 7.5 Hz, 2H, H₄), 7.53 (t, *J* = 7.7 Hz, 4H, H₃). **¹³C{¹H}-NMR** (151 MHz, CDCl₃, 300 K): δ [ppm] = 188.2, 148.7, 137.5, 133.9, 133.1, 129.5, 128.8. **IR**: $\tilde{\nu}$ [cm⁻¹] = 3119+3053+2925+2853 (C_{ar}-H), 1631 (C=O). **MS** (ESI): *m/z* = 315.0457 calculated for [C₁₈H₁₂O₂NaS]⁺ = 315.0450.

4.2.10 Poly[2,5-thiophenylene-1,2-diphenylvinylene] (PTV-DP)



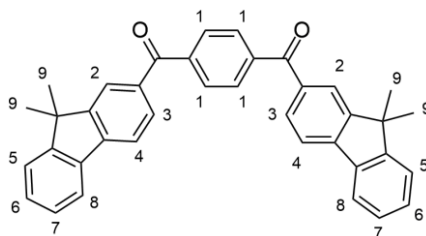
Chlorobenzene (20 ml) was added to 2,5-dibenzoylthiophene (1.00 g, 3.42 mmol, 1.0 eq.) and phosphorus pentachloride (2.85 g, 13.7 mmol, 4.0 eq.) in a Schlenk tube under argon

atmosphere. The solution was stirred for 24 hours at 120 °C. Subsequently, the solvent, phosphorus oxychloride, and excess phosphorus pentachloride were removed by distillation under reduced pressure. The resulting 2,5-bis[dichloro(phenyl)methyl]thiophene was used without further purification.

2,5-Bis[dichloro(phenyl)methyl]thiophene (1.37 g, 3.42 mmol, 1.0 eq.) and dicobalt octacarbonyl (2.99 g, 8.75 mmol, 2.6 eq.) were dissolved in chlorobenzene (10 ml) under argon atmosphere. The solution was heated to 100 °C for 50 minutes. Then, 1,2-dichloroethane (10 ml) was added and stirred for further 10 minutes. The polymer was precipitated into acidified (2 M HCl) cold methanol, filtrated, and washed with methanol. The crude product was purified by Soxhlet extraction (MeOH, acetone, EtOAc, CHCl₃). The ethyl acetate and chloroform fractions were redissolved in chloroform (ca. 10 ml) and reprecipitated into acidified (2 M HCl) cold methanol. The products were obtained as dark orange/brownish solids (ethyl acetate fraction: 12.2 mg, 0.04 mmol, 1%; chloroform fraction: 20.1 mg, 0.08 mmol, 2%).

¹H-NMR (400 MHz, C₂D₂Cl₄, 353 K): δ [ppm] = 7.63-6.67 (m, 12H, H₁₋₄). **¹³C{¹H}-NMR** (101 MHz, C₂D₂Cl₄, 353 K): δ [ppm] = 147.2, 142.5, 131.0, 128.8, 128.0. **GPC** (THF) ethyl acetate fraction: M_n = 2000 g/mol, M_w = 2900 g/mol, PDI = 1.44; chloroform fraction: M_n = 2100 g/mol, M_w = 3000 g/mol, PDI = 1.47. **UV/Vis** (THF solution): λ_{max}. [nm] = 262 sh, 460; (film): λ_{max}. [nm] = 257 sh, 456. **PL** (THF solution, λ_{exc}. [nm] = 460 nm): λ_{max}. [nm] = 534, 619, PLQY = N/A; (film, λ_{exc}. [nm] = 460 nm): λ_{max} [nm] = 625, PLQY = 0.6%. **BET** (N₂ adsorption): S_{BET} [m²/g] = 1; Total pore volume [cm³/g] = 0.004.

4.2.11 1,4-Bis(2-(9,9-dimethyl-9H-fluorenyl))benzene (PDK-DF)

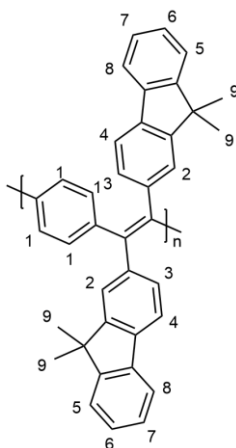


9,9-Dimethyl-9H-fluorene (5.75 g, 29.6 mmol, 4.0 eq.) was added to terephthaloyl chloride (1.51 g, 7.44 mmol, 1.0 eq.) and aluminium chloride (2.17 g, 16.3 mmol, 2.2 eq.) in dichloroethane (30 ml) under argon atmosphere. The solution was stirred at 85 °C for 4 hours. Subsequently, the solution was cooled to room temperature and a large amount of cold water was

added. The mixture was extracted with chloroform, the organic phase dried over magnesium sulfate, and the solvent removed by evaporation. The crude product was purified by column chromatography (hexane/CHCl₃ 3:2). The product was obtained as white crystals (3.86 g, 7.44 mmol, >99%).

¹H-NMR (400 MHz, CDCl₃, 300 K): δ [ppm] = 8.00 (s, 2H, H₂), 7.95 (s, 4H, H₁), 7.87-7.78 (m, 6H, H_{3/4+5/8+6/7}), 7.53-7.47 (m, 2H, H_{5/8}), 7.44-7.36 (m, 4H, H_{3/4+6/7}), 1.55 (s, 12H, H₉). **¹³C{¹H}-NMR** (101 MHz, CDCl₃, 300 K): δ [ppm] = 196.2, 155.0, 154.1, 144.4, 141.4, 138.0, 135.8, 130.5, 129.8, 128.9, 127.5, 124.6, 123.0, 121.2, 119.8, 47.3, 27.1. **IR:** $\tilde{\nu}$ [cm⁻¹] = 3053+3009 (C_{ar}-H), 2962+2923+2867 (C_{alkyl}-H) 1640 (C=O). **MS** (ESI): m/z = 519.2321 calculated for [C₃₈H₃₁O₂]⁺ = 519.2319.

4.2.12 Poly[1,4-phenylene-1,2-bis(2-(9,9-dimethyl-9H-fluorenyl))vinylene] (PPV-DF)



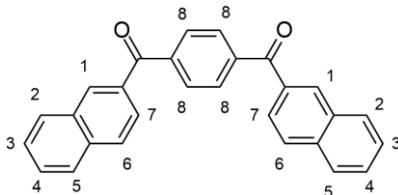
Chlorobenzene (20 ml) was added to 1,4-bis(2-(9,9-dimethyl-9H-fluorenyl))benzene (1.00 g, 1.93 mmol, 1.0 eq.) and phosphorus pentachloride (1.61 g, 7.73 mmol, 4.0 eq.) in a Schlenk tube under argon atmosphere. The solution was stirred for 24 hours at 120 °C. Subsequently, the solvent, phosphorus oxychloride, and excess phosphorus pentachloride were removed by distillation under reduced pressure. The resulting 1,4-bis[dichloro(2-(9,9-dimethyl-9H-fluorenyl))methyl]benzene was used without further purification.

1,4-Bis[dichloro(2-(9,9-dimethyl-9H-fluorenyl))methyl]benzene (1.21 g, 1.93 mmol, 1.0 eq.) and dicobalt octacarbonyl (1.80 g, 5.26 mmol, 2.7 eq.) were dissolved in chlorobenzene (10 ml) under argon atmosphere. The solution was heated to 100 °C for 50 minutes. Then, 1,2-dichloroethane (10 ml) was added and stirred for further 10 minutes. The polymer was precipitated

into acidified (2 M HCl) cold methanol, filtrated, and washed with methanol. The crude product was purified by Soxhlet extraction (MeOH, acetone, EtOAc, CHCl₃). The ethyl acetate and chloroform fractions were redissolved in chloroform (ca. 10 ml) and reprecipitated into acidified (2 M HCl) cold methanol. The products were obtained as light orange solids (ethyl acetate fraction: 0.17 g, 0.35 mmol, 18%; chloroform fraction: 0.51 g, 1.05 mmol, 54%).

¹H-NMR (600 MHz, C₂D₂Cl₄, 353 K): δ [ppm] = 8.72-6.13 (m, 18H, H₁₋₈), 1.95-0.29 (m, 12H, H₉). **¹³C{H}-NMR** (151 MHz, C₂D₂Cl₄, 353 K): δ [ppm] = 154.5, 153.7, 143.7, 142.5, 139.5, 137.8, 131.3, 127.3, 126.3, 122.9, 120.3, 119.6, 46.8, 27.5. **GPC** (THF) ethyl acetate fraction: M_n = 6900 g/mol, M_w = 10800 g/mol, PDI = 1.57; chloroform fraction: M_n = 11400 g/mol, M_w = 18500 g/mol, PDI = 1.63. **UV/Vis** (THF solution): λ_{max}. [nm] = 285, 322, 391 sh; (film): λ_{max}. [nm] = 287, 319 sh, 375 sh. **PL** (THF solution, λ_{exc.} [nm] = 375 nm): λ_{max}. [nm] = 569, PLQY = 13%; (film, λ_{exc.} [nm] = 380 nm): λ_{max} [nm] = 565, PLQY = 26%. **BET** (N₂ adsorption): S_{BET} [m²/g] = 3; Total pore volume [cm³/g] = 0.01.

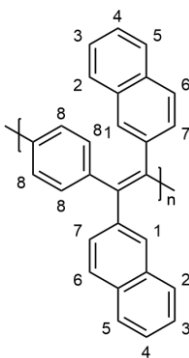
4.2.13 1,4-Bis(2-naphthoyl)benzene (PDK-DN)



Terephthaloyl chloride (2.63 g, 13.0 mmol, 1.0 eq.) was added to naphthalene (3.65 g, 28.5 mmol, 2.2 eq.) and aluminium chloride (3.80 g, 28.5 mmol, 2.2 eq.) in dichloroethane (130 ml) under argon at 0°C. The solution was stirred at room temperature for 20 hours. Subsequently, cold water was added. Then, the aqueous phase was separated and the organic layer was dried over magnesium sulfate. The solvent was evaporated in vacuo and the crude product was purified by column chromatography (gradient: hexane → CH₂Cl₂). The product was obtained as white solid (0.45 g, 1.16 mmol, 9%).

¹H-NMR (600 MHz, CDCl₃, 300 K): δ [ppm] = 8.32 (s, 2H, H₁), 8.03-7.97 (m, 8H, H_{2,5,8}), 7.96-7.92 (m, 4H, H_{6,7}), 7.65 (t, J=7.4 Hz, 2H, H_{3/4}), 7.59 (t, J = 7.5 Hz, 2H, H_{3/4}). **¹³C{H}-NMR** (151 MHz, CDCl₃, 300 K): δ [ppm] = 196.2, 141.2, 135.7, 134.4, 132.5, 132.4, 130.0, 129.7, 128.8, 128.7, 128.1, 127.2, 125.7. **IR**: $\tilde{\nu}$ [cm⁻¹] = 3053+2922+2852 (C_{ar}-H), 1648 (C=O). **MS** (ESI): m/z = 409.1175 calculated for [C₂₈H₁₈O₂Na]⁺ = 409.1199.

4.2.14 Poly[1,4-phenylene-1,2-bis(2-naphthyl)vinylene] (PPV-DN)

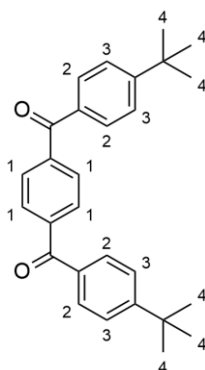


Chlorobenzene (10 ml) was added to 1,4-bis(2-naphthoyl)benzene (0.45 g, 1.16 mmol, 1.0 eq.) and phosphorus pentachloride (0.97 g, 4.66 mmol, 4.0 eq.) in a Schlenk tube under argon atmosphere. The solution was stirred for 24 hours at 120 °C. Subsequently, the solvent, phosphorus oxychloride, and excess phosphorus pentachloride were removed by distillation under reduced pressure. The resulting 1,4-bis[dichloro(2-naphthyl)methyl]benzene was used without further purification.

1,4-Bis[dichloro(2-naphthyl)methyl]benzene (0.58 g, 1.16 mmol, 1.0 eq.) and dicobalt octacarbonyl (1.08 g, 3.17 mmol, 2.7 eq.) were dissolved in chlorobenzene (10 ml) under argon atmosphere. The solution was heated to 100 °C for 50 minutes. Then, 1,2-dichloroethane (10 ml) was added and stirred for further 10 minutes. The polymer was precipitated into acidified (2 M HCl) cold methanol, filtrated, and washed with methanol. The crude product was purified by Soxhlet extraction (MeOH, acetone, EtOAc, CHCl₃). The ethyl acetate and chloroform fractions were redissolved in chloroform (ca. 10 ml) and reprecipitated into acidified (2 M HCl) cold methanol. The products were obtained as orange solids (ethyl acetate fraction: 0.08 g, 0.23 mmol, 20%; chloroform fraction: 0.29 g, 0.81 mmol, 69%).

¹H-NMR (600 MHz, C₂D₂Cl₄, 353 K): δ [ppm] = 7.82-6.45 (m, 18H, H₁₋₈). **¹³C{¹H}-NMR** (151 MHz, C₂D₂Cl₄, 353 K): δ [ppm] = 142.6, 141.5, 133.6, 132.6, 131.5, 131.0, 129.8, 128.5, 127.9, 127.2, 126.1. **GPC** (THF) ethyl acetate fraction: M_n = 4500 g/mol, M_w = 6000 g/mol, PDI = 1.33; chloroform fraction: M_n = 11600 g/mol, M_w = 17800 g/mol, PDI = 1.54. **UV/Vis** (THF solution): λ_{max} . [nm] = 222, 258 sh, 307 sh, 343 sh; (film): λ_{max} . [nm] = 222, 258 sh, 307 sh, 351. **PL** (THF solution): λ_{max} . [nm] = 545, PLQY = 2.8%; (film): λ_{max} [nm] = 553, PLQY = 1.0%. **BET** (N₂ adsorption): S_{BET} [m²/g] = 14; Total pore volume [cm³/g] = 0.07.

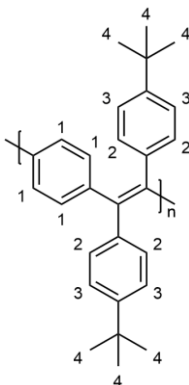
4.2.15 4,4'-Bis(*tert*-butyl)terephthalophenone (PDK-DPtBu)



Terephthaloyl chloride (4.00 g, 19.7 mmol, 1.0 eq.) was added to *tert*-butylbenzene (40.0 ml, 0.26 mol, 13 eq.) and aluminium chloride (5.78 g, 43.3 mmol, 2.2 eq.) in a dry flask under argon at 0 °C. The solution was stirred at room temperature for 2.5 hours. Subsequently, a large amount of cold water was added. The mixture was extracted with chloroform, the organic phase dried over magnesium sulfate, and the solvent removed by evaporation. The crude product was purified by column chromatography (hexane/CHCl₃ 7:3) followed by recrystallization from ethyl acetate to yield a white crystalline solid (4.71 g, 11.83 mmol, 60%).

¹H-NMR (400 MHz, CDCl₃, 300 K): δ [ppm] = 7.88 (s, 4H, H₁), 7.80 (d, *J* = 8.4 Hz, 4H, H_{2/3}), 7.53 (d, *J* = 8.4 Hz, 4H, H_{2/3}), 1.38 (s, 18H, H₄). **¹³C{¹H}-NMR** (101 MHz, CDCl₃, 300 K): δ [ppm] = 195.9, 157.0, 141.0, 134.4, 130.4, 129.7, 125.6, 35.3, 31.3. **IR**: $\tilde{\nu}$ [cm⁻¹] = 3093+3063+3039 (C_{ar}-H), 2957+2902+2867 (C_{alkyl}-H), 1645 (C=O). **MS** (APCI): *m/z* = 399.2347 calculated for [C₂₈H₃₁O₂]⁺ = 399.2319.

4.2.16 Poly[1,4-phenylene-1,2-bis(4-*tert*-butylphenyl)vinylene] (PPV-DPtBu)

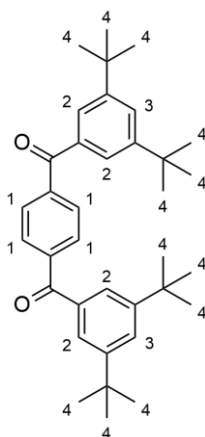


Chlorobenzene (45 ml) was added to 4,4'-bis(*tert*-butyl)terephthalophenone (1.81 g, 4.54 mmol, 1.0 eq.) and phosphorus pentachloride (3.78 g, 18.2 mmol, 4.0 eq.) in a Schlenk tube under argon atmosphere. The solution was stirred for 4 days at 120 °C. Subsequently, the solvent, phosphorus oxychloride, and excess phosphorus pentachloride were removed by distillation under reduced pressure. The resulting 1,4-bis[dichloro(4-*tert*-butylphenyl)methyl]benzene was used without further purification.

1,4-Bis[dichloro(4-*tert*-butylphenyl)methyl]benzene (2.31 g, 4.54 mmol, 1.0 eq.) and dicobalt octacarbonyl (4.24 g, 12.4 mmol, 2.7 eq.) were dissolved in chlorobenzene (10 ml) under argon atmosphere. The solution was heated to 100 °C for 50 minutes. Then, 1,2-dichloroethane (10 ml) was added and stirred for further 10 minutes. The polymer was precipitated into acidified (2 M HCl) cold methanol, filtrated, and washed with methanol. The crude product was purified by Soxhlet extraction (MeOH, acetone, EtOAc, CHCl₃). The ethyl acetate and chloroform fractions were redissolved in chloroform (ca. 10 ml) and reprecipitated into acidified (2 M HCl) cold methanol. The products were obtained as yellow solids (ethyl acetate fraction: 0.34 g, 0.92 mmol, 20%; chloroform fraction: 0.70 g, 1.90 mmol, 42%).

¹H-NMR (600 MHz, C₂D₂Cl₄, 353 K): δ [ppm] = 7.30-6.45 (m, 12H, H₁₋₃), 1.45-1.07 (m, 18H, H₄). **¹³C{¹H}-NMR** (151 MHz, C₂D₂Cl₄, 353 K): δ [ppm] = 149.5, 142.6, 141.2, 141.0, 131.4, 131.0, 124.4, 34.7, 31.8. **GPC** (CHCl₃) ethyl acetate fraction: M_n = 9900 g/mol, M_w = 39000 g/mol, PDI = 3.91; chloroform fraction: M_n = 29300 g/mol, M_w = 164000 g/mol, PDI = 5.62. **UV/Vis** (THF solution): λ_{max}. [nm] = 250, 282 sh, 366; (film): λ_{max}. [nm] = 252, 292 sh, 355. **PL** (THF solution): λ_{max}. [nm] = 530, PLQY = 4.6%; (film): λ_{max} [nm] = 537, PLQY = 64%. **BET** (N₂ adsorption): S_{BET} [m²/g] = 417; Total pore volume [cm³/g] = 0.42.

4.2.17 3,3',5,5'-Tetrakis(*tert*-butyl)terephthalophenone (PDK-DPDtBu)



1-Bromo-3,5-di-*tert*-butylbenzene (8.02 g, 29.8 mmol, 4.0 eq.) was added to a stirred mixture of magnesium turnings (0.80 g, 37.0 mmol, 4.9 eq.) in dry tetrahydrofuran (30 ml) under argon atmosphere. The solution was carefully heated until the reaction has started. Then, it was stirred at room temperature until the boiling stopped. Subsequently, the solution was heated to 65 °C for 1 hour.

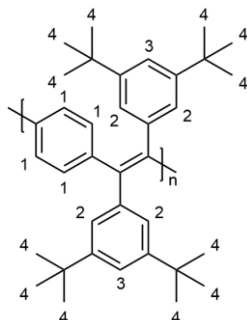
The resulting (3,5-di-*tert*-butylphenyl)magnesium bromide solution was added drop-wise to a solution of terephthalaldehyde (1.00 g, 7.46 mmol, 1.0 eq.) in dry tetrahydrofuran (75 ml) at 40 °C. The resulting solution was then allowed to warm up to room temperature and stirred at the same temperature for 1 hour. The reaction was quenched by adding saturated aqueous ammonium chloride solution very slowly at -30 °C. The reaction mixture was stirred at room temperature for 5 minutes and then, the aqueous solution was extracted with chloroform (3x 200 ml). The organic phases were combined and dried over magnesium sulfate. The solvent was evaporated under reduced pressure.

The resulting solid was dissolved in dichloromethane (50 ml). Celite® (0.5 g) and pyridinium chlorochromate (16.07 g, 74.6 mmol, 10 eq.) was added and the resulting slurry was stirred at room temperature for 2 hours. The reaction mixture was diluted with chloroform (100 ml). Then, the suspension was filtered through Celite®, and the filtrate was concentrated under reduced pressure. The resulting raw product was purified by flash chromatography on silica gel (hexane/CHCl₃ 7:3). The product was obtained as white solid (1.30 g, 2.54 mmol, 34%).

¹H-NMR (400 MHz, CDCl₃, 300 K): δ [ppm] = 7.91 (s, 4H, H₁), 7.71-7.69 (m, 2H, H₃), 7.69-7.66 (m, 4H, H₂), 1.36 (s, 36H, H₄). ¹³C{¹H}-NMR (101 MHz, CDCl₃, 300 K): δ [ppm] = 197.0,

151.3, 141.2, 136.7, 129.9, 127.2, 124.7, 35.2, 31.5. **IR:** $\tilde{\nu}$ [cm^{-1}] = 2951+2903+2866 ($\text{C}_{\text{alkyl}}\text{-H}$), 1648 (C=O). **MS** (APCI): m/z = 533.3389 calculated for $[\text{C}_{36}\text{H}_{46}\text{O}_2\text{Na}]^+$ = 533.3390.

4.2.18 Poly[1,4-phenylene-1,2-bis(3,5-di-*tert*-butylphenyl)vinylene] (PPV-DPDtBu)



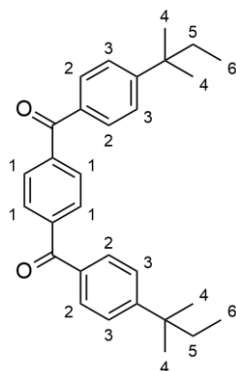
Chlorobenzene (20 ml) was added to 3,3',5,5'-tetrakis(*tert*-butyl)terephthalophenone (1.05 g, 2.06 mmol, 1.0 eq.) and phosphorus pentachloride (1.71 g, 8.22 mmol, 4.0 eq.) in a Schlenk tube under argon atmosphere. The solution was stirred for 4 days at 120 °C. Subsequently, the solvent, phosphorus oxychloride, and excess phosphorus pentachloride were removed by distillation under reduced pressure. The resulting 1,4-bis[dichloro(3,5-di-*tert*-butylphenyl)methyl]benzene was used without further purification.

1,4-Bis[dichloro(3,5-di-*tert*-butylphenyl)methyl]benzene (1.28 g, 2.06 mmol, 1.0 eq.) and dicobalt octacarbonyl (1.90 g, 5.55 mmol, 2.7 eq.) were dissolved in chlorobenzene (10 ml) under argon atmosphere. The solution was heated to 100 °C for 50 minutes. Then, 1,2-dichloroethane (10 ml) was added and stirred for further 10 minutes. The polymer was precipitated into acidified (2 M HCl) cold methanol, filtrated, and washed with methanol. The crude product was purified by Soxhlet extraction (MeOH, acetone, EtOAc, CHCl_3). The ethyl acetate and chloroform fractions were redissolved in chloroform (ca. 10 ml) and reprecipitated into acidified (2 M HCl) cold methanol. The products were obtained as yellow solids (ethyl acetate fraction: 0.46 g, 0.93 mmol, 47%; chloroform fraction: 0.04 g, 0.08 mmol, 4%).

$^1\text{H-NMR}$ (600 MHz, $\text{C}_2\text{D}_2\text{Cl}_4$, 353 K): δ [ppm] = 7.27-6.27 (m, 10H, H_{1-3}), 1.43-0.59 (m, 36H, H_4). **$^{13}\text{C}\{\text{H}\}\text{-NMR}$** (151 MHz, $\text{C}_2\text{D}_2\text{Cl}_4$, 353 K): δ [ppm] = 149.8, 143.1, 130.9, 126.2, 119.9, 34.8, 31.9. **GPC** (CHCl_3) ethyl acetate fraction: M_n = 12900 g/mol, M_w = 17800 g/mol, PDI = 1.38; chloroform fraction: M_n = 12300 g/mol, M_w = 25600 g/mol, PDI = 2.07. **UV/Vis** (THF solution): λ_{max} [nm] = 249, 376; (film): λ_{max} [nm] = 244 sh, 375. **PL** (THF solution,

$\lambda_{\text{exc.}} [\text{nm}] = 380 \text{ nm}$; $\lambda_{\text{max.}} [\text{nm}] = 536$, PLQY = 18%; (film, $\lambda_{\text{exc.}} [\text{nm}] = 380 \text{ nm}$): $\lambda_{\text{max}} [\text{nm}] = 525$, PLQY = 27%. **BET** (N_2 adsorption): $S_{\text{BET}} [\text{m}^2/\text{g}] = 7$; Total pore volume $[\text{cm}^3/\text{g}] = 0.02$.

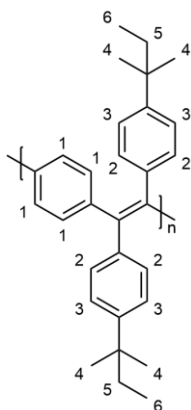
4.2.19 4,4'-Bis(*tert*-pentyl)terephthalophenone (PDK-DPtPent)



Terephthaloyl chloride (2.00 g, 9.85 mmol, 1.0 eq.) was added to *tert*-pentylbenzene (4.0 ml, 23.5 mmol, 2.4 eq.) and aluminium chloride (2.89 g, 21.7 mmol, 2.2 eq.) in a dry flask under argon. The solution was stirred at 85 °C for 4 hours. Subsequently, the solution was cooled to room temperature and a large amount of cold water was added. The mixture was extracted with chloroform, the organic phase dried over magnesium sulfate, and the solvent removed by evaporation. The crude product was purified by column chromatography (hexane/EtOAc 19:1), followed by recrystallization from ethyl acetate. The product was obtained as white solid (1.64 g, 3.84 mmol, 39%).

$^1\text{H-NMR}$ (400 MHz, CDCl_3 , 300 K): δ [ppm] = 7.88 (s, 4H, H_1), 7.80 (d, $J = 8.6$ Hz, 4H, $\text{H}_{2/3}$), 7.47 (d, $J = 8.6$ Hz, 4H, $\text{H}_{2/3}$), 1.71 (q, $J = 7.4$ Hz, 4H, H_5), 1.34 (s, 12H, H_4), 0.72 (t, $J = 7.4$ Hz, 6H, H_6). **$^{13}\text{C}\{\text{H}\}\text{-NMR}$** (101 MHz, CDCl_3 , 300 K): δ [ppm] = 196.0, 155.6, 141.1, 134.4, 130.3, 129.7, 126.3, 38.7, 36.9, 28.4, 9.2. **IR**: $\tilde{\nu} [\text{cm}^{-1}] = 3059$ ($\text{C}_{\text{ar}}\text{-H}$), 2962+2913+2873+2848 ($\text{C}_{\text{alkyl}}\text{-H}$), 1643+1603 ($\text{C}=\text{O}$). **MS** (ESI): $m/z = 427.2637$ calculated for $[\text{C}_{30}\text{H}_{35}\text{O}_2]^+ = 427.2632$.

4.2.20 Poly[1,4-phenylene-1,2-bis(4-*tert*-pentylphenyl)vinylene] (PPV-DP_tPent)

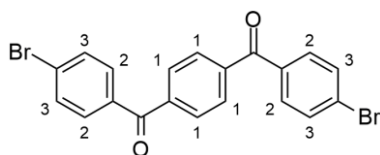


Chlorobenzene (20 ml) was added to 4,4'-bis(*tert*-pentyl)terephthalophenone (0.90 g, 2.10 mmol, 1.0 eq.) and phosphorus pentachloride (1.75 g, 8.40 mmol, 4.0 eq.) in a Schlenk tube under argon atmosphere. The solution was stirred for 4 days at 120 °C. Subsequently, the solvent, phosphorus oxychloride, and excess phosphorus pentachloride were removed by distillation under reduced pressure. The resulting 1,4-bis[dichloro(4-*tert*-pentylphenyl)methyl]benzene was used without further purification.

1,4-Bis[dichloro(4-*tert*-pentylphenyl)methyl]benzene (1.13 g, 2.10 mmol, 1.0 eq.) and dicobalt octacarbonyl (1.94 g, 5.67 mmol, 2.7 eq.) were dissolved in chlorobenzene (10 ml) under argon atmosphere. The solution was heated to 100 °C for 50 minutes. Then, 1,2-dichloroethane (10 ml) was added and stirred for further 10 minutes. The polymer was precipitated into acidified (2 M HCl) cold methanol, filtrated, and washed with methanol. The crude product was purified by Soxhlet extraction (MeOH, acetone, EtOAc, CHCl₃). The ethyl acetate and chloroform fractions were redissolved in chloroform (ca. 10 ml) and reprecipitated into acidified (2 M HCl) cold methanol. The products were obtained as yellow solids (ethyl acetate fraction: 0.30 g, 0.77 mmol, 37%; chloroform fraction: 0.04 g, 0.11 mmol, 5%).

¹H-NMR (600 MHz, C₂D₂Cl₄, 353 K): δ [ppm] = 7.37-6.43 (m, 12H, H₁₋₃), 2.22-0.23 (m, 22H, H₄₋₆). **¹³C{¹H}-NMR** (151 MHz, C₂D₂Cl₄, 353 K): δ [ppm] = 148.0, 142.4, 141.1, 131.3, 131.0, 127.0, 125.0, 37.9, 37.4, 28.7, 9.34. **GPC** (CHCl₃) ethyl acetate fraction: M_n = 9900 g/mol, M_w = 16400 g/mol, PDI = 1.65; chloroform fraction: M_n = 21400 g/mol, M_w = 75400 g/mol, PDI = 3.53. **UV/Vis** (THF solution): λ_{max}. [nm] = 242, 359 sh; (film): λ_{max}. [nm] = 253, 292 sh, 362. **PL** (THF solution, λ_{exc}. [nm] = 360 nm): λ_{max}. [nm] = 539, PLQY = 0.4%; (film, λ_{exc}. [nm] = 360 nm): λ_{max} [nm] = 537, PLQY = 13%. **BET** (N₂ adsorption): S_{BET} [m²/g] = 3; Total pore volume [cm³/g] = 0.01.

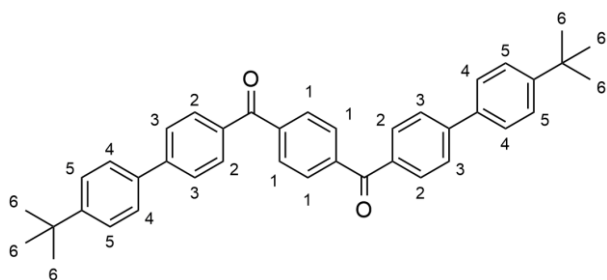
4.2.21 4,4'-Dibromoterephthalophenone (11)



Terephthaloyl dichloride (2.00 g, 9.85 mmol, 1.0 eq.) was added to bromobenzene (15 ml, 142 mmol, 14 eq.) under argon atmosphere. Then, aluminium chloride (3.15 g, 23.6 mmol, 2.4 eq.) was added. The mixture was stirred at 90 °C for 18 hours. Subsequently, the mixture was allowed to cool down to room temperature, and a large amount of cold water was added. The solid that precipitated was filtered and washed with water. After drying in air, the crude product was recrystallized from a mixture of methanol and chloroform. The product was obtained as white solid (2.80 g, 6.31 mmol, 64%).

¹H-NMR (600 MHz, CDCl₃, 323 K): δ [ppm] = 7.86 (s, 4H, H₁), 7.71 (d, *J* = 8.7 Hz, 4H, H_{2/3}), 7.67 (d, *J* = 8.7 Hz, 4H, H_{2/3}). **¹³C{¹H}-NMR** (151 MHz, CDCl₃, 323 K): δ [ppm] = 194.8, 140.8, 136.0, 132.1, 131.7, 129.8, 128.4. **IR**: $\tilde{\nu}$ [cm⁻¹] = 3093+3035 (C_{ar}-H), 1644 (C=O). **MS** (ESI): *m/z* = 464.9080 calculated for [C₂₀H₁₂O₂Br₂]⁺ = 464.9096.

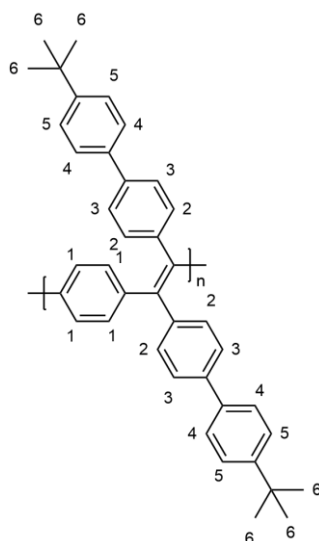
4.2.22 4,4'-Bis(4''-*tert*-butylphenyl)terephthalophenone (PDK-DBtBu)



2 M Sodium carbonate aqueous solution (30 ml, 60.0 mmol, 23 eq.), 4-*tert*-butylbenzeneboronic acid (1.29 g, 7.25 mmol, 2.8 eq.), and a few drops of Aliquat® 336 were added to a solution of 4,4'-dibromoterephthalophenone (1.15 g, 2.59 mmol, 1.0 eq.) in toluene (25 ml). The solution was bubbled with argon for 15 minutes. Then, tetrakis(triphenylphosphine)palladium(0) (0.15 g, 0.13 mmol, 0.05 eq.) was added under argon atmosphere. The mixture was heated to 120°C for 48 hours. Subsequently, the precipitated solid was filtered off and washed with chloroform. The solvent was concentrated and cooled, until further product precipitates. The product was obtained as a white solid (1.11 g, 2.01 mmol, 77%).

$^1\text{H-NMR}$ (600 MHz, CDCl_3 , 300 K): δ [ppm] = 7.93 (m, 8H, $\text{H}_{1,2/3/4/5}$), 7.74 (d, $J = 8.3$ Hz, 4H, $\text{H}_{2/3/4/5}$), 7.62 (d, $J = 8.4$ Hz, 4H, $\text{H}_{2/3/4/5}$), 7.52 (d, $J = 8.4$ Hz, 4H, $\text{H}_{2/3/4/5}$), 1.38 (s, 18H, H_6).
 $^{13}\text{C}\{\text{H}\}$ -NMR (151 MHz, CDCl_3 , 300 K): δ [ppm] = 195.8, 151.8, 145.8, 141.0, 137.0, 135.5, 131.0, 127.1, 127.1, 126.2, 34.8, 31.5. **IR:** $\tilde{\nu}$ [cm^{-1}] = 2957+2902+2866 ($\text{C}_{\text{alkyl-H}}$), 1642 (C=O).
MS (ESI): $m/z = 573.2762$ calculated for $[\text{C}_{40}\text{H}_{38}\text{O}_2\text{Na}]^+ = 573.2764$.

4.2.23 Poly[1,4-phenylene-1,2-bis(4-(4'-*tert*-butyl)biphenyl)vinylene] (PPV-DBtBu)



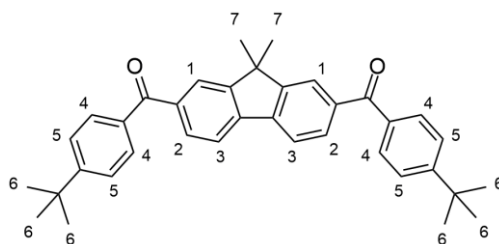
Chlorobenzene (20 ml) was added to 4,4'-bis(4'-*tert*-butylphenyl)terephthalophenone (1.00 g, 1.82 mmol, 1.0 eq.) and phosphorus pentachloride (1.51 g, 7.26 mmol, 4.0 eq.) in a Schlenk tube under argon atmosphere. The solution was stirred for 4 days at 120 °C. Subsequently, the solvent, phosphorus oxychloride, and excess phosphorus pentachloride were removed by distillation under reduced pressure. The resulting 1,4-bis[dichloro(4-(4'-*tert*-butyl)biphenyl)methyl]benzene was used without further purification.

1,4-Bis[dichloro(4-(4'-*tert*-butyl)biphenyl)methyl]benzene (1.20 g, 1.82 mmol, 1.0 eq.) and dicobalt octacarbonyl (1.68 g, 4.90 mmol, 2.7 eq.) were dissolved in chlorobenzene (10 ml) under argon atmosphere. The solution was heated to 100 °C for 50 minutes. Then, 1,2-dichloroethane (10 ml) was added and stirred for further 10 minutes. The polymer was precipitated into acidified (2 M HCl) cold methanol, filtrated, and washed with methanol. The crude product was purified by Soxhlet extraction (MeOH, acetone, EtOAc, CHCl_3). The ethyl acetate and chloroform fractions were redissolved in chloroform (ca. 10 ml) and reprecipitated into acidified (2 M

HCl) cold methanol. The products were obtained as yellow solids (ethyl acetate fraction: 0.45 g, 0.86 mmol, 47%; chloroform fraction: 0.30 g, 0.58 mmol, 32%).

¹H-NMR (400 MHz, C₂D₂Cl₄, 353 K): δ [ppm] = 8.14-6.38 (m, 20H, H₁₋₅), 1.55-0.67 (m, 18H, H₆). **¹³C{¹H}-NMR** (101 MHz, C₂D₂Cl₄, 353 K): δ [ppm] = 150.5, 142.5, 140.9, 138.8, 137.7, 132.0, 131.1, 129.4, 126.6, 125.8, 34.6, 31.6. **GPC** (THF) ethyl acetate fraction: M_n = 12000 g/mol, M_w = 19600 g/mol, PDI = 1.63; chloroform fraction: M_n = 23100 g/mol, M_w = 72600 g/mol, PDI = 3.15. **UV/Vis** (THF solution): λ_{max}. [nm] = 285, 305 sh, 365 sh; (film): λ_{max}. [nm] = 285, 307 sh, 365. **PL** (THF solution, λ_{exc}. [nm] = 360 nm): λ_{max}. [nm] = 554, PLQY = 7.4%; (film, λ_{exc}. [nm] = 370 nm): λ_{max} [nm] = 557, PLQY = 36%. **BET** (N₂ adsorption): S_{BET} [m²/g] = 7; Total pore volume [cm³/g] = 0.03.

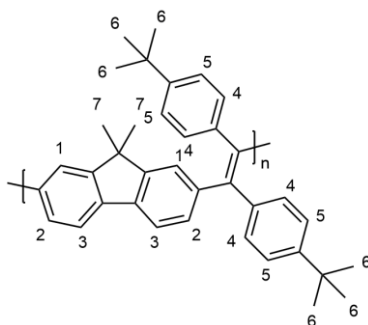
4.2.24 2,7-(4-(*tert*-Butyl)benzoyl)-9,9-dimethyl-9*H*-fluorene (FDK-DPtBu)



4-(*tert*-Butyl)benzoyl chloride (3.4 ml, 18.5 mmol, 2.4 eq.) was added to 9,9-dimethyl-9*H*-fluorene (1.50 g, 7.72 mmol, 1.0 eq.) and aluminium chloride (2.27 g, 17.0 mmol, 2.2 eq.) in dichloroethane (20 ml) under argon atmosphere. The solution was stirred at 85°C for 4 hours. Subsequently, the solution was cooled down to room temperature, and a large amount of cold water was added. The mixture was extracted with chloroform, the organic phase dried over magnesium sulfate, and the solvent removed by evaporation. The crude product was purified by column chromatography twice (hexane/CHCl₃ 7:3; hexane/EtOAc 9:1). The product was obtained as a white powder (0.98 g, 1.90 mmol, 25%).

¹H-NMR (400 MHz, CDCl₃, 300 K): δ [ppm] = 7.97 (s, 2H, H₁), 7.89-7.78 (m, 8H, H_{2,3+4/5}), 7.53 (d, *J* = 8.6 Hz, 4H, H_{4/5}), 1.58 (s, 6H, H₇), 1.39 (s, 18H, H₆). **¹³C{¹H}-NMR** (101 MHz, CDCl₃, 300 K): δ [ppm] = 196.4, 156.3, 154.9, 142.2, 137.9, 135.3, 130.3, 130.2, 125.5, 124.6, 120.5, 47.5, 35.3, 31.3, 27.0. **IR**: $\tilde{\nu}$ [cm⁻¹] = 3058 (C_{ar}-H), 2960+2905+2869 (C_{alkyl}-H), 1652 (C=O). **MS** (ESI): *m/z* = 537.2764 calculated for [C₃₇H₃₈O₂Na]⁺ = 537.2764.

4.2.25 Poly[2,7-(9,9-dimethyl-9H-fluorenylene)-1,2-bis(4-tert-butylphenyl)vinylene] (PFV-DPtBu)



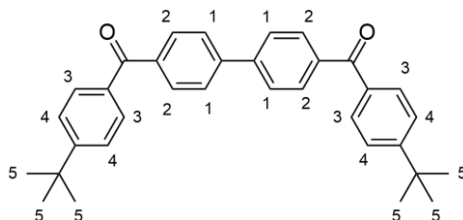
Chlorobenzene (20 ml) was added to 2,7-(4-(*tert*-butyl)benzoyl)-9,9-dimethyl-9*H*-fluorene (0.98 g, 1.90 mmol, 1.0 eq.) and phosphorus pentachloride (1.58 g, 7.61 mmol, 4.0 eq.) in a Schlenk tube under argon atmosphere. The solution was stirred for 72 hours at 120 °C. Subsequently, the solvent, phosphorus oxychloride, and excess phosphorus pentachloride were removed by distillation under reduced pressure. The resulting 2,7-bis[dichloro(4-*tert*-butylphenyl)methyl]-9,9-dimethyl-9*H*-fluorenylene benzene was used without further purification.

2,7-Bis[dichloro(4-*tert*-butylphenylene)methyl]-9,9-dimethyl-9*H*-fluorenylene (1.19 g, 1.90 mmol, 1.0 eq.) and dicobalt octacarbonyl (1.76 g, 5.14 mmol, 2.7 eq.) were dissolved in chlorobenzene (10 ml) under argon atmosphere. The solution was heated to 100 °C for 50 minutes. Then, 1,2-dichloroethane (10 ml) was added and stirred for further 10 minutes. The polymer was precipitated into acidified (2 M HCl) cold methanol, filtrated, and washed with methanol. The crude product was purified by Soxhlet extraction (MeOH, acetone, EtOAc, CHCl₃). The ethyl acetate and chloroform fractions were redissolved in chloroform (ca. 10 ml) and reprecipitated into acidified (2 M HCl) cold methanol. The products were obtained as yellow solids (ethyl acetate fraction: 0.35 g, 0.72 mmol, 38%; chloroform fraction: 0.42 g, 0.86 mmol, 45%).

¹H-NMR (600 MHz, C₂D₂Cl₄, 353 K): δ [ppm] = 7.93-6.45 (m, 14H, H₁₋₅), 1.41-1.09 (m, 18H, H₆), 1.04-0.79 (m, 6H, H₇). **¹³C{¹H}-NMR** (151 MHz, C₂D₂Cl₄, 353 K): δ [ppm] = 153.7, 149.8, 143.6, 141.6, 141.4, 137.4, 131.5, 130.5, 124.9, 124.6, 119.3, 46.3, 34.7, 31.7, 27.1. **GPC** (THF) ethyl acetate fraction: M_n = 6700 g/mol, M_w = 8800 g/mol, PDI = 1.30; chloroform fraction: M_n = 15000 g/mol, M_w = 24200 g/mol, PDI = 1.61. **UV/Vis** (THF solution): λ_{max}. [nm] = 280, 380; (film): λ_{max}. [nm] = 282, 379. **PL** (THF solution, λ_{exc}. [nm] = 380 nm): λ_{max}. [nm] = 545,

PLQY = 4.8%; (film, λ_{exc} [nm] = 370 nm): λ_{max} [nm] = 559, PLQY = 21%. **BET** (N_2 adsorption): S_{BET} [m^2/g] = 351; Total pore volume [cm^3/g] = 0.37.

4.2.26 4,4'-Bis(4-*tert*-butylbenzoyl)biphenyl (BDK-DPtBu)

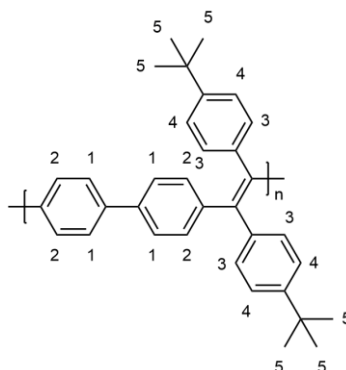


Thionyl chloride (6.0 ml, 82.2 mmol, 10 eq.) and dry dimethylformamide (0.13 ml, 1.68 mmol, 0.2 eq.) were added to 4,4'-biphenyldicarboxylic acid (2.00 g, 8.26 mmol, 1.0 eq.) under argon atmosphere. The solution was heated to 75 °C for 18 hours. Then, the solvent and excess thionyl chloride were evaporated under reduced pressure. The resulting 4,4'-biphenyldicarbonyl chloride was used without further purification.

tert-Butylbenzene (43 ml, 279 mmol, 34 eq.) was added to 4,4'-biphenyldicarbonyl chloride (2.306 g, 8.26 mmol, 1.0 eq.) and aluminium chloride (2.35 g, 17.6 mmol, 2.1 eq.) under argon atmosphere. The solution was stirred at 85 °C for 4 hours. Subsequently, a large amount of cold water was added. The mixture was extracted with chloroform, the organic phase dried over magnesium sulfate, and the solvent removed by evaporation. The crude product was purified by column chromatography (hexane/ CHCl_3 6:4). The product was obtained as white solid (1.28 g, 2.69 mmol, 33%).

$^1\text{H-NMR}$ (600 MHz, CDCl_3 , 300 K): δ [ppm] = 7.93 (d, J = 8.3 Hz, 4H, $\text{H}_{1/2}$), 7.81 (d, J = 8.4 Hz, 4H, $\text{H}_{3/4}$), 7.76 (d, J = 8.3 Hz, 4H, $\text{H}_{1/2}$), 7.53 (d, J = 8.3 Hz, 4H, $\text{H}_{3/4}$), 1.39 (s, 18H, H_5). **$^{13}\text{C}\{\text{H}\}\text{-NMR}$** (151 MHz, CDCl_3 , 300 K): δ [ppm] = 196.0, 156.5, 143.9, 137.5, 135.0, 130.9, 130.3, 127.3, 125.5, 35.3, 31.3. **IR**: $\tilde{\nu}$ [cm^{-1}] = 3055+3035 ($\text{C}_{\text{ar}}\text{-H}$), 2903+2866 ($\text{C}_{\text{alkyl}}\text{-H}$), 1650+1602 (C=O). **MS** (ESI): m/z = 497.2488 calculated for $[\text{C}_{34}\text{H}_{34}\text{O}_2\text{Na}]^+$ = 497.2451.

4.2.27 Poly[4,4'-biphenyldiyl-1,2-bis(4-*tert*-butylphenyl)vinylene] (PBV-DPtBu)

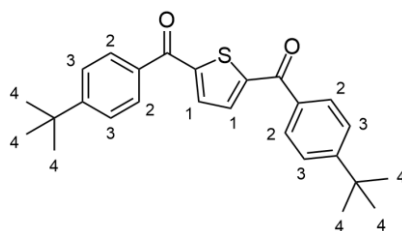


Chlorobenzene (20 ml) was added to 4,4'-bis(4-*tert*-butylbenzoyl)biphenyl (1.07 g, 2.25 mmol, 1.0 eq.) and phosphorus pentachloride (1.88 g, 9.02 mmol, 4.0 eq.) in a Schlenk tube under argon atmosphere. The solution was stirred for 3 days at 120 °C. Subsequently, the solvent, phosphorus oxychloride, and excess phosphorus pentachloride were removed by distillation under reduced pressure. The resulting 4,4'-bis[dichloro(4-*tert*-butylphenyl)methyl]biphenyl was used without further purification.

4,4'-Bis[dichloro(4-*tert*-butylphenyl)methyl]biphenyl (1.32 g, 2.25 mmol, 1.0 eq.) and dicobalt octacarbonyl (2.08 g, 6.09 mmol, 2.7 eq.) were dissolved in chlorobenzene (10 ml) under argon atmosphere. The solution was heated to 100 °C for 50 minutes. Then, 1,2-dichloroethane (10 ml) was added and stirred for further 10 minutes. The polymer was precipitated into acidified (2 M HCl) cold methanol, filtrated, and washed with methanol. The crude product was purified by Soxhlet extraction (MeOH, acetone, EtOAc, CHCl₃). The ethyl acetate and chloroform fractions were redissolved in chloroform (ca. 10 ml) and reprecipitated into acidified (2 M HCl) cold methanol. The products were obtained as yellow solids (ethyl acetate fraction: 0.12 g, 0.28 mmol, 12%; chloroform fraction: 0.12 g, 0.28 mmol, 12%).

¹H-NMR (600 MHz, C₂D₂Cl₄, 353 K): δ [ppm] = 8.39-6.40 (m, 16H, H₁₋₄), 2.13-0.40 (m, 18H, H₅). **¹³C{¹H}-NMR** (151 MHz, C₂D₂Cl₄, 353 K): δ [ppm] = 149.6, 147.9, 143.2, 140.8, 138.5, 131.9, 131.1, 126.1, 124.7, 34.5, 31.5. **GPC** (THF) ethyl acetate fraction: M_n = 8800 g/mol, M_w = 16100 g/mol, PDI = 1.83; chloroform fraction: M_n = 26100 g/mol, M_w = 65700 g/mol, PDI = 2.51. **UV/Vis** (THF solution): λ_{max}. [nm] = 270 sh, 349; (film): λ_{max}. [nm] = 268, 351. **PL** (THF solution, λ_{exc}. [nm] = 350 nm): λ_{max}. [nm] = 532, PLQY = 3.8%; (film, λ_{exc}. [nm] = 350 nm): λ_{max} [nm] = 538, PLQY = 11%. **BET** (N₂ adsorption): S_{BET} [m²/g] = 85; Total pore volume [cm³/g] = 0.46.

4.2.28 2,5-(4-*tert*-Butylbenzoyl)thiophene (TDK-DPtBu)

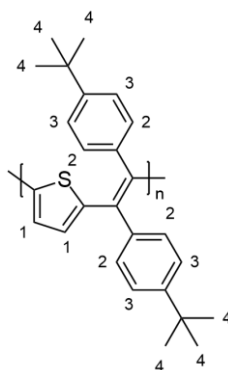


Thionyl chloride (6.4 ml, 87.0 mmol, 10 eq.) and dry dimethylformamide (0.14 ml, 1.74 mmol, 0.2 eq.) were added to 2,5-thiophenedicarboxylic acid (1.50 g, 8.71 mmol, 1.0 eq.) under argon atmosphere. The solution was heated to 75 °C for 4 hours. Then, the solvent and excess thionyl chloride were evaporated under reduced pressure. The resulting 2,5-thiophenedicarbonyl chloride was used without further purification.

tert-Butylbenzene (20 ml, 130 mmol, 15 eq.) was added to 2,5-thiophenedicarbonyl chloride (1.82 g, 8.71 mmol, 1.0 eq.) and aluminium chloride (19.1 mmol, 2.2 eq.) under argon atmosphere. The solution was stirred at 85°C for 17 hours. Subsequently, the solution was cooled down to room temperature and a large amount of cold water was added. The mixture was extracted with chloroform (3x 100 ml), the combined organic phases dried over magnesium sulfate, and the solvent removed by evaporation. The crude product was purified by column chromatography (hexane/EtOAc 9:1). The product was obtained as yellow solid (2.00 g, 4.94 mmol, 57%).

¹H-NMR (400 MHz, CDCl₃, 300 K): δ [ppm] = 7.88 (d, *J* = 8.7 Hz, 4H, H_{2/3}), 7.70 (s, 2H, H₁), 7.54 (s, *J* = 8.7 Hz, 4H, H_{2/3}), 1.38 (s, 18H, H₄). **¹³C{¹H}-NMR** (101 MHz, CDCl₃, 300 K): δ [ppm] = 187.9, 157.0, 148.6, 134.8, 133.6, 129.6, 125.7, 35.3, 31.3. **IR**: $\tilde{\nu}$ [cm⁻¹] = 3086 (C_{ar}-H), 2962+2902+2864 (C_{alkyl}-H), 1629 (C=O). **MS** (ESI): *m/z* = 427.1700 calculated for [C₂₆H₂₈O₂NaS]⁺ = 427.1702.

4.2.29 Poly[2,5-thiophenylene-1,2-bis(4-*tert*-butylphenyl)vinylene] (PTV-DPtBu)

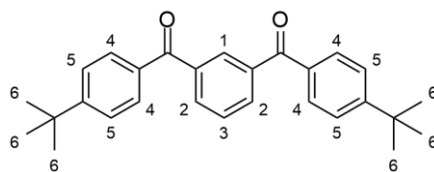


Chlorobenzene (20 ml) was added to 2,5-(4-*tert*-butylbenzoyl)thiophene (1.00 g, 2.47 mmol, 1.0 eq.) and phosphorus pentachloride (2.06 g, 9.89 mmol, 4.0 eq.) in a Schlenk tube under argon atmosphere. The solution was stirred for 4 days at 120 °C. Subsequently, the solvent, phosphorus oxychloride, and excess phosphorus pentachloride were removed by distillation under reduced pressure. The resulting 2,5-bis[dichloro(4-*tert*-butylphenyl)methyl]thiophene was used without further purification.

2,5-Bis[dichloro(4-*tert*-butylphenyl)methyl]thiophene (1.27 g, 2.47 mmol, 1.0 eq.) and dicobalt octacarbonyl (2.28 g, 6.67 mmol, 2.7 eq.) were dissolved in chlorobenzene (10 ml) under argon atmosphere. The solution was heated to 100 °C for 50 minutes. Then, 1,2-dichloroethane (10 ml) was added and stirred for further 10 minutes. The polymer was precipitated into acidified (2 M HCl) cold methanol, filtrated, and washed with methanol. The crude product was purified by Soxhlet extraction (MeOH, acetone, EtOAc, CHCl₃). The ethyl acetate and chloroform fractions were redissolved in chloroform (ca. 10 ml) and reprecipitated into acidified (2 M HCl) cold methanol. The products were obtained as dark orange/brownish solids (ethyl acetate fraction: 0.19 g, 0.52 mmol, 21%; chloroform fraction: 0.12 g, 0.32 mmol, 13%).

¹H-NMR (600 MHz, C₂D₂Cl₄, 353 K): δ [ppm] = 7.89-6.07 (m, 10H, H₁₋₃), 2.01-0.48 (m, 18H, H₄). **¹³C{¹H}-NMR** (151 MHz, C₂D₂Cl₄, 353 K): δ [ppm] = 130.8, 129.3, 128.8, 128.5, 125.5, 34.6, 31.6. **GPC** (THF) ethyl acetate fraction: M_n = 4200 g/mol, M_w = 7000 g/mol, PDI = 1.67; chloroform fraction: M_n = 6900 g/mol, M_w = 20300 g/mol, PDI = 2.93. **UV/Vis** (THF solution): λ_{max}. [nm] = 256, 410; (film): λ_{max}. [nm] = 254, 404. **PL** (THF solution, λ_{exc}. [nm] = 400 nm): λ_{max}. [nm] = 588, PLQY = N/A; (film, λ_{exc}. [nm] = 400 nm): λ_{max} [nm] = 619, PLQY = N/A. **BET** (N₂ adsorption): S_{BET} [m²/g] = 34; Total pore volume [cm³/g] = 0.35.

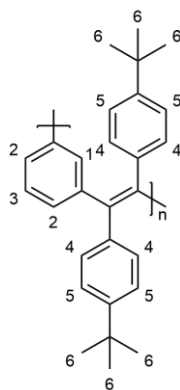
4.2.30 4,4'-Bis(*tert*-butyl)isophthalophenone (mPDK-DPtBu)



tert-Butylbenzene (3.6 ml, 23.3 mmol, 2.4 eq.) was added to isophthaloyl chloride (2.01 g, 9.90 mmol, 1.0 eq.) and aluminium chloride (2.93 g, 21.9 mmol, 2.2 eq.) in dichloroethane (30 ml) under argon atmosphere. The solution was stirred at room temperature for 24 hours. Subsequently, a large amount of cold water was added. The mixture was extracted with chloroform, the organic phase dried over magnesium sulfate, and the solvent removed by evaporation. The crude product was purified by column chromatography (hexane/CHCl₃ 3:2). The product was obtained as a light yellow solid (3.49 g, 8.75 mmol, 88%).

¹H-NMR (400 MHz, CDCl₃, 300 K): δ [ppm] = 8.18 (s, 1H, H₁), 8.02 (d, *J* = 7.7 Hz, 2H, H₂), 7.78 (d, *J* = 8.7 Hz, 4H, H_{4/5}), 7.62 (t, *J* = 7.7 Hz, 1H, H₃), 7.51 (d, *J* = 8.7 Hz, 4H, H_{4/5}), 1.37 (s, 18H, H₆). ¹³C{¹H}-NMR (101 MHz, CDCl₃, 300 K): δ [ppm] = 195.7, 156.8, 138.2, 134.5, 133.3, 131.3, 130.3, 128.6, 125.6, 35.3, 31.3. IR: $\tilde{\nu}$ [cm⁻¹] = 3065 (C_{ar}-H), 2956+2903+2865 (C_{alkyl}-H), 1656 (C=O). MS (ESI): *m/z* = 421.2134 calculated for [C₂₈H₃₀O₂Na]⁺ = 421.2138.

4.2.31 Poly[1,3-phenylene-1,2-bis(4-*tert*-butylphenyl)vinylene] (PmPV-DPtBu)



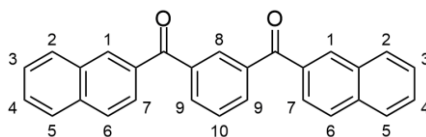
Chlorobenzene (20 ml) was added to 4,4'-bis(*tert*-butyl)isophthalophenone (1.00 g, 2.51 mmol, 1.0 eq.) and phosphorus pentachloride (2.07 g, 9.94 mmol, 4.0 eq.) in a Schlenk tube under argon atmosphere. The solution was stirred for 17 hours at 120 °C. Subsequently, the solvent, phosphorus oxychloride, and excess phosphorus pentachloride were removed by

distillation under reduced pressure. The resulting 1,3-bis[dichloro(4-*tert*-butylphenyl)methyl]benzene was used without further purification.

1,3-Bis[dichloro(4-*tert*-butylphenyl)methyl]benzene (1.28 g, 2.51 mmol, 1.0 eq.) and dicobalt octacarbonyl (2.32 g, 6.78 mmol, 2.7 eq.) were dissolved in chlorobenzene (10 ml) under argon atmosphere. The solution was heated to 100 °C for 50 minutes. Then, 1,2-dichloroethane (10 ml) was added and stirred for further 10 minutes. The polymer was precipitated into acidified (2 M HCl) cold methanol, filtrated, and washed with methanol. The crude product was purified by Soxhlet extraction (MeOH, acetone, EtOAc, CHCl₃). The ethyl acetate and chloroform fractions were redissolved in chloroform (ca. 10 ml) and reprecipitated into acidified (2 M HCl) cold methanol. The products were obtained as light yellow solids (ethyl acetate fraction: 0.40 g, 1.08 mmol, 43%; chloroform fraction: 1.3 mg, 0.004 mmol, 0.1%).

¹H-NMR (400 MHz, C₂D₂Cl₄, 353 K): δ [ppm] = 8.91-7.54 (m, 12H, H₁₋₅), 2.86-1.81 (m, 18H, H₆). **¹³C{¹H}-NMR** (101 MHz, C₂D₂Cl₄, 353 K): δ [ppm] = 152.0, 146.7, 143.5, 137.0, 133.9, 132.3, 130.9, 129.9, 127.1, 37.4, 34.6. **GPC** (THF) ethyl acetate fraction: M_n = 7700 g/mol, M_w = 12800 g/mol, PDI = 1.67; chloroform fraction: M_n = 16600 g/mol, M_w = 112000 g/mol, PDI = 6.72. **UV/Vis** (THF solution): λ_{max}. [nm] = 248, 319; (film): λ_{max}. [nm] = 246, 317. **PL** (THF solution, λ_{exc}. [nm] = 320 nm): λ_{max}. [nm] = 507, PLQY = 3.6%; (film, λ_{exc}. [nm] = 320 nm): λ_{max} [nm] = 498, PLQY = 13%. **BET** (N₂ adsorption): S_{BET} [m²/g] = 1; Total pore volume [cm³/g] = 0.004.

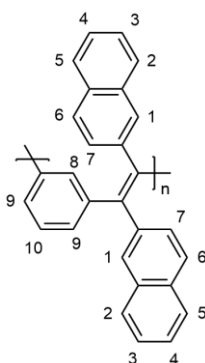
4.2.32 1,3-Bis(2-naphthoyl)benzene (mPDK-DN)



Isophthaloyl chloride (0.10 g, 0.49 mmol, 1.0 eq.) was added to naphthalene (0.14 g, 1.08 mmol, 2.2 eq.) and aluminium chloride (0.14 g, 1.08 mmol, 2.2 eq.) in dichloroethane (5 ml) under argon. The solution was stirred at room temperature for 20 hours. Subsequently, cold water was added. Then, the aqueous phase was separated and the organic layer was dried over magnesium sulfate. The solvent was evaporated in vacuo and the crude product was purified by column chromatography (hexane/CH₂Cl₂ 1:1) The product was obtained as a white solid (0.01 g, 0.04 mmol, 8%) yield.

¹H-NMR (400 MHz, CDCl₃, 300 K): δ [ppm] = 8.33-8.28 (m, 3H, H_{1,8}), 8.13 (d, *J* = 7.7 Hz, 2H, H₉), 8.00-7.87 (m, 8H, H_{2,5,6,7}), 7.71 (t, *J*=7.7 Hz, 1H, H₁₀), 7.62 (t, *J* = 8.2 Hz, 2H, H_{3/4}), 7.58 (t, *J* = 8.1 Hz, 2H, H_{3/4}). **¹³C{¹H}-NMR** (101 MHz, CDCl₃, 300 K): δ [ppm] = 196.0, 138.4, 135.6, 134.4, 133.6, 132.4, 132.2, 131.4, 129.7, 128.8, 128.7, 128.7, 128.0, 127.1, 125.7. **IR:** $\tilde{\nu}$ [cm⁻¹] = 3052+2919+2850 (C_{ar}-H), 1654 (C=O). **MS** (ESI): *m/z* = 409.1191 calculated for [C₂₈H₁₈O₂Na]⁺ = 409.1199.

4.2.33 Poly[1,3-phenylene-1,2-bis(2-naphthyl)vinylene] (PmPV-DN)

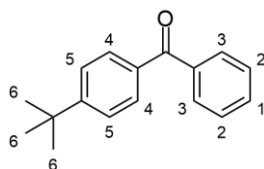


Chlorobenzene (10 ml) was added to 1,3-bis(2-naphthoyl)benzene (0.44 g, 1.15 mmol, 1.0 eq.) and phosphorus pentachloride (0.96 g, 4.59 mmol, 4.0 eq.) in a Schlenk tube under argon atmosphere. The solution was stirred for 24 hours at 120 °C. Subsequently, the solvent, phosphorus oxychloride, and excess phosphorus pentachloride were removed by distillation under reduced pressure. The resulting 1,3-bis[dichloro(2-naphthyl)methyl]-benzene was used without further purification.

1,3-Bis[dichloro(2-naphthyl)methyl]benzene (0.57 g, 1.15 mmol, 1.0 eq.) and dicobalt octacarbonyl (1.07 g, 3.12 mmol, 2.7 eq.) were dissolved in chlorobenzene (10 ml) under argon atmosphere. The solution was heated to 100 °C for 50 minutes. Then, 1,2-dichloroethane (10 ml) was added and stirred for further 10 minutes. The polymer was precipitated into acidified (2 M HCl) cold methanol, filtrated, and washed with methanol. The crude product was purified by Soxhlet extraction (MeOH, acetone, EtOAc, CHCl₃). The ethyl acetate and chloroform fractions were redissolved in chloroform (ca. 10 ml) and reprecipitated into acidified (2 M HCl) cold methanol. The products were obtained as orange solids (ethyl acetate fraction: 0.07 g, 0.19 mmol, 16%; chloroform fraction: 0.27 g, 0.75 mmol, 65%).

¹H-NMR (600 MHz, C₂D₂Cl₄, 353 K): δ [ppm] = 7.92-6.41 (m, 18H, H₁₋₁₀). **¹³C{¹H}-NMR** (151 MHz, C₂D₂Cl₄, 353 K): δ [ppm] = 143.9, 143.4, 141.6, 141.0, 133.5, 132.4, 130.4, 129.8, 129.5, 128.4, 128.0, 127.8, 127.1, 126.0. **GPC** (THF) ethyl acetate fraction: M_n = 2600 g/mol, M_w = 3600 g/mol, PDI = 1.37; chloroform fraction: M_n = 5300 g/mol, M_w = 9400 g/mol, PDI = 1.77. **UV/Vis** (THF solution): λ_{max}. [nm] = 221, 335; (film): λ_{max}. [nm] = 268, 348. **PL** (THF solution): λ_{max}. [nm] = 518, PLQY = 0.8%; (film): λ_{max} [nm] = 611, PLQY = 0.2%. **BET** (N₂ adsorption): S_{BET} [m²/g] = 17; Total pore volume [cm³/g] = 0.11.

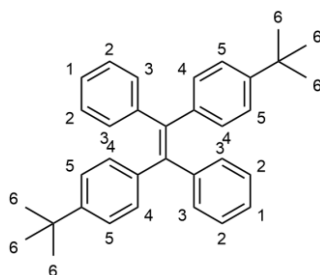
4.2.34 1-Benzoyl-4-*tert*-butylbenzene (17)



In a dry flask benzoyl chloride (1.0 ml, 8.68 mmol 1.0 eq.) was added to a solution of *tert*-butylbenzene (1.5 ml, 9.72 mmol 1.1 eq.) and aluminium chloride (1.39 g, 10.4 mmol, 1.2 eq.) in dichloroethane (3 ml) under argon atmosphere. The solution was stirred for 4 hours at room temperature. Subsequently, a large amount of cold water was added and the aqueous phase was extracted with chloroform (3x 20 ml), the organic phase dried over magnesium sulfate, and the solvent was evaporated in vacuo. The crude product was purified by flash column chromatography (hexane/CHCl₃ 1:0 → 8:2). The product was obtained as colourless oil (1.46 g, 6.11 mmol, 70%).

¹H-NMR (400 MHz, CDCl₃, 300 K): δ [ppm] = 7.81 (d, *J* = 7.0 Hz, 2H, H₃), 7.77 (d, *J* = 8.7 Hz, 2H, H₄), 7.58 (t, *J* = 7.4 Hz, 1H, H₁), 7.52-7.43 (m, 4H, H_{2,5}), 1.37 (s, 9H, H₆). **¹³C{¹H}-NMR** (101 MHz, CDCl₃, 300 K): δ [ppm] = 196.6, 156.3, 138.1, 135.0, 132.3, 130.3, 130.2, 128.3, 125.4, 35.3, 31.3. **IR**: $\tilde{\nu}$ [cm⁻¹] = 3082+3061+3031 (C_{ar}-H), 2962+2904+2867 (C_{alkyl}-H) 1656+1604 (C=O). **MS** (ESI): *m/z* = 261.1249 calculated for [C₁₇H₁₈ONa]⁺ = 261.1250.

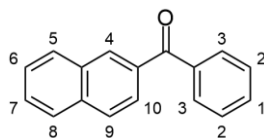
4.2.35 *E*-1,2-Bis(4-*tert*-butylphenyl)-1,2-diphenylethylene (TPE-DtBu)



A suspension of zinc (1.60 g, 24.5 mmol, 4.0 eq.) in dry tetrahydrofuran (15 ml) was stirred under argon at 0 °C. Titanium tetrachloride (1.4 ml, 12.7 mmol, 2.1 eq.) was added slowly and the ice bath was removed. The mixture was heated to 70 °C for 3.5 hours. Then, 1-benzoyl-4-*tert*-butylbenzene (1.46 g, 6.11 mmol, 1.0 eq.) in THF (7 ml) was added. The mixture was stirred at 70 °C for 44 hours. The solution was cooled to room temperature and quenched with a saturated solution of aqueous ammonium chloride (30 ml). Then, the mixture was extracted with chloroform, the organic phase dried over magnesium sulfate, and the solvent removed by evaporation. The *E/Z*-Isomers (1.36 g, 3.05 mmol, >99%) were separated by recrystallization from a mixture of hexane and toluene. The *E*-isomer was obtained as white solid (0.15 g, 0.34 mmol, 11%).

¹H-NMR (400 MHz, CDCl₃, 300 K): δ [ppm] = 7.10-7.07 (m, 10H, H_{1,2/3/4/5}), 7.06-7.02 (m, 4H, H_{2/3/4/5}), 6.92 (d, *J* = 8.5 Hz, 4H, H_{3/4/5}), 1.25 (s, 18H, H₆). **¹³C{¹H}-NMR** (101 MHz, CDCl₃, 300 K): δ [ppm] = 149.3, 144.3, 140.9, 140.6, 131.5, 131.1, 127.6, 126.3, 124.5, 34.5, 31.5. **IR**: $\tilde{\nu}$ [cm⁻¹] = 3080+3058+3038 (C_{ar}-H), 2962+2901+2863 (C_{alkyl}-H). **MS** (ESI): *m/z* = 467.2635 calculated for [C₃₄H₃₆Na]⁺ = 467.2709. **UV/Vis** (THF solution): λ_{max}. [nm] = 242, 314; (film): λ_{max}. [nm] = 245, 320. **PL** (THF solution): λ_{max}. [nm] = 358, 490, PLQY = 2.4%; (film): λ_{max} [nm] = 473, PLQY = 4.6%. **BET** (N₂ adsorption): S_{BET} [m²/g] = 1; Total pore volume [cm³/g] = 0.01.

4.2.36 2-Benzoylnaphthalene

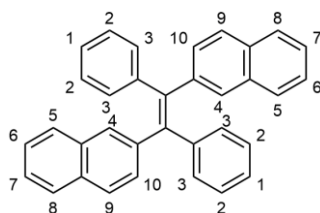


In a flame-dried flask benzoyl chloride (3.0 ml, 26.0 mmol 1.0 eq.) was added to a solution of naphthalene (3.67, 28.6 mmol 1.1 eq.) and aluminium chloride (4.17 g, 31.3 mmol, 1.2 eq.) in

chloroform (250 ml) under argon atmosphere. The solution was stirred for 17 hours at room temperature. Subsequently, a large amount of cold water was added and the aqueous phase was extracted with chloroform (3x 200 ml), the organic phase dried over magnesium sulfate, and the solvent was evaporated in vacuo. The crude product was purified by twofold flash column chromatography (hexane/CH₂Cl₂ 1:0 → 0:1; hexane/CH₂Cl₂ 8:2). The product was obtained as a yellow solid (0.73 g, 3.14 mmol, 12%).

¹H-NMR (400 MHz, CDCl₃, 300 K): δ [ppm] = 8.30 (s, 1H, H₄), 7.98 (d, *J* = 1.2 Hz, 2H, H_{9,10}), 7.96-7.92 (m, 2H, H_{5,8}), 7.89 (d, *J* = 8.3 Hz, 2H, H₃) 7.69-7.62 (m, 2H, H_{6,7}), 7.61-7.51 (m, 3H, H_{1,2}). **¹³C{¹H}-NMR** (101 MHz, CDCl₃, 300 K): δ [ppm] = 196.7, 138.0, 135.3, 134.9, 132.4, 132.3, 131.8, 130.1, 129.4, 128.3, 128.3, 128.3, 127.8, 126.8, 125.8. **IR**: $\tilde{\nu}$ [cm⁻¹] = 3057+3025 (C_{ar}-H), 1653+1623 (C=O). **MS** (ESI): *m/z* = 233.0961 calculated for [C₁₇H₁₃O]⁺ = 233.0961.

4.2.37 *E*-1,2-Bis(2-naphthenyl)-1,2-diphenylethylene (DPE-DN)

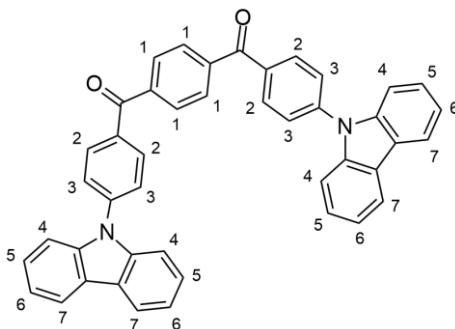


A suspension of zinc (0.82 g, 12.6 mmol, 4.0 eq.) in dry tetrahydrofuran (12 ml) was stirred under argon at 0 °C. Titanium tetrachloride (0.7 ml, 6.35 mmol, 2.0 eq.) was added slowly and the ice bath was removed. The mixture was heated to 70 °C for 3.5 hours. Then, 2-benzoylnaphthalene (0.73 g, 3.14 mmol, 1.0 eq.) in THF (7 ml) was added. The mixture was stirred at 70 °C for 19 hours. The solution was cooled to room temperature and quenched with a saturated solution of aqueous ammonium chloride (30 ml). Then, the mixture was extracted with chloroform, the organic phase dried over magnesium sulfate, and the solvent removed by evaporation. The *E/Z*-isomers (0.66 g, 1.53 mmol, 97%) were separated by recrystallization from a mixture of hexane and toluene. The *E*-isomer was obtained as white solid (0.20, 0.46, 29%).

¹H-NMR (400 MHz, CDCl₃, 300 K): δ [ppm] = 7.74 (d, *J* = 7.5 Hz, 2H, H_{5/8}), 7.63-7.52 (m, 6H, H_{4,5/8,10}), 7.44-7.35 (m, 4H, H_{6,7}), 7.21 (dd, *J* = 8.4, 1.7 Hz, 2H, H₉) 7.14-7.06 (m, 10H, H₁₋₃). **¹³C{¹H}-NMR** (101 MHz, CDCl₃, 300 K): δ [ppm] = 143.9, 141.6, 141.5, 133.4, 132.3, 131.7, 130.7, 129.7, 128.2, 128.0, 127.6, 127.1, 126.8, 125.9, 125.9. **IR**: $\tilde{\nu}$ [cm⁻¹] = 3078+3050+3020 (C_{ar}-H). **MS** (ESI): *m/z* = 455.1789 calculated for [C₃₄H₂₄Na]⁺ = 455.1770.

UV/Vis (THF solution): λ_{\max} . [nm] = 220, 334; (film): λ_{\max} . [nm] = 226, 337. **PL** (THF solution): λ_{\max} . [nm] = 407, 490 sh, PLQY = 0.3%; (film): λ_{\max} [nm] = 479, PLQY = 1.2%. **BET** (N_2 adsorption): S_{BET} [m^2/g] = 1; Total pore volume [cm^3/g] = 0.01.

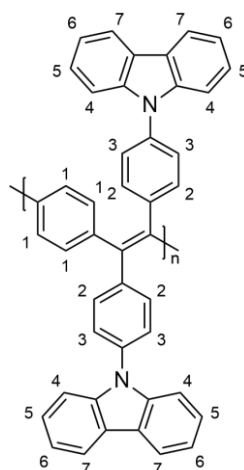
4.2.38 4,4'-Bis(9-carbazoyl)terephthalophenone (PDK-DPC)



Potassium carbonate (6.02 g, 43.6 mmol, 8.0 eq.), tri-*tert*-butylphosphine (0.26 ml, 1.09 mmol, 0.2 eq.), palladium(II) acetate (0.12 g, 0.54 mmol, 0.1 eq.), 9*H*-carbazole (1.82 g, 10.9 mmol, 2 eq.), and 4,4'-dibromoterephthalophenone (2.42 g, 5.45 mmol, 1.0 eq.) were dissolved in toluene (30 ml) and heated to 120 °C under argon atmosphere. After 48 hours, the mixture was cooled to room temperature, water was added, and the mixture extracted with chloroform (3x100 ml). The combined organic phases were dried over magnesium sulfate and the solvent evaporated. The crude product was purified by twofold recrystallization from acetonitrile. The product was obtained as beige powder (2.09 g, 3.39 mmol, 62%).

$^1\text{H-NMR}$ (600 MHz, CDCl_3 , 300 K): δ [ppm] = 8.16 (m, 8H, $\text{H}_{2/3+4/7}$), 8.06 (s, 4H, H_1), 7.80 (d, $J = 8.5$ Hz, 4H, $\text{H}_{4/7}$), 7.55 (d, $J = 8.2$ Hz, 4H, $\text{H}_{2/3}$), 7.46 (t, $J = 7.7$ Hz, 4H, $\text{H}_{5/6}$), 7.35 (t, $J = 7.4$ Hz, 4H, H_4 , $\text{H}_{5/6}$). **$^{13}\text{C}\{\text{H}\}\text{-NMR}$** (151 MHz, CDCl_3 , 300 K): δ [ppm] = 194.9, 142.4, 140.9, 140.4, 135.4, 132.1, 130.0, 126.6, 126.4, 124.1, 120.9, 120.7, 109.9. **IR**: $\tilde{\nu}$ [cm^{-1}] = 3047+3018+2952+2923+2847 ($\text{C}_{\text{ar}}\text{-H}$), 1659 ($\text{C}=\text{O}$). **MS** (FD): $m/z = 616.2112$ calculated for $[\text{C}_{37}\text{H}_{38}\text{O}_2\text{Na}]^+ = 616.2151$.

4.2.39 Poly[1,4-phenylene-1,2-bis(4-(9-carbazoyl)phenyl)vinylene] (PPV-DPC)



Chlorobenzene (100 ml) was added to 4,4'-bis(9-carbazoyl)terephthalophenone (1.07 g, 1.74 mmol, 1.0 eq.) and phosphorus pentachloride (1.45 g, 6.94 mmol, 4.0 eq.) in a Schlenk tube under argon atmosphere. The solution was stirred for 3 days at 120 °C. Subsequently, the solvent, phosphorus oxychloride, and excess phosphorus pentachloride were removed by distillation under reduced pressure. The resulting 1,4-bis[dichloro(4-(9-carbazoyl)phenyl)methyl]benzene was used without further purification.

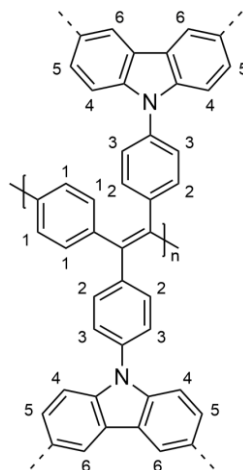
1,4-Bis[dichloro(4-(9-carbazoyl)phenyl)methyl]benzene (1.20 g, 1.65 mmol, 1.0 eq.) and dicobalt octacarbonyl (1.53 g, 4.46 mmol, 2.7 eq.) were dissolved in dimethylformamide (120 ml) under argon atmosphere. The solution was heated to 100 °C for 1 hour. Subsequently, the temperature was increased to 160 °C for 2.5 hours. Then, 1,2-dichloroethane (10 ml) was added at 100 °C and stirred for further 10 minutes. The polymer was precipitated into cold methanol, filtrated, and washed with methanol. The crude product was purified by Soxhlet extraction (MeOH, acetone, EtOAc, CHCl₃). The ethyl acetate and chloroform fractions were reprecipitated into cold methanol. The products were obtained as yellow solids (ethyl acetate fraction: 0.09 g, 0.15 mmol, 10%; chloroform fraction: 0.65 g, 1.11 mmol, 67%; contains 26% monomer estimated from GPC).

M-PPV-DPC:

¹H-NMR (600 MHz, C₂D₂Cl₄, 353 K): δ [ppm] = 8.26-6.71 (m, 28H, H₁₋₇). **¹³C{¹H}-NMR** (151 MHz, C₂D₂Cl₄, 353 K): δ [ppm] = 194.9, 143.5, 143.3, 141.5, 140.9, 140.1, 136.0, 133.2, 132.3, 131.6, 130.2, 127.2, 126.6, 124.1, 121.6, 120.8, 111.3, 110.3. **IR:** $\tilde{\nu}$ [cm⁻¹] = 3060+3035 (C_{ar}-H), 1653 (C=O). **GPC** ethyl acetate fraction (CHCl₃): M_n = 2100 g/mol, M_w = 2400 g/mol, PDI = 1.12; chloroform fraction (TCB): M_n = 5100 g/mol, M_w = 6100 g/mol, PDI = 1.20.

UV/Vis (THF solution): λ_{\max} [nm] = 237, 291, 349; (film): λ_{\max} [nm] = 217, 249, 304, 349. **PL** (THF solution, λ_{exc} [nm] = 350 nm): λ_{\max} [nm] = 545, PLQY = 4.9%; (film, λ_{exc} [nm] = 350 nm): λ_{\max} [nm] = 539, PLQY = 40%. **BET** (N_2 adsorption): S_{BET} [m^2/g] = 20; Total pore volume [cm^3/g] = 0.20.

4.2.40 Network N1

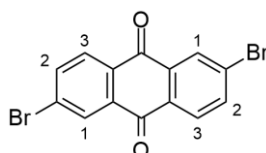


In the 10 ml-reaction cell a solution of 1.8 mg **M-PPV-DPC** and tetrabutylammonium hexafluorophosphate (386 mg, 0.1 mmol) in dichloromethane (10 ml) was purged with argon. The network was generated on ITO glass by cyclic voltammetry in the range of 0-1.5 V with a scan rate of 0.1 Vs^{-1} . After 20 cycles the film was removed from the glass surface by washing with acetonitrile.

IR: $\tilde{\nu}$ [cm^{-1}] = 3079+3060+3025+2920+2847 ($\text{C}_{\text{ar}}\text{-H}$), 1661 ($\text{C}=\text{O}$). **UV/Vis** (film on ITO): λ_{\max} [nm] = 300, 349 sh. **PL** (film on ITO, λ_{exc} [nm] = 350 nm): λ_{\max} [nm] = 533, PLQY = <1%. **BET** (Kr adsorption): S_{BET} [m^2/g] = 5; Total pore volume [cm^3/g] = 0.003.

4.3 Syntheses from chapter 3

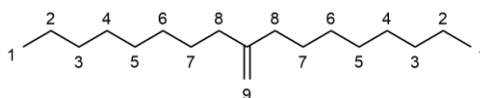
4.3.1 2,6-Dibromoanthraquinone (30)



To a refluxing mixture of *tert*-butyl nitrite (8.4 ml, 63.6 mmol, 3.0 eq.), copper(II) bromide (11.91 g, 53.3 mmol, 2.5 eq.), and dry acetonitrile (350 ml) under argon atmosphere 2,6-diaminoanthraquinone (5.00 g, 21.0 mmol, 1.0 eq.) was slowly added. After 4 hours the mixture was cooled down to room temperature and poured into a 1 M aqueous hydrochloric acid solution. The crude 2,6-dibromoanthraquinone which precipitates was filtered off and purified by recrystallization from chloroform. The product was obtained as a light yellow solid (6.74 g, 18.43 mmol, 88%).

¹H-NMR (600 MHz, CDCl₃, 323 K): δ [ppm] = 8.44 (d, *J* = 2.0 Hz, 2H, H₁), 8.17 (d, *J* = 8.3 Hz, 2H, H₃), 7.94 (dd, *J* = 8.3, 2H, 2.0 Hz, H₂). **¹³C{¹H}-NMR** (151 MHz, CDCl₃, 323 K): δ [ppm] = 181.4, 137.5, 134.7, 132.2, 130.6, 130.4, 129.3. **IR:** $\tilde{\nu}$ [cm⁻¹] = 3084+3067 (C_{ar}-H), 1674 (C=O). **MS** (FD): *m/z* = 363.8816, calculated for [C₁₄H₆O₂Br₂]⁺ = 363.8735.

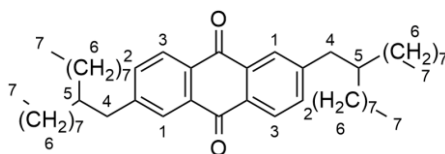
4.3.2 9-Methyleneheptadecane (32)



A dispersion of 60% sodium hydride in mineral oil (0.79 g, 19.7 mmol, 1.0 eq.) was added to dry dimethyl sulfoxide (8 ml) under argon atmosphere and heated to 75 °C for 20 minutes. Then, the mixture was cooled down to 0 °C, and methyltriphenylphosphonium bromide (7.02 g, 19.7 mmol, 1.0 eq.) dissolved in warm dimethyl sulfoxide (20 ml) was added. The resulting solution was stirred for 10 minutes at room temperature. Subsequently, 9-heptadecanone (5.00 g, 19.7 mmol, 1.0 eq.) was added and stirred for 20 hours. Then, saturated aqueous ammonium chloride solution (20 ml) was added under cooling. The solution was extracted with pentane, dried over magnesium sulfate, and evaporated. The crude product was purified by column chromatography (hexane) to yield a colourless liquid (4.60 g, 18.2 mmol, 93%).

¹H-NMR (400 MHz, CDCl₃, 300 K): δ [ppm] = 4.69 (s, 2H, H₉), 2.00 (t, *J* = 7.6 Hz, 4H, H₈), 1.48-1.20 (m, 24H, H₂₋₇), 0.89 (t, *J* = 6.9 Hz, 6H, H₁). **¹³C{¹H}-NMR** (101 MHz, CDCl₃, 300 K): δ [ppm] = 150.6, 108.5, 36.3, 32.1, 29.7, 29.6, 29.5, 28.0, 22.9, 14.3. **IR:** $\tilde{\nu}$ [cm⁻¹] = 2956+2922+2853 (C_{alkyl}-H), 1645 (C=C). **MS** (FD): *m/z* = 252.2931, calculated for [C₁₈H₃₆]⁺ = 252.2817.

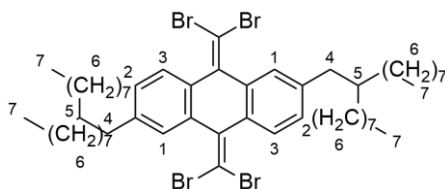
4.3.3 2,6-Bis(2-octyldecyl)anthraquinone (33)



0.5 M 9-Borabicyclo[3.3.1]nonane solution in THF (62 ml, 31.0 mmol, 2.7 eq.) was slowly added to 9-methyleneheptadecane (7.13 g, 28.2 mmol, 2.5 eq.) at room temperature under argon atmosphere. The mixture was stirred for 23 hours. Then 2.4 M potassium carbonate aqueous solution (10 ml, 23.5 mmol, 2.1 eq.), 2,6-dibromoanthraquinone (4.14 g, 11.3 mmol, 1.0 eq.), and tetrakis(triphenylphosphine)palladium(0) (0.52 g, 0.45 mmol, 0.04 eq.) were added and the mixture was heated to 75 °C for further 23 hours. Then, the reaction was allowed to cool down to room temperature, extracted with dichloromethane (3x 100 ml), the combined organic phases were dried over magnesium sulfate, and the solvent removed by evaporation. The crude product was purified by column chromatography (hexane/CH₂Cl₂ 1:0 → 3:1). The product was obtained as a yellow oil (2.24 g, 3.14 mmol, 28%).

¹H-NMR (600 MHz, CDCl₃, 300 K): δ [ppm] = 8.21 (d, *J* = 7.9 Hz, 2H, H₃), 8.07 (d, *J* = 1.5 Hz, 2H, H₁), 7.55 (dd, *J* = 7.9, 1.7 Hz, 2H, H₂), 2.70 (d, *J* = 7.1 Hz, 4H, H₄), 1.72 (s, 2H, H₅), 1.37-1.15 (m, 56H, H₆), 0.86 (t, *J* = 7.0 Hz, 12H, H₇). **¹³C{¹H}-NMR** (151 MHz, CDCl₃, 300 K): δ [ppm] = 183.6, 149.6, 135.0, 133.6, 131.7, 127.7, 127.4, 41.1, 39.8, 33.4, 32.0, 30.1, 29.7, 29.5, 26.7, 22.8, 14.2. **IR:** $\tilde{\nu}$ [cm⁻¹] = 2920+2852 (C_{alkyl}-H), 1674 (C=O). **MS** (FD): *m/z* = 712.6186, calculated for [C₅₀H₈₀O₂]⁺ = 712.6158.

4.3.4 9,10-Bis(dibromomethylene)-2,6-bis(2-octyldecyl)-9,10-dihydroanthracene (28)

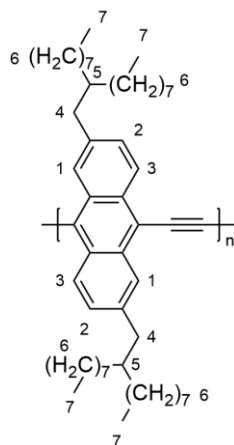


Dry toluene (5 ml) was added to triphenylphosphine (2.31 g, 8.79 mmol, 8.0 eq.) and tetrabromomethane (1.64 g, 4.95 mmol, 4.5 eq.) under argon atmosphere. The mixture was stirred for 20 minutes at room temperature. Then 2,6-bis(2-octyldecyl)anthraquinone (0.78 g, 1.10 mmol, 1.0 eq.) in toluene (5 ml) was added and the solution was heated to 80 °C for 24 hours. The suspension was cooled down to room temperature and filtered. The remaining solid was washed

with toluene and the filtrate evaporated. The crude product was purified by column chromatography (hexane). The product was obtained as a colourless oil (0.97, 0.95 mmol, 86%).

$^1\text{H-NMR}$ (600 MHz, CDCl_3 , 300 K): δ [ppm] = 7.73 (d, J = 8.0 Hz, 2H, H_3), 7.60 (d, J = 1.5 Hz, 2H, H_1), 7.04 (dd, J = 8.0, 1.7 Hz, 2H, H_2), 2.52 (d, J = 6.8, 4H, H_4), 1.63 (m, 2H, H_5), 1.34-1.17 (m, 56H, H_6), 0.88 (t, J = 7.1 Hz, 12H, H_7). **$^{13}\text{C}\{\text{H}\}\text{-NMR}$** (151 MHz, CDCl_3 , 300 K): δ [ppm] = 141.1, 139.9, 135.9, 133.3, 128.4, 127.9, 127.4, 89.4, 40.6, 39.8, 33.5, 33.2, 32.1, 30.2, 30.1, 29.8, 29.7, 29.5, 29.4, 27.1, 26.9, 26.6, 22.8, 14.3. **IR:** $\tilde{\nu}$ [cm^{-1}] = 2920+2850 ($\text{C}_{\text{alkyl}}\text{-H}$). **MS** (FD): m/z = 1020.2935, calculated for $[\text{C}_{50}\text{H}_{80}\text{Br}_4]^+$ = 1020.2994.

4.3.5 Poly[2,6-(2-octyldecyl)anthrylene-9,10-ethynylene] (PAAE)



A solution of 9,10-bis(dibromomethylene)-2,6-bis(2-octyldecyl)-9,10-dihydroanthracene (1.34 g, 1.31 mmol, 1.0 eq.) in dry tetrahydrofuran (10 ml) was cooled down to <-90 °C using a cooling bath of acetone and liquid nitrogen. Then, 1.6 M *n*-butyllithium solution in hexane (1.64 ml, 2.62 mmol, 2.0 eq.) was slowly added. The solution was stirred for 1 hour. Subsequently, copper(I) cyanide (0.12 g, 1.31 mmol, 1.0 eq.) was added and the solution slowly allowed to reach room temperature over a period of 4 hours. It was stirred at room temperature for 18 hours. The reaction was diluted with chloroform and extracted with 25% aqueous ammonia solution (2x). Then, most of the solvent was evaporated and the polymer was precipitated into acidified (2 M HCl) cold methanol, filtrated, and washed with methanol. The crude product was purified by Soxhlet extraction (MeOH, acetone, EtOAc, CHCl_3). The products were obtained as a dark red, viscous materials (ethyl acetate fraction: 0.49 g, 0.70 mmol, 53%; chloroform fraction: 0.01 g, 0.01 mmol, 1%).

¹H-NMR (400 MHz, C₂D₂Cl₄, 353 K): δ [ppm] = 9.21-6.48 (m, 6H, H₁₋₃), 3.25-0.25 (m, 74H, H₄₋₇). **¹³C{¹H}-NMR** (101 MHz, C₂D₂Cl₄, 353 K): δ [ppm] = 128.5, 42.0, 39.9, 34.1, 32.3, 30.4, 30.0, 29.6, 27.2, 23.0, 14.3. **GPC** (THF) ethyl acetate fraction: M_n = 7100 g/mol, M_w = 16600 g/mol, PDI = 2.33; chloroform fraction: M_n = 13000 g/mol, M_w = 44400 g/mol, PDI = 3.41. **UV/Vis** (CHCl₃ solution): λ_{max} . [nm] = 261, 502; (film): λ_{max} . [nm] = 263, 506. **PL** (CHCl₃ solution, λ_{exc} . [nm] = 500 nm): λ_{max} . [nm] = 611, PLQY = 7.2%; (film, λ_{exc} . [nm] = 500 nm): λ_{max} [nm] = 687, PLQY = 3.8%. **Energies/Bandgap** E_{HOMO} [eV] = -5.49; E_{LUMO} [eV] = -3.25; E_g [eV] = 2.24.

5 Appendix

5.1 List of Abbreviations

9-BBN	9-borabicyclo[3.3.1]nonane
Abs.	absorption
A.C.	autocorrelation function
Ac	acetyl
ACN	acetonitrile
ACQ	aggregation-caused quenching
AEE	aggregation-enhanced emission
AFM	atomic force microscopy
AIE	aggregation-induced emission
AIEgen	aggregation-induced emission luminogens
APCI	atmospheric pressure chemical ionization
Ar	aryl
BET	Brunauer, Emmett, Teller
Bu	butyl
COD	1,5-cyclooctadiene
C-PIM	conjugated polymer of intrinsic microporosity
cps	counts per second
d	days
DCE	dichloroethane

DCM	dichloromethane
DMF	dimethylformamide
DMSO	dimethyl sulfoxide
DP	degree of polymerization
DSC	differential scanning calorimetry
EA	ethyl acetate
EDTA	ethylenediaminetetraacetic acid
E_g	bandgap energy
eq.	equivalents
EQCM	electrochemical quartz crystal microbalance
ESI	electrospray ionization
Et	ethyl
exc.	excitation
FD	field desorption
f_w	water fraction
GPC	gel permeation chromatography
h	hours
HOMO	highest occupied molecular orbital
IR	infrared
ITO	indium tin oxide
LUMO	lowest unoccupied molecular orbital
MALDI	matrix-assisted laser desorption ionization

max.	maximum
Me	methyl
min	minutes
M_n	number average
MS	mass spectrometry
M_w	weight average
N/A	not applicable
NHE	normal hydrogen electrode
NMR	nuclear magnetic resonance spectroscopy
OFET	organic field-effect transistor
OLED	organic light-emitting diode
PAE	poly(arylene ethynylene)
PAV	poly(arylene vinylene)
PCC	pyridinium chlorochromate
PDI	polydispersity index
PET	photoinduced electron transfer
Ph	phenyl
PL	photoluminescence
PPE	poly(<i>para</i> -phenylene ethynylene)
ppm	parts per million
PPV	poly(<i>para</i> -phenylene vinylene)
PPV-DP	poly(1,4-phenylene-1,2-diphenylvinylene)

PTFE	polytetrafluoroethylene
quat	quaternary
QY	quantum yield
R	residue
RIM	restriction of intramolecular motions
rt	room temperature
SCE	saturated calomel electrode
sh	shoulder
STP	standard temperature and pressure
<i>t</i>	tert
TBAP	tetrabutylammonium perchlorate
TBAPF ₆	tetrabutylammonium hexafluorophosphate
TCB	1,2,4-trichlorobenzene
TGA	thermogravimetric analysis
THF	tetrahydrofuran
TNP	picric acid
TPE	tetraphenylethylene
UV/Vis	ultraviolet-visible spectroscopy
W.R.	weighted residuals

5.2 References

- [1] M. Kim, S. U. Ryu, S. A. Park, K. Choi, T. Kim, D. Chung, T. Park, *Adv. Funct. Mater.* **2019**, *10*, 1904545.
- [2] F. So, B. Krummacher, M. K. Mathai, D. Poplavskyy, S. A. Choulis, V.-E. Choong, *J. Appl. Phys.* **2007**, *102*, 91101.
- [3] R. Ragni, A. Operamolla, G. M. Farinola in *Organic Light-Emitting Diodes (OLEDs)*, Elsevier, **2013**, pp. 3–48.
- [4] J. H. Burroughes, D. D. C. Bradley, A. R. Brown, R. N. Marks, K. Mackay, R. H. Friend, P. L. Burns, A. B. Holmes, *Nature* **1990**, *347*, 539.
- [5] Y. Wang, L. Feng, S. Wang, *Adv. Funct. Mater.* **2019**, *29*, 1806818.
- [6] P. Baek, L. Voorhaar, D. Barker, J. Travas-Sejdic, *Acc. Chem. Res.* **2018**, *51*, 1581.
- [7] H. Zhou, M. H. Chua, B. Z. Tang, J. Xu, *Polym. Chem.* **2019**, *10*, 3822.
- [8] S. Günes, H. Neugebauer, N. S. Sariciftci, *Chem. Rev.* **2007**, *107*, 1324.
- [9] A. Kraft, A. C. Grimsdale, A. B. Holmes, *Angew. Chem. Int. Ed. Engl.* **1998**, *37*, 402.
- [10] U. H. F. Bunz, *Macromol. Rapid Commun.* **2009**, *30*, 772.
- [11] W. Holzer, A. Penzkofer, M. Pichlmaier, D.D.C. Bradley, W. J. Blau, *Chem. Phys.* **1999**, *248*, 273.
- [12] R. Jakubiak, C. J. Collison, W. C. Wan, L. J. Rothberg, B. R. Hsieh, *J. Phys. Chem. A* **1999**, *103*, 2394.
- [13] P. M. Cotts, T. M. Swager, Q. Zhou, *Macromolecules* **1996**, *29*, 7323.
- [14] J. R. Lakowicz, *Principles of fluorescence spectroscopy*, Springer, Boston, **2006**.
- [15] C. A. Hunter, J. K. M. Sanders, *J. Am. Chem. Soc.* **1990**, *112*, 5525.
- [16] J. Luo, Z. Xie, J. W. Lam, L. Cheng, H. Chen, C. Qiu, H. S. Kwok, X. Zhan, Y. Liu, D. Zhu, B. Z. Tang, *Chem. Commun.* **2001**, *18*, 1740.
- [17] D. A. M. Egbe, C. P. Roll, E. Birckner, U.-W. Grummt, R. Stockmann, E. Klemm, *Macromolecules* **2002**, *35*, 3825.
- [18] S. De, S. Das, A. Girigoswami, *Spectrochim. Acta A* **2005**, *61*, 1821.
- [19] Y. Huang, J. Xing, Q. Gong, L.-C. Chen, G. Liu, C. Yao, Z. Wang, H.-L. Zhang, Z. Chen, Q. Zhang, *Nat. Commun.* **2019**, *10*, 169.
- [20] D. A. M. Egbe, B. Cornelia, J. Nowotny, W. Günther, E. Klemm, *Macromolecules* **2003**, *36*, 5459.
- [21] D.M. Johansson, M. Theander, O. Inganäs, M. R. Andersson, *Synth. Met.* **2000**, *113*, 293.

- [22] W. Z. Yuan, P. Lu, S. Chen, J. W. Y. Lam, Z. Wang, Y. Liu, H. S. Kwok, Y. Ma, B. Z. Tang, *Adv. Mater.* **2010**, *22*, 2159.
- [23] Q. Zhao, X. A. Zhang, Q. Wei, J. Wang, X. Y. Shen, A. Qin, J. Z. Sun, B. Z. Tang, *Chem. Commun.* **2012**, *48*, 11671.
- [24] M. A. Díaz-García, F. Hide, B. J. Schwartz, M. D. McGehee, M. R. Andersson, A. J. Heeger, *Appl. Phys. Lett.* **1997**, *70*, 3191.
- [25] G. Lyu, J. Kendall, I. Meazzini, E. Preis, S. Bayseç, U. Scherf, S. Clément, R. C. Evans, *ACS Appl. Polym. Mater.* **2019**, *1*, 3039.
- [26] S. Baysec, E. Preis, S. Allard, U. Scherf, *Macromol. Rapid Commun.* **2016**, *37*, 1802.
- [27] R. Hu, N. L. C. Leung, B. Z. Tang, *Chem. Soc. Rev.* **2014**, *43*, 4494.
- [28] F. Würthner, *Angew. Chem. Int. Ed. Engl.* **2020**, *59*, 2.
- [29] G. C. Schmidt, *Ann. Phys. Chem.* **1896**, *294*, 103.
- [30] Y. Cai, L. Du, K. Samedov, X. Gu, F. Qi, H. H. Y. Sung, B. O. Patrick, Z. Yan, X. Jiang, H. Zhang, J. W. Y. Lam, I. D. Williams, D. Lee Phillips, A. Qin, B. Z. Tang, *Chem. Sci.* **2018**, *9*, 4662.
- [31] N. L. C. Leung, N. Xie, W. Yuan, Y. Liu, Q. Wu, Q. Peng, Q. Miao, J. W. Y. Lam, B. Z. Tang, *Chemistry* **2014**, *20*, 15349.
- [32] Z. Qiu, Z. Yang, W.-C. Chen, L. Xing, S. Hu, S. Ji, Q. Yang, N. Cai, X. Ouyang, Y. Huo, *J. Mater. Chem. C* **2020**, *8*, 4139.
- [33] J. Zhou, Z. Chang, Y. Jiang, B. He, M. Du, P. Lu, Y. Hong, H. S. Kwok, A. Qin, H. Qiu, Z. Zhao, B. Z. Tang, *Chem. Commun.* **2013**, *49*, 2491.
- [34] A. C. B. Rodrigues, J. Pina, W. Dong, M. Forster, U. Scherf, J. S. Seixas de Melo, *Macromolecules* **2018**, *51*, 8501.
- [35] H.-H. Hörhold, D. Raabe, *Acta Polym.* **1979**, *30*, 86.
- [36] W. Dong, T. Fei, U. Scherf, *RSC Adv.* **2018**, *8*, 5760.
- [37] M. P. Aldred, C. Li, G.-F. Zhang, W.-L. Gong, A. D. Q. Li, Y. Dai, D. Ma, M.-Q. Zhu, *J. Mater. Chem.* **2012**, *22*, 7515.
- [38] W. Dong, Y. Pan, M. Fritsch, U. Scherf, *J. Polym. Sci. Part A: Polym. Chem.* **2015**, *53*, 1753.
- [39] W. Dong, T. Fei, A. Palma-Cando, U. Scherf, *Polym. Chem.* **2014**, *5*, 4048.
- [40] F. Cacialli, R. Daik, W.J. Feast, R. H. Friend, C. Lartigau, *Opt. Mater.* **1999**, *12*, 315.
- [41] T. Jenkins, *Talanta* **2001**, *54*, 501.
- [42] Bureau of Alcohol, Tobacco, Firearms and Explosives (ATF), *Fed. Regist.* **2010**, *75*, 70291.

- [43] W. Dong, J. Pina, Y. Pan, E. Preis, J. S. Seixas de Melo, U. Scherf, *Polymer* **2015**, *76*, 173.
- [44] P. Lu, J. W. Y. Lam, J. Liu, C. K. W. Jim, W. Yuan, C. Y. K. Chan, N. Xie, Q. Hu, K. K. L. Cheuk, B. Z. Tang, *Macromolecules* **2011**, *44*, 5977.
- [45] H. Zhou, X. Wang, T. T. Lin, J. Song, B. Z. Tang, J. Xu, *Polym. Chem.* **2016**, *7*, 6309.
- [46] J. Liu, Y. Zhong, P. Lu, Y. Hong, J. W. Y. Lam, M. Faisal, Y. Yu, K. S. Wong, B. Z. Tang, *Polym. Chem.* **2010**, *1*, 426.
- [47] E. Preis, W. Dong, G. Brunklaus, U. Scherf, *J. Mater. Chem. C* **2015**, *3*, 1582.
- [48] S. Pramanik, C. Zheng, X. Zhang, T. J. Emge, J. Li, *J. Am. Chem. Soc.* **2011**, *133*, 4153.
- [49] C. Gu, N. Huang, Y. Wu, H. Xu, D. Jiang, *Angew. Chem. Int. Ed. Engl.* **2015**, *54*, 11540.
- [50] A. Palma-Cando, D. Woitassek, G. Brunklaus, U. Scherf, *Mater. Chem. Front.* **2017**, *1*, 1118.
- [51] S. Dalapati, S. Jin, J. Gao, Y. Xu, A. Nagai, D. Jiang, *J. Am. Chem. Soc.* **2013**, *135*, 17310.
- [52] E. Preis, C. Widling, U. Scherf, S. Patil, G. Brunklaus, J. Schmidt, A. Thomas, *Polym. Chem.* **2011**, *2*, 2186.
- [53] A. Raupke, A. Palma-Cando, E. Shkura, P. Teckhausen, A. Polywka, P. Gornn, U. Scherf, T. Riedl, *Sci. Rep.* **2016**, *6*, 29118.
- [54] V. S. Mothika, A. Raupke, K. O. Brinkmann, T. Riedl, G. Brunklaus, U. Scherf, *ACS Appl. Nano Mater.* **2018**, *1*, 6483.
- [55] A. Palma-Cando, U. Scherf, *ACS Appl. Mater. Interfaces* **2015**, *7*, 11127.
- [56] G. Inzelt, M. Pineri, J.W. Schultze, M.A. Vorotyntsev, *Electrochim. Acta* **2000**, *45*, 2403.
- [57] K. Karon, M. Lapkowski, *J. Solid State Electrochem.* **2015**, *19*, 2601.
- [58] F. Martnez, J. Retuert, G. Neculqueo, H. Naarmann, *Int. J. Polym. Mater.* **1995**, *28*, 51.
- [59] G. Cheng, B. Bonillo, R. S. Sprick, D. J. Adams, T. Hasell, A. I. Cooper, *Adv. Funct. Mater.* **2014**, *24*, 5219.
- [60] P. Klein, H. J. Jotzen, C. M. Aitchison, R. Clowes, E. Preis, A. I. Cooper, R. S. Sprick, U. Scherf, *Polym. Chem.* **2019**, *10*, 5200.
- [61] W.-E. Lee, D.-C. Han, D.-H. Han, H.-J. Choi, T. Sakaguchi, C.-L. Lee, G. Kwak, *Macromol. Rapid Commun.* **2011**, *32*, 1047.
- [62] T. Masuda, E. Isobe, T. Higashimura, K. Takada, *J. Am. Chem. Soc.* **1983**, *105*, 7473.

- [63] G. Cheng, T. Hasell, A. Trewin, D. J. Adams, A. I. Cooper, *Angew. Chem. Int. Ed. Engl.* **2012**, *51*, 12727.
- [64] R. S. Sprick, J.-X. Jiang, B. Bonillo, S. Ren, T. Ratvijitvech, P. Guiglion, M. A. Zwijnenburg, D. J. Adams, A. I. Cooper, *J. Am. Chem. Soc.* **2015**, *137*, 3265.
- [65] R. S. Sprick, Y. Bai, A. A. Y. Guilbert, M. Zbiri, C. M. Aitchison, L. Wilbraham, Y. Yan, D. J. Woods, M. A. Zwijnenburg, A. I. Cooper, *Chem. Mater.* **2019**, *31*, 305.
- [66] H.-H. Hörhold, J. Gottschaldt, J. Opfermann, *J. Prakt. Chem.* **1977**, *319*, 611.
- [67] C. Friedel, J.-M. Crafts, *Compt. Rend.* **1877**, 1392.
- [68] T. Mukaiyama, T. Sato, J. Hanna, *Chem. Lett.* **1973**, *2*, 1041.
- [69] B. Helferich, W. Schaefer, *Org. Synth.* **1929**, *9*, 32.
- [70] R. N. Ram, V. Singh, *Tetrahedron Lett.* **2006**, *47*, 7625.
- [71] N. Miyaura, A. Suzuki, *J. Chem. Soc., Chem. Commun.* **1979**, 866.
- [72] X. Pu, X. Qi, J. M. Ready, *J. Am. Chem. Soc.* **2009**, *131*, 10364.
- [73] H. Reisch, U. Wiesler, U. Scherf, N. Tuytuykov, *Macromolecules* **1996**, *29*, 8204.
- [74] L. H. Slauch, J. H. Raley, *Tetrahedron* **1964**, *20*, 1005.
- [75] T. J. Bruno, P. D. N. Svoronos, Bruno-Svoronos, *Handbook of basic tables for chemical analysis*, CRC Press, Boca Raton, **2011**.
- [76] J. Stampfl, W. Graupner, G. Leising, U. Scherf, *J. Lumin.* **1995**, *63*, 117.
- [77] A. C. Grimsdale, K. Müllen, *Adv. Polym. Sci.* **2008**, *212*, 1.
- [78] C.-Y. Yu, A. Polisenawati, *Polym. Bull.* **2016**, *73*, 463.
- [79] U. Müller, M. Adam, K. Müllen, *Chem. Ber.* **1994**, *127*, 437.
- [80] A. Dammers-de Klerk, *Mol. Phys.* **1958**, *1*, 141.
- [81] J. E. Anthony, *Clin. Chem.* **2006**, *106*, 5028.
- [82] J. Seixas de Melo, H. D. Burrows, M. Svensson, M. R. Andersson, A. P. Monkman, *J. Chem. Phys.* **2003**, *118*, 1550.
- [83] J. S. de Melo, L. M. Silva, L. G. Arnaut, R. S. Becker, *J. Chem. Phys.* **1999**, *111*, 5427.
- [84] G. Ginocchetti, U. Mazzucato, A. Spalletti, *J. Photochem. Photobiol.* **2008**, *196*, 233.
- [85] W. J. Feast, F. Cacialli, A. T. H. Koch, R. Daik, C. Lartigau, R. H. Friend, D. Beljonne, J.-L. Brédas, *J. Mater. Chem.* **2007**, *17*, 907.
- [86] S. Brunauer, P. H. Emmett, E. Teller, *J. Am. Chem. Soc.* **1938**, *60*, 309.
- [87] K. S. W. Sing, *Pure Appl. Chem.* **1985**, *57*, 603.
- [88] J. Jeromenok, J. Weber, *Langmuir* **2013**, *29*, 12982.
- [89] A. C. B. Rodrigues, I. S. Geisler, P. Klein, J. Pina, F. J. H. Neuhaus, E. Dreher, C. W. Lehmann, U. Scherf, J. S. Seixas de Melo, *J. Mater. Chem. C* **2020**, *8*, 2248.

- [90] T. Mukaiyama, T. Sato, J. Hanna, *Chem. Lett.* **1973**, 2, 1041.
- [91] B.-K. An, S.-K. Kwon, S.-D. Jung, S. Y. Park, *J. Am. Chem. Soc.* **2002**, 124, 14410.
- [92] C. S. de Castro, T. F.G.G. Cova, A. C.C. Pais, D. Pinheiro, C. Nuñez, C. Lodeiro, J. S. Seixas de Melo, *Dyes Pigm.* **2016**, 134, 601.
- [93] J. F. Ambrose, R. F. Nelson, *J. Electrochem. Soc.* **1968**, 115, 1159.
- [94] M. Li, S. Tang, F. Shen, M. Liu, W. Xie, H. Xia, L. Liu, L. Tian, Z. Xie, P. Lu, M. Hanif, D. Lu, G. Cheng, Y. Ma, *Chem. Commun.* **2006**, 3393.
- [95] P. Taranekar, T. Fulghum, D. Patton, R. Ponnampati, G. Clyde, R. Advincula, *J. Am. Chem. Soc.* **2007**, 129, 12537.
- [96] L. Qin, S. Zhang, J. Xu, B. Lu, X. Duan, D. Zhu, Y. Huang, *Int. J. Electrochem. Sci.* **2013**, 8, 5299.
- [97] J. Heinze, *Angew. Chem. Int. Ed. Engl.* **1984**, 23, 831.
- [98] V. V. Pavlishchuk, A. W. Addison, *Inorg. Chim. Acta* **2000**, 298, 97.
- [99] Y. Wei, C. C. Chan, J. Tian, G. W. Jang, K. F. Hsueh, *Chem. Mater.* **1991**, 3, 888.
- [100] D. B. Wurm, Y.-T. Kim, *Langmuir* **2000**, 16, 4533.
- [101] G. Sauerbrey, *Z. Physik* **1959**, 155, 206.
- [102] E. Tamburri, S. Orlanducci, F. Toschi, M. L. Terranova, D. Passeri, *Synth. Met.* **2009**, 159, 406.
- [103] G. Li, L. Qin, C. Yao, Y. Xu, *Sci. Rep.* **2017**, 7, 15394.
- [104] R. T. K. Kwok, J. Geng, J. W. Y. Lam, E. Zhao, G. Wang, R. Zhan, B. Liu, B. Z. Tang, *J. Mater. Chem. B* **2014**, 2, 4134.
- [105] Q. Pang, X. Fan, *ChemistrySelect* **2020**, 5, 7959.
- [106] J. Ma, H. Zhu, W. Huang, T. Lin, X. Pan, W. Wang, *Chin. J. Chem.* **2015**, 33, 1380.
- [107] C. Yang, J. Jacob, K. Müllen, *Macromol. Chem. Phys.* **2006**, 207, 1107.
- [108] D. F. Eaton, *Pure Appl. Chem.* **1988**, 60, 1107.
- [109] A. Sánchez-Grande, B. de La Torre, J. Santos, B. Cirera, K. Lauwaet, T. Chutora, S. Edalatmanesh, P. Mutombo, J. Rosen, R. Zbořil, R. Miranda, J. Björk, P. Jelínek, N. Martín, D. Écija, *Angew. Chem. Int. Ed. Engl.* **2019**, 58, 6559.
- [110] S. Tarkuç, R. Eelkema, F. C. Grozema, *Tetrahedron* **2017**, 73, 4994.
- [111] G. A. Parada, Z. K. Goldsmith, S. Kolmar, B. Pettersson Rimgard, B. Q. Mercado, L. Hammarström, S. Hammes-Schiffer, J. M. Mayer, *Science* **2019**, 364, 471.
- [112] M. Y. Vorona, N. J. Yutronkie, O. A. Melville, A. J. Daszczyński, K. T. Agyei, J. S. Ovens, J. L. Brusso, B. H. Lessard, *Materials* **2019**, 12, 2726.

- [113] H.-Y. Wen, T.-S. Huang, H.-D. Zhang, M.-Y. Chang, W.-Y. Huang, *ACS Appl. Polym. Mater.* **2019**, *1*, 3343.
- [114] S. Haldar, D. Chakraborty, B. Roy, G. Banappanavar, K. Rinku, D. Mullangi, P. Hazra, D. Kabra, R. Vaidhyanathan, *J. Am. Chem. Soc.* **2018**, *140*, 13367.
- [115] H.-M. Shih, C.-J. Lin, S.-R. Tseng, C.-H. Lin, C.-S. Hsu, *Macromol. Chem. Phys.* **2011**, *212*, 1100.
- [116] T. M. Vember, A. S. Cherkasov, *Theor. Exp. Chem.* **1973**, *7*, 332.
- [117] S. C. Ganguly, N. K. Choudhury, *Z. Physik* **1953**, *135*, 255.
- [118] M. Uejima, T. Sato, K. Tanaka, H. Kaji, *Chem. Phys.* **2014**, *430*, 47.
- [119] N. K. Choudhury, *Z. Physik* **1958**, *151*, 93.
- [120] J. Men, H. Ting, Y. Li, W. Wang, G. Gao, L. Xiao, Z. Chen, S. Wang, Q. Gong, *Chem. Phys. Lett.* **2014**, *609*, 33.
- [121] T. Miteva, A. Meisel, M. Grell, H. G. Nothofer, D. Lupo, A. Yasuda, W. Knoll, L. Kloppenburg, U.H.F. Bunz, U. Scherf, D. Neher, *Synth. Met.* **2000**, *111-112*, 173.
- [122] A. Senes, S. C. J. Meskers, W. M. Dijkstra, J. J. van Franeker, S. Altazin, J. S. Wilson, R. A. J. Janssen, *J. Mater. Chem. C* **2016**, *4*, 6302.
- [123] J. Frischeisen, D. Yokoyama, A. Endo, C. Adachi, W. Brütting, *Org. Electron.* **2011**, *12*, 809.
- [124] N. Seidel, T. Hahn, S. Liebing, W. Seichter, J. Kortus, E. Weber, *New J. Chem.* **2013**, *37*, 601.
- [125] S. Pola, C.-H. Kuo, W.-T. Peng, M. M. Islam, I. Chao, Y.-T. Tao, *Chem. Mater.* **2012**, *24*, 2566.
- [126] R. E. Buckles, G. M. Matlack, *Org. Synth.* **1951**, *31*, 104.
- [127] R. J. Rawson, I. T. Harrison, *J. Org. Chem.* **1970**, *35*, 2057.
- [128] M. Iyoda, H. Otani, M. Oda, *Angew. Chem.* **1988**, *100*, 1131.
- [129] T. Nishioka, K. Kuroda, M. Akita, M. Yoshizawa, *Angew. Chem. Int. Ed. Engl.* **2019**, *58*, 6579.
- [130] P. Keg, A. Dell'Aquila, F. Marinelli, O. L. Kapitanchuk, D. Fichou, P. Mastroilli, G. Romanazzi, G. P. Suranna, L. Torsi, Y. M. Lam, S. G. Mhaisalkar, *J. Mater. Chem.* **2010**, *20*, 2448.
- [131] A. Dell'Aquila, F. Marinelli, J. Tey, P. Keg, Y.-M. Lam, O. L. Kapitanchuk, P. Mastroilli, C. F. Nobile, P. Cosma, A. Marchenko, D. Fichou, S. G. Mhaisalkar, G. P. Suranna, L. Torsi, *J. Mater. Chem.* **2008**, *18*, 786.

- [132] C. A. Heller, R. A. Henry, B. A. McLaughlin, D. E. Bliss, *J. Chem. Eng. Data* **1974**, *19*, 214.
- [133] M. Levitus, M. A. Garcia-Garibay, *J. Phys. Chem. A* **2000**, *104*, 8632.
- [134] B. Souharce, *Dissertation*, Bergische Universität Wuppertal, **2008**.
- [135] L. Zhao, R. I. Kaiser, W. Lu, M. Ahmed, M. M. Evseev, E. K. Bashkirov, V. N. Azyazov, C. Tönshoff, F. Reicherter, H. F. Bettinger, A. M. Mebel, *Angew. Chem. Int. Ed.* **2020**, *59*, 11334.
- [136] A. J. Tilley, R. D. Pensack, E. L. Kynaston, G. D. Scholes, D. S. Seferos, *Chem. Mater.* **2018**, *30*, 4409.
- [137] G. M. Sheldrick, *Acta Crystallogr. A: Found. Adv.* **2015**, *71*, 3.
- [138] G. M. Sheldrick, *Acta Crystallogr. C: Struct. Chem.* **2015**, *71*, 3.
- [139] O. V. Dolomanov, L. J. Bourhis, R. J. Gildea, J. A. K. Howard, H. Puschmann, *J. Appl. Crystallogr.* **2009**, *42*, 339.
- [140] J. Pina, J. Seixas de Melo, H. D. Burrows, A. Bilge, T. Farrell, M. Forster, U. Scherf, *J. Phys. Chem. B* **2006**, *110*, 15100.
- [141] D. Law, A. Blakeney, R. Tkachuk, *J. Near Infrared Spectrosc.* **1996**, *4*, 189.
- [142] G. Striker, V. Subramaniam, C. A. M. Seidel, A. Volkmer, *J. Phys. Chem. B* **1999**, *103*, 8612.

5.3 Acknowledgements

First of all, I would like to express my sincere gratitude towards Prof. Dr. Ullrich Scherf for the warm welcome to the group and the opportunity to work on this interesting and challenging topic. Furthermore, I would like to thank him for the support and guidance whenever needed. I am also thankful for the given freedom to develop and work on my own scientific ideas.

I am very thankful to Prof. Dr. Michael W. Tausch for reviewing this thesis.

Special thanks also go to Dr. Sybille Allard, Dr. Michael Forster, Anke Helfer, Sylwia Adamczyk and Kerstin Müller for their administrative and technical support.

I would like to thank Patrick Klein, Christin Barron, Dr. Sybille Allard and Felix Pfaffe for the revision of this thesis.

Furthermore, I am grateful to Jannis Tent for introducing me to the electrochemistry, his support during the measurements and for the revision of the corresponding chapter in this work.

I thank Prof. PhD J. Sérgio Seixas de Melo and Ana Clara B. Rodrigues from the chemistry department of the University of Coimbra for the successful collaboration and the optical measurements of the PAVs and model compounds.

Also, I would like to thank Prof. Dr. John Lupton and Jakob Schedlbauer from the physics department of the University of Regensburg for the collaboration and the anisotropy measurements of the anthrylene ethynylene compounds.

Furthermore, I am grateful to the group of Prof. Dr. Christian W. Lehmann at the Max-Planck-Institut für Kohlenforschung for providing me with the crystal structures of my TPE model compounds.

For plenty analytical measurements of my samples I would like to thank Anke Helfer, Sylwia Adamczyk, Andreas Siebert, Ilka Polanz and Simone Bettinger.

I would like to thank my current and former coworkers in the macromolecular chemistry group for all the scientific discussions, mutual support and a lot fun times spent together, especially Dario Wetterling, Jannis Tent, Christin Barron, Yazhou Xu, Dr. Tina Keller, Patrik Klein, Dr. Florian Trilling, Dr. Markus Mühlinghaus, Dr. Florian Körber and Robin Ammenhäuser.

A special regard goes to Patrick Klein for inspiring my topic and shearing his tert-butyl polymer with me.

Thank you to Kerstin Müller for always having an open ear and all the organizational support.

Also, I want to thank my Bachelor student Fabian Neuhaus and all the other students that supported me with their synthesis-work.

Last but not least, I would like to express my deepest gratitude towards my mother Brigitte, my fiancée Felix, my whole family and my friends: Thank you for all your support, love and encouragement. I could not have made this without you.